Characterizing and Managing Risk from Environmental Release of Pathogens of Concern

A Thesis

Submitted to the Faculty

of

Drexel University

by

Tao Hong

in partial fulfillment of the

requirements for the degree

of

Doctor of Philosophy

December 2011

Acknowledgements

First and foremost I would like to acknowledge Dr. Patrick Gurian, my academic supervisor, for his guidance, dedication, and support in the course of my graduate studies at Drexel University. I am deeply impressed by his enthusiasm, inspiration, knowledge, wisdom, and keen insight. He has invested enormous efforts and provided tremendous help in every aspect throughout all phases of this venture, and I could not have completed this work without him.

I would also like to express my appreciation to my thesis committee members, Dr. Charles Haas, Dr. Wen Jin, Dr. Anu Pradhan, and Dr. John Domzalski, for their valuable comments, suggestions, and recommendations. My thanks also go to my Master thesis committee members, Dr. Joan Rose and Dr. Mira Olson. In addition, it was both an honor and a privilege to work with Dr. Haas and Dr. Rose, true pioneers in this field.

Moreover, I am grateful to the financial support through the Center for Advancing Microbial Risk Assessment, by the U.S. Environmental Protection Agency and U.S. Department of Homeland Security, under the Science to Achieve Results (STAR) grant program (grant number: R83236201).

Last but definitely not least, many thanks are extended to my colleagues and friends for their assistance in many different ways during my stay at Drexel University.

Table of Contents

List of Tables

List of Figures

ABSTRACT

Characterizing and Managing Risk from Environmental Release of Pathogens of Concern
Tao Hong
Patrick L. Gurian, Ph.D., Supervisor

The 2001 anthrax letter attacks not only caused the deaths of 5 people, the distribution of prophylactic antibiotic therapy to more than 30,000 people, and the cost of hundreds of millions of dollars to decontaminate the affected buildings, but also reminded decision makers of the urgency of having a risk management framework for response and recovery from a biological incident in a timely manner. In order to address this concern, the overall objective of this dissertation is to develop mathematical models to promote the understanding of a biological attack, to reduce uncertainty and variability in risk assessments of bioterrorism agents, and to provide information for decision-making steps to minimize the associated mortality and economic loss. This dissertation first adopted the Bayesian Monte Carlo (BMC) method to validate a previously published risk assessment framework by the author, which developed surface concentration standards for *B. anthracis* by linking surface contamination levels with estimates of risk to exposed individuals. The benefit of this analysis significantly reduced uncertainties in the estimated human health risk, which provided more accurate information for the decision makers seeking to identify the proper response. Then this dissertation focused on characterizing the risk of a biological release. It developed a 7-step evaluation framework for choosing the sampling and modeling approach which most accurately recovers details of a release from surface samples. The findings of this analysis not only answered the question "what is the best place to sample?", but also provided insights as to the quantity

of samples that should be taken. The last chapter of this dissertation extends the fate, transport, and risk assessment model by synthesizing available information on five Category A pathogens (*Bacillus anthracis*, *Yersinia pestis*, *Francisella tularensis*, *Variola major* and Lassa) to develop quantitative guidelines for how environmental pathogen concentrations may be related to human health risk. These findings provide critical information for developing a risk-informed biological attack response system. Questions such as "how to estimate if risks warrant the distribution of prophylactic antibiotics?", and "how to choose between active or passive decontamination approaches?" were addressed.

CHAPTER 1: BACKGROUND

It has been ten years since Al Qaeda's terrorist attacks on the World Trade Center and the Pentagon, which were followed by the mailing out of a series of letters containing *B. anthraces* spores to multiple destinations in 2001. Since then, attention and resources (billions of dollars) have been spent by the US government in order to prevent future domestic terrorist attacks and to improve its emergency response system [109, 209]. Quantitative microbial risk assessment (QMRA), derived from chemical risk assessment, is a robust tool to prepare such a response system. It is designed to deliver critical information to decision makers, by estimating the casualties of a terrorist attack, and prioritizing different mitigation options [70, 71]. A standard QMRA framework is composed of four elements, hazard identification, dose-response evaluation, exposure assessment, and risk characterization [117]. However, a major challenge to a QMRA framework is the difficulty of handling uncertainty and variability, which can be due to a lack of precise knowledge or an inherent property of the factors under consideration [12, 25, 122]. Thus, the overall objective of this dissertation is to develop mathematical models to promote the understanding of a biological attack, and reduce uncertainty in the risk assessment.

1.1 The history of biological attack

According to the Centers for Disease Control and Prevention's (CDC) definition, bioterrorism is "the deliberate release of viruses, bacteria, or other germs (agents) used to

cause illness or death in people, animals, or plants" [31]. A narrower view expressed by Carus is that nonideologically motivated uses of biological agents belong to the category of biocrimes.[29]. Compared to conventional weapons, biological ones, also known as "the poor man's atom bomb" [144], can produce panic, havoc and casualties which profoundly disrupt the stability of a society [190]. Four reasons can explain the emergence of bioterrorism: 1) natural access to the pathogens, 2) fewer technical challenges, 3) relatively low costs to launch an attack, and 4) more difficulty in detecting the victims' infection due to the pathogens' incubation period and the fact that many diseases not caused by bioterrorism have similar symptoms [192].

Historically, the earliest record of employing biological agents as a warfare weapon can be traced back to ancient Roman civilization. The Romans threw carrion into their enemies' wells to pollute the drinking water [13]. In the 14th century, the Tatars utilized bubonic plague as a weapon to infiltrate the city of Kaffa, resulting in some of the inhabitants escaping in ships with infected rats and fleas. Later, those ships' multiple entrance to various Italian ports became the source of the Black Death, which wiped out nearly a third of Western Europe [13]. In the modern era, infamous instances of biological warfare happened during World War II (WWII), including the Japanese military's release of plague in China, and the Soviets' tularemia attack towards German Panzer troops [13]. Even after WWII, investigations of biological weapons were still continued. It was reported that more than 10 types of pathogens were able to be effectively delivered in forms of aerosol spray or bomblets [126, 190].

In recent years, prior to the 2001 anthrax letter attacks, identified bioterrorism attacks and biocrimes included the release of *Salmonella typhimurium* to eleven restaurants' salad bars in order to influence an election in the city of Portland in 1984, causing the infection of 750 people; the release of *Shigella dysenteriae* into pastries by a co-worker, sending 12 people to the hospital in Dallas in 1996 [70]; and the release of *Bacillus anthracis* spores in Tokyo by the religious group Aum Shinrikyo between 1990 and 1995, which failed to infect any people [13, 157]. After comparing attacks that happened before and after the 1990s, terrorist scholars found there was a revolutionary transformation in nature of terrorism, since the 'new terrorism' 1) is more inspired by religious beliefs; 2) has amorphous irreconcilable objectives; 3) has global targets; 4) has a horizontal and loose network; 5) pursues symbolic violence; 6) employs more lethal and indiscriminate violent tactics; and 7) is closely related to weapons of mass destruction [7, 64, 83, 105, 145, 165, 208].

1.2 The 2001 anthrax letter attacks

The 2001 anthrax letter attacks have changed the realm of public health [95]. These letters not only caused the deaths of 5 people and the distribution of prophylactic antibiotic therapy to more than 30,000 people, but also required hundreds of millions of dollars to decontaminated the affected buildings [163]. Although the 2001 anthrax letter attacks are considered to be the "worst case of bioterrorism in U.S. history", they are treated as relative small scale attacks compared to the ones with the potential to bring thousands of deaths [65]. In 1970, the World Health Organization (WHO) predicted that

if 50 kg of *B. anthracis* spores were released by aircraft over an area with a population of 5 million, the number of casualties would be around 25,000 [206]. In 1993, the US Congressional Office of Technology Assessment estimated that the lethality of releasing 100kg of *B. anthracis* spores upwind of Washington, DC area was equivalent to a hydrogen bomb, causing 3 million deaths [187]. In a recently study, Wein et. al. indicated that if the released amount of *B. anthracis* spores were reduced to 1 kg with 50% dissemination efficiency over a large U.S. city of 1.39 million people, there could be as many as 146,269 mortalities [197]. Based on the above three estimates and the 2001 anthrax letter attacks, a large-scale biological attack on a U.S. city could contaminate both indoor and outdoor environments, requiring a resource consuming decontamination, and rendering a city uninhabitable for long time period [65].

From the 2001 anthrax letter attacks, decision makers realized the urgency of having a risk management framework, for response and recovery from a biological incident in a timely manner [136, 188]. This framework should address a number of critical knowledge gaps in perspectives of risk characterization and future damage control, including propagating the uncertainties in the risk assessment, developing consensus-based surface sampling methods and validating their results, justifying the selection of a decontamination endpoint, and creating a publicly acceptable prophylactic antibiotic storage and distribution plan [67, 176].

1.3 Pathogens of Interest

In the year 1999, the Centers for Disease Control (CDC) reclassified biologic agents into three categories based on their ease of transmission, mortality rate, disruption of social order, and level of public panic. Table 1-1 lists the features of the three categories of pathogens and their representatives [30, 150, 190]. In this study, five pathogens (*Bacillus anthracis*, *Yersinia. pestis*, *Francisella tularensis*, Variola major and Lassa) from Category A are selected, and their risk to exposed people will be investigated.

Table 1-1 Features and representatives of biological agents

Category	Feature	Pathogens
Category A	• Easily to disseminate • High mortality rates • Might cause public panic and social disruption • Require special action for public health preparedness	• *Bacillus anthracis* • *Clostridium botulinum* toxin • *Yersinia pestis* • Variola major • *Francisella tularensis* • Ebola, and Lassa
Category B	• Moderately easy to disseminate • Moderate or low mortality rates • Require specific enhancements of CDC's diagnostic capacity and enhanced disease surveillance	• *Brucella species* • *Clostridium perfringens* • *Salmonella species* • *Burkholderia mallei* • *Burkholderia pseudomallei* • *Chlamydia psittaci* • *Coxiella burnetii* • *Ricinus communis* • *Staphylococcal enterotoxin B* • *Rickettsia prowazekii* • *Alphaviruses* • *Vibrio cholerae* • *Cryptosporidium parvum*
Category C	• Available to be engineered and disseminated • Low mortality risk	• *Emerging infectious diseases such as Nipah virus and hantavirus*

Information extracted from [30, 150, 190]

1.3.1 *Bacillus anthracis*

Bacillus anthracis is an aerobic, Gram-positive, non-motile, spore-forming bacterial species which is the causative agent of anthrax, a potentially fatal bacterial infection. The bacteria will sporulate when the environment is not suitable for continuous multiplication. *Bacillus anthracis* spores are resistant to heat, ultraviolet, drying, and many chemical disinfectants [50, 191]. Two reasons can be explained for terrorists using *Bacillus anthracis* spores as their weapon. One is that *Bacillus anthracis* particles can be readily obtained from scientific and natural sources, cultivated, possibly "weaponized", stored, transported, and released as aerosols using a variety of delivery systems [94]; the other reason is the high mortality rate once people are infected.

1.3.1.1 Forms of anthrax

a) Cutaneous anthrax

Cutaneous anthrax is the most common form of anthrax and accounts for 90%-95% of anthrax infections all over the world [50, 191]. Neck, head and extremities are common areas where infection may initiate after direct or indirect contact with infected animals or their products, while transmission by insects after feeding on infected animal is rare [143]. Antibiotic treatment is recommended for cutaneous anthrax which can reduce the mortality from 20% to almost 0% [50, 94].

b) Inhalational anthrax

Inhalational anthrax is less common. It occurs after spores entering the upper respiratory system are engulfed and transported by alveolar macrophages to the

peribronchial lymph nodes, where the spores germinate and spread throughout the body in blood [50]. Only 18 cases of inhalational anthrax were reported in the US in the 20th century, most due to occupational exposure, such as meat-packing, animal hair-sorting and tanning [82, 94]. The early diagnosis of inhalational anthrax is difficult unless there is a known outbreak. However, the onset of symptoms can occur after several weeks from exposure [50]. Historically, the mortality rate of inhalational anthrax is over 90%, but the 2001 anthrax letter attacks indicated that early antibiotic treatment could reduce the mortality rate to 45% [84].

c) Gastrointestinal anthrax

Gastrointestinal anthrax is more common in herbivorous animals than in humans and usually occurs in undeveloped countries as a result of ingesting undercooked infected meat. There were no records of gastrointestinal anthrax in the USA before 1999 [50] or Britain before 1994 [191]. However, 24 cases of oral-oropharyngeal anthrax were attributed to ingesting contaminated water buffalo meat in the north part of Thailand, and 6 infections were reported in Turkey in 1986 [168]. Since the symptoms of gastrointestinal anthrax are not specific, difficulties in diagnosing the disease may miss the recommended treatment period, which contributes to a relatively broad mortality rate range from 4% to 50% [167, 191].

1.3.1.2 Epidemiology of anthrax

Accidental human infection with *Bacillus anthracis* is very rare. It is estimated that there were only 2000 cases worldwide annually in the 1980s, and 80% of these cases

were initiated by industrial exposure [57]. The largest outbreak in the USA happened in 1957. Nine (9) goat hair-processing plant workers were infected and 4 of them died. At worldwide level, 79 persons contracted anthrax and 68 of them died because of an accidental release of *B. anthracis* spores from a military laboratory in Sverdlovsk, 1979 [1, 118]. It is estimated that aggressive antibiotic treatment could have increased the survival rate to 20% for people who suffered inhalational anthrax in Sverdlovsk [118]. Between 1979 and 1980, 182 died of anthrax out of 10,000 human infection cases in Zimbabwe; in Tibet, China, 162 deaths out of 507 infections occurred in 1989; and in western mountainous part of China, there were 898 human infections reported in 1996 with a 5% fatality rate, and 1,210 human infections with a 3% fatality rate reported in 1997. There are high numbers of human anthrax cases in Spain, from 152 in 1990 to 50 in 1996 [57, 92]. Though the threat from accidental exposure to *Bacillus anthracis* has been reduced with the improvement of industrial hygiene and development of vaccines, the potential of employing this Category A agent as a weapon causing massive casualties is evidently high.

1.3.1.3 *Bacillus Anthracis* as a weapon

Before 2001, bioterrorism-related anthrax was a concern only in tabletop exercises [17]. However, since terrorists have employed *Bacillus anthracis* as a biologic weapon, the realm of public health has been changed. On September 18th, envelopes containing *Bacillus anthracis* spores were mailed to news media companies and government officials, leading to the first bioterrorism-related cases of anthrax in the United States [95, 135]. Around October 9th, a letter containing threatening language

along with *Bacillus anthracis* spores was opened in the mail handing area of a Senate office suite in the Hart Senate Office Building, Washington, DC [135, 199]. These attacks caused the deaths of 5 people and cost hundreds of millions of dollars to clean the contaminated buildings [163].

1.3.2 *Yersinia pestis*

Yersinia. pestis (Y. pestis) is a facultative anaerobic, Gram-negative, non-motile, nonsporulating bacterial species which is the causative agent of plague, an acute and potentially fatal bacterial infection. Unlike *B. anthracis*, *Y. pestis* is susceptible to heat, ultraviolet, drying, and chemical disinfectants [76, 126].

1.3.2.1 Forms of plague

a) Bubonic Plague

Bubonic Plague is the most common form of plague. It is transmitted via the bite of an infected rodent flea which might inoculate up to thousands of organisms into patients' skin [27]. Surviving *Y. pestis* pathogens can enter the bloodstream, migrate to lymph nodes, cause hemorrhaging, and create painful buboes [44]. It is reported that 80% of bubonic plague cases can develop bactermia, 25% can develop septicemia and 10% can develop pneumonia as a complication, resulting in a 50%-60% mortality rate for infected people without medical interference [76]. Thus, antibiotic treatment is recommended for bubonic plague which can significantly reduce the mortality [32].

b) Pneumonic Plague

Similar to anthrax, pneumonic plague is less common. But it is human to human transmissible via close contacts (within 2 meters) with a final-stage patient whose red sputum contains an enormous number of pure culture bacilli [119]. Pneumonic plague occurs after *Y. pestis* is inhaled into the respiratory system [76]. Sometimes pneumonic plague can be misdiagnosed as influenza which may miss the best time for medical treatment [27, 100]. Literature reports indicate that appropriate antibiotic treatment can increase the survival rate to 85% from 0% survival probability without treatment.

c) Septicemic Plague

In septicemic plague, disseminated intravascular coagulation is caused by bacterial endotoxins, forming tiny clots throughout the body and uncontrollable bleeding. Usually, untreated septicemic plague is fatal, but early treatment with antibiotics is able to reduce the mortality rate to 4%-15% [27, 44].

1.3.2.2 Epidemiology of plague

Historically, at least 3 pandemics were caused by plague. The first recorded plague pandemic began in AD 541 afflicting the Eastern Roman Empire and caused the death of 100 million people (50% to 60% population loses) which is also known as the Justinian plague. The second pandemic, the black death, began in 1346 peaking in Europe which killed 30% to 60% of Europe's population (20 to 30 million). The third pandemic spread China in 1855, which killed more than 12 million people including people in India [44, 100, 115, 142, 169].

The improvement of living condition, public hygiene level, and antibiotic therapy have blocked the possibility of plague-caused pandemics [44]. During the decade of 1994 to 2003, the number of both suspected and confirmed human-plague cases was 28,530, with a fatality rate of 7.1% resulting in 2015 deaths, as reported by the World Health Organization (WHO) [203]. In the United States, 390 cases of plague were reported from 1947 to 1996, with a median of 7 cases of plague per year approximately [33, 44, 76].

1.3.2.3 *Y. pestis* as a weapon

Although it is technically challenging to weaponize *Y. pestis*, the feature of secondary person-to-person transmission makes it become a favorable biological weapon to some. In WWII, a secret branch of the Japanese army, Unit 731, attempted to use plague as a weapon in Harbin, the northern part of China. The former Soviet Union successfully created large quantities of *Y. pestis* that can be placed into weapons, while U.S. scientists failed due to pathogen's lack of persistence in the environment. Unlike naturally occurring plague, an outbreak of pneumonic plague, whose initial symptoms are similar to other severe respiratory illnesses, would be likely to happen if aerosolized *Y. pestis* were disseminated [44, 75, 99, 126]. In 1970, the WHO estimated that if 50 kg of *Y. pestis* were intentional aerosolized over a city with 5 million population, as many as 36,000 people would die of pneumonic plague based on a mortality rate of 24% [202].

1.3.3 *Francisella tularensis*

Francisella tularensis (F. tularensis) is an aerobic, Gram-negative, non-motile, nonsporulating bacterial species which is the causative agent of tularemia. Humans are

very sensitive to tularemia, and it is reported that as few as 10 organisms are able to cause disease. Similar to *Y. pestis*, *F. tularensis* is often transmitted to humans via the bites of infected fleas [81, 144].

1.3.3.1 Forms of tularemia

a) Ulceroglandular Tularemia

Ulceroglandular tularemia is the most common form of tularemia accounting for over 90% of cases in European countries. Ulceroglandular tularemia is usually caused through vectorborne transmission or direct skin contacts with infected animals, such as rabbits, moles, muskrats, and some domestic animals [81, 140, 180]. Once infected, a mosquito bite-like ulcer is developed, becoming tender and palpable by draining lymph nodes [62]. Other rare but initiated by membrane contact forms of tularemia includes oculoglandular tularemia, and oropharyngeal tularemia [62, 77].

b) Pneumonic Tularemia

If pathogens are inhaled through the respiratory system, pneumonic tularemia is likely to occur. The disease is transmissible from person to person. Although the mortality rate of inhalational tularemia is up to 30% without medical intervention, antibiotic treatment will greatly lower the rate to less than 2% [45, 48].

1.3.3.2 Epidemiology of tularemia

The geographical distribution of tularemia is uneven with low prevalence in the southern hemisphere. Regions of high prevalence include Scandinavia, Russia, and the

United States. For the United States, the number of tularemia cases has been reduced from several thousand per year before 1950 to 125 during the last decade [15, 34, 35, 44]. High correlation has been reported between the outbreaks of human tularemia and rodent tularemia. For example, tularemia in voles and hares has been associated with human outbreaks in Sweden [181].

1.3.3.3 *F. tularesis* as a weapon

F. tularesis has been viewed as a candidate biological weapon for ages due to its combination of high infectivity and severe illness in humans [159]. It is one of the pathogens investigated by Unit 731, a branch of Japanese secret army, during the Second World War. Scientists from the U.S. developed weapons aerosolizing *F. tularesis* between the 1950s and 1960s, which were gradually destroyed after 1969. The former Soviet Union was reported to develop antibiotic-resistant *F. tularesis,* and a former scientist, Ken Alibek, implied the usage of tularaemia as a bioweapon during WWII on the Eastern Front [45, 99, 140]. In 1969, a group of experts from WHO estimated that if 50 kg of virulent *F. tularesis* were intentional aerosolized over a metropolitan area with a population of 5 million, the number of causalities would be 250,000 including 19,000 deaths [202]. The Centers for Disease Control and Prevention (CDC) estimated that the economic loss caused by a terrorist releasing *F. tularesis* would be $5.4 million per 100,000 exposed persons, which is based on WHO's model [98].

1.3.4 Variola major

As a member of Poxviridae, Variola major is one of the most complex viruses. It is the causative agent of smallpox with a fatality rate of 30% [125]. Similarly to *Y. pestis* and *F. tularensis*, smallpox can be transmitted by directly contacting an infectious person's droplet nuclei or aerosols expelled from the oropharynx [194].

1.3.4.1 Forms of smallpox

Clinically, there are two types of smallpox, variola major and minor, where the former one is the severe and most common one. Four types of smallpox caused by these viruses have been identified. The most frequent type is ordinary smallpox, which accounts for 90% or more of cases. The second type is modified smallpox, which is mild but can infect previously vaccinated persons. The third and fourth types are named flat and hemorrhagic smallpox, which are rare but fatal. Variola minor is a less common presentation of smallpox, and a much less severe disease, with death rates historically of 1% or less [125, 126, 150].

1.3.4.2 Epidemiology of smallpox

The earliest evidence of smallpox is found in the Egyptian mummies from 3000 years ago [89]. Historically, smallpox has been spread throughout the world [81]. In the mid-18th century, smallpox was considered a major endemic disease, since it infected people globally, and killed 400,000 people per year [79]. In the 20th century, around 300-500 million people died due to smallpox [155]. To eradicate smallpox, an intensified global eradication program began in 1967, which aimed to vaccinate over 80% of the

population, and to develop a system of detecting and containing cases and outbreaks [155]. The eradication of smallpox was certified by WHO in the year 1979 [125, 155].

1.3.4.3 Variola major as a weapon

Smallpox is a good bioterrorism agent because it is easy to grow and can resist heat [78]. It was first used as a biological weapon during the French and Indian Wars by the British, who distributed blankets used by smallpox patients to the American Indians, killing more than 50% for the affected tribes [54, 78]. In 1980, the WHO recommended that all remaining samples of the variola major virus should be destroyed or transferred to the reference laboratories in the US and Russia [78]. However, concerns about whether or not these virus samples were securely held were raised after the emergence of a report by Ken Alibek, a former deputy director of the Soviet Union's civilian bioweapons program. Alibek believed that the smallpox based bioweapons, such as bombs and intercontinental ballistic missiles, were secretly prepared until at least 1992. If this is true, it would cause serious problems once terrorists have access to these weapons, since the financial support for those research agencies has been sharply declined recently, which provide motivation for rogue scientists to sell organisms to terrorist groups [13, 78].

1.3.5 Lassa virus

Lassa virus, the causative agent of Lassa fever, is transmitted by rats and was not identified until 1969 in the town of Lassa, Nigeria [151]. The Lass virus is an enveloped, single-stranded, bisegmented RNA virus [138]. Humans can contract this disease from the bite of an infected arthropod, from the aerosol of infected rodent excreta, or from

direct contact with infected animal carcasses [107]. Lassa fever can be transmitted between humans via close contacts [14].

1.3.5.1 Symptoms of Lassa fever

Clinically, the symptoms of Lassa fever are indistinguishable from other hemorrhagic fevers such as Ebola and Marburg. After an incubation period of six to twenty-one days, an acute illness with multiorgan involvement develops. Symptoms include fever, sore throat, and vomiting, while complications include mucosal bleeding, sensorineural hearing deficit, pleural effusion, pericardial effusion, and hemorrhage [151].

1.3.5.2 Epidemiology of Lassa fever

Lass virus is endemic in West African countries, where there are 300,000 to 500,000 infections annually, with approximately 5,000 deaths [138]. It is estimated that about 15-20% of hospitalized Lassa fever patients will die from the illness, while this number can increase to 50% during epidemics [51, 151]. The prevalence of antibodies to the virus in the populations is 8-52% in Sierra Leone, 4-55% in Guinea, and 21% in Nigeria [151].

1.3.5.3 Lassa virus as a weapon

In 1999, CDC classified the Lass virus as Category A agent because it has the ability to cause widespread illness and death, is easy to disseminate, and be transmitted from person to person transmission. Large quantities of Lass virus-based weapons were produced by the former Soviet Union and Russia until 1992 [14].

1.4 Objective of this dissertation

To address gaps identified in the 2001 anthrax letter attacks, the overall objective of this dissertation is to develop mathematical models to promote the understanding of a biological attack, to reduce uncertainty and variability in risk assessments of bioterrorism agents, and to provide information for decision-making steps to minimize the associated mortality and economic loss, which is explained by three sub-objectives (Figure 1-1).

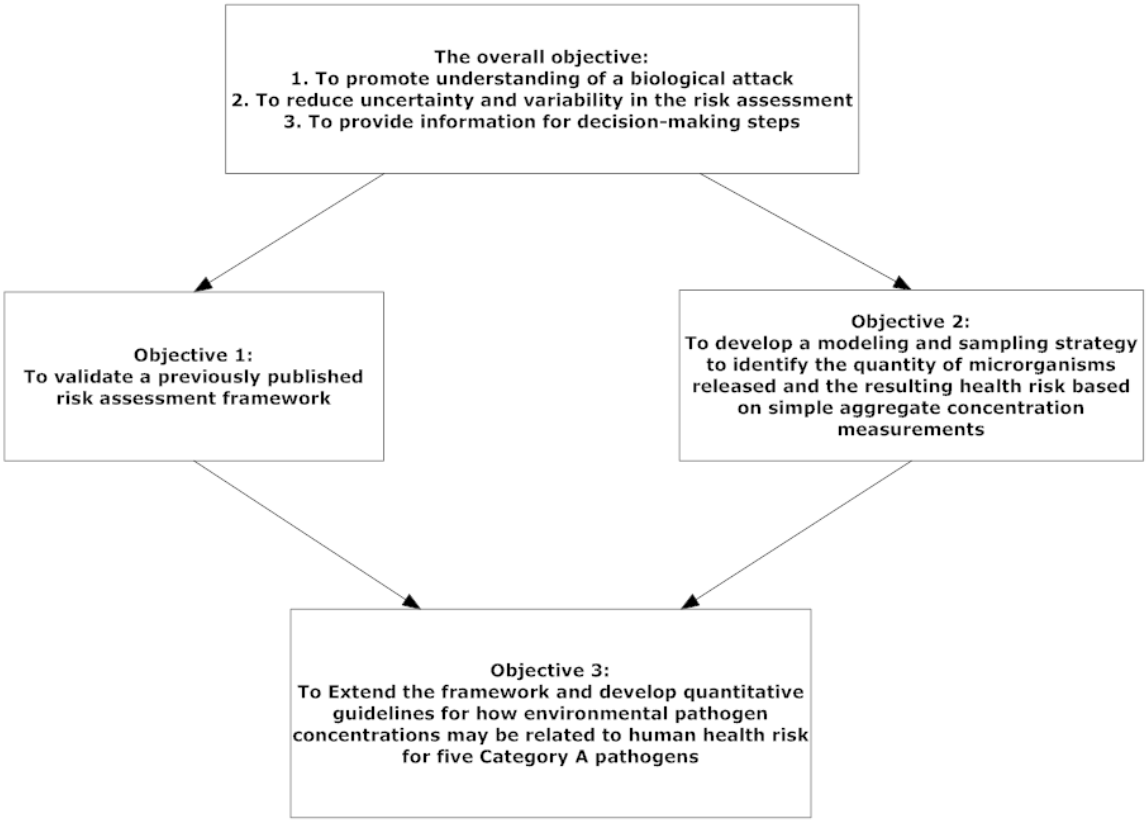

Figure 1-1 Dissertation Analysis Plan

The first objective is to validate a previously published risk assessment framework by the author, which developed surface concentration standards for *B. anthracis* by linking surface contamination levels with estimates of risk to exposed individuals [85]. The objective is accomplished by applying the Bayesian Monte Carlo (BMC) method to the indoor particle fate and transport model developed by Sextro et al. [162] and used by Hong et al. [85]. Field data [199] collected from the Hart Senate Office Building, after a letter containing *B. anthracis* spores was opened, are employed to update distributions for model parameter values (e.g., turbulence intensity, particle density, setting velocity, resuspension rate, sample recovery efficiency, risk to exposed people, etc.). While the available field data may not be sufficient to fully identify all parameters using classical model calibration techniques, when used in a BMC updating procedure they may allow for more informative parameter distributions to be developed. At a minimum, the BMC procedure can ascertain if the observations conflict substantively with the surrogate-based parameter estimates used previously [85, 162].

The second objective aims to address the question of whether the risk due to a microbial release can be identified based on simple aggregate concentration measurements, such as could reasonably be made after an actual release. The successful estimation of this information is valuable in predicting the subsequent dispersion and human health risks. In order to assess how much detail on release can realistically be identified from surface sampling results, a variety of alternative model formulations and sampling schemes are considered, whose results are tested by a 7-step evaluation framework. The recommended sampling schemes are further investigated by applying

them to concentration measurements from a large scale field test, which aims to provide insights between a sampling scheme's uncertainty and its required sample size.

The last objective extends the framework validated in Objective 1. It synthesizes available information on five Category A pathogens (*Bacillus anthracis, Yersinia* pestis, *Francisella tularensis,* Variola major and Lassa) to develop quantitative guidelines for how environmental pathogen concentrations may be related to human health risk. An integrated model of environmental transport and human health exposure to biological pathogens is constructed which 1) includes the effects of environmental attenuation, 2) considers fomite contact exposure (ingestion or dermal risk) as well as inhalational exposure, and 3) includes an uncertainty analysis to identify key input uncertainties. A reduced form model is also derived which allows for approximate estimation of risk without the need to conduct matrix manipulations. The findings from this study will provide a framework for developing many different environmental standards that are needed for making risk-informed response decisions, such as when prophylactic antibiotics should be distributed, and whether or not a contaminated area should be cleaned up [190].

CHAPTER 2: A BAYESIAN APPROACH TO MODEL CALIBRATION FOR *B. ANTHRACIS* RISK ASSESSMENT

Abstract

In this study, the Bayesian Monte Carlo (BMC) method was applied to an indoor pathogen fate and transport model [85]. Uncertainty distributions for model parameters (i.e., release quantity, risk to exposed people, the amount of spores exiting the room, particle density, setting velocity, resuspension rate, sample recovery efficiency, etc.) were updated by comparing model predictions with measurements of *B. anthracis* spores made after one of the 2001 anthrax letter attacks [199]. The results indicated that uncertainties associated with the total quantity of spores released, the amount exiting the room, and risk to occupants could be significantly reduced. However, posterior distributions for fate and transport parameters and sample recovery efficiency were not greatly changed from their prior values, indicating that literature estimates of these parameters are not inconsistent with the observations made by Weis et al. [199]. Posterior estimates of risk for people in the room when the spores were released are on the order of 4.7×10^{-3} to 2.2×10^{-2}, which supports the decision to administer prophylactic antibiotics. Risks associated with spores leaving the room where spores were released are more difficult to characterize but a recommendation to perform risk assessments even for individuals outside the room when the release occurred appears justified. In addition, analyses were conducted to assess how effective different combinations of measurements were at reducing uncertainty in the estimate risk. This analysis revealed that if the size distribution of the released particulates is known, then environmental sampling can be

limited to accurately characterizing floor concentrations, otherwise samples from multiple locations, as well as particulate and building air circulation parameters need to be measured.

2.1. Introduction

The series of 2001 anthrax letter attacks not only caused the deaths of 5 people and hundreds of millions of dollars in clean up costs [163, 178], but also highlighted the difficulties in assessing risks associated with bioterrorism agents [85]. Risk characterization of a biological attack requires a practical approach to estimate the total release quantity, as well as ground-truthed mathematical models to evaluate the subsequent dispersion and human health risks [146].

Many researchers have developed models describing the fate and transport of various particulates in the indoor environmental [120, 131, 146, 149, 152, 162, 171, 173, 184, 183, 189]. For instance, Hong et al. [85] applied the fate and transport model of Sextro et al. [162] in a risk assessment framework to inform the development of surface concentration standards for *B. anthracis*. However, predictions from these models are dependent on the quality of their inputs, which inevitably contain significant amounts of uncertainties given current knowledge. In particular, the parameter estimates for these models are based on surrogates, typically household dust, which may not be representative of the behavior of weaponized *B. anthracis* spores. One of the few sources of information on the environmental fate and transport of *B. anthracis* spores released during an actual bioterrorism event is a study by Weis et al. [199] which reported field data on the behavior of *B. anthracis* spores used in the 2001 anthrax letter attacks. These data may provide some basis for assessing whether the model parameter estimates used by Sextro et al. [162] and Hong et al. [85] are appropriate for a *B. anthracis* bioterrorism incident. However, the large number of parameters in these models may allow multiple

sets of different parameter values to fit the data equally well. In cases such as these, where parameter identifiability is a concern, the use of Bayesian Monte Carlo (BMC) techniques may be helpful [18].

The BMC approach [18] is a robust tool for model calibration. While classical model calibration methods require inputs to be either parameters fit to match the calibration data or fixed constants, the BMC approach allows inputs to be defined by probability distributions that reflect prior knowledge of their likely values. Posterior probability distributions are then developed by comparing the model predictions with observed data. Informative prior distributions can be developed in this domain because many parameters describing the indoor environment, such as turbulence intensity and air exchange rates, fluctuate within bounds that can be defined to some extent by available technical knowledge. BMC provides an approach to employ this prior knowledge of plausible parameter ranges to calibrate the model [18, 69, 160]. By drawing not only on the data, but also prior knowledge, BMC methods may be able applied in situations where classical model calibration would be unable to identify parameters (i.e., cases where the model would be overfit to the available data). There are numerous successful examples of BMC approaches, including applications to water quality evaluation [49], environmental health risk assessment [18, 40], traffic queue modeling [69], fate and transport of DDT in the environment [160], and identification of contaminant source characteristics from sensor network observations [41, 174, 175]. In many BMC studies the posterior distribution is estimated by reweighting the results of a Monte Carlo simulation. In this study due to the high dimensionality of the model being estimated (19

parameters), it becomes unlikely that any combination of prior model parameters will fall in a region of substantial posterior density. For this reason a Markov Chain Monte Carlo (MCMC) method is used to sample the posterior distribution. While the computational method used here differs from many previous studies, the framework of updating prior model parameters distributions with data is unchanged, and hence we consider this study to be an application of the BMC approach.

In this paper, the BMC method is applied to the indoor particle fate and transport model developed by Sextro et al. [162] and applied by Hong et al. [85]. Field data [199] collected from the Hart Senate Office Building, after a letter containing *B. anthracis* spores was opened, are employed to update distributions for model parameter values. While the available field data may not be sufficient to fully identify all parameters using classical model calibration techniques, when used in a BMC updating procedure they may allow for more informative parameter distributions to be developed. At a minimum, the BMC procedure can ascertain if the observations conflict substantively with the surrogate-based parameter estimates used previously [85, 162].

2.2 Methods

2.2.1 Risk assessment model

The risk assessment model of Hong et al. [85] has two components, a fate and transport model, predicting the distribution of released *B. anthracis* spores in an office,

and a dose-response model, estimating human health risk from inhalation of the released *B. anthracis* spores. A schematic plot of the modeled office is provided in Figure 2-1.

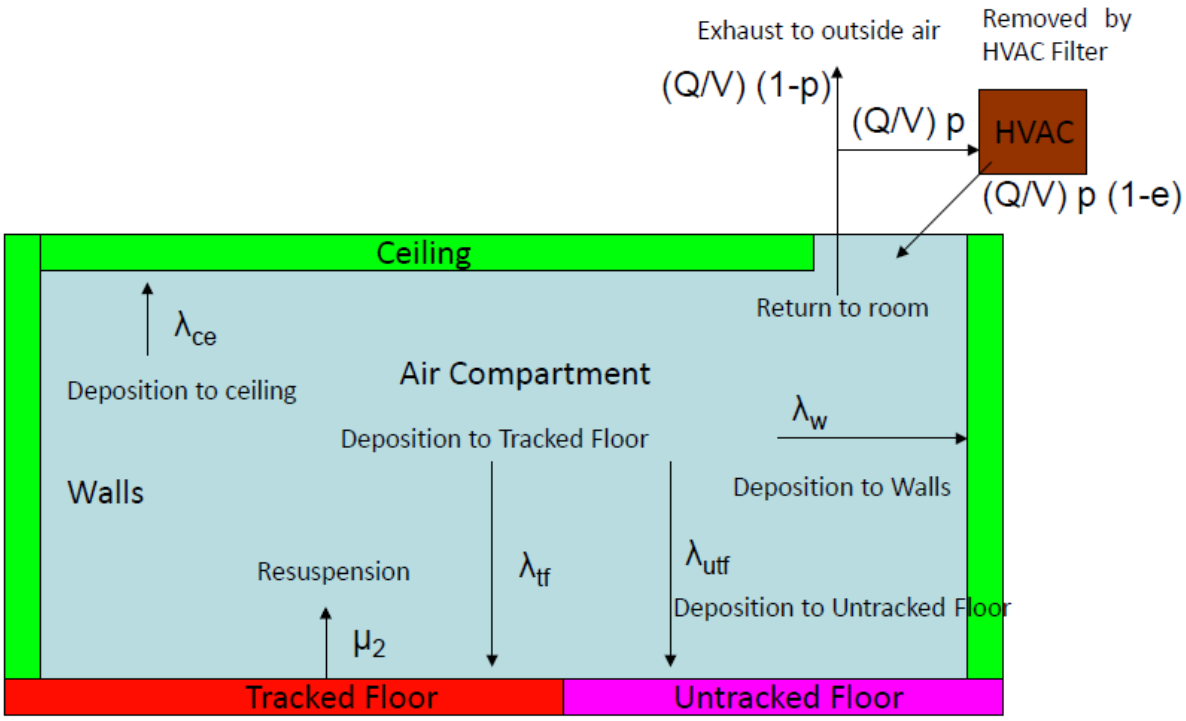

Figure 2-1 Schematic of the modeled office

The office includes seven compartments: air, tracked floor, untracked floor, walls, ceiling, heating ventilation and air conditioning (HVAC), and the nasal passages of occupants of the office. *B. anthracis* spores are modeled as being released instantaneously to the air compartment and completed mixed. Spores deposit to the tracked floor, untracked floor, walls, and ceilings, can be removed by the HVAC filter, can exit the office after passing the HVAC filter, and can be inhaled by the occupants. Most of the movements are irreversible, however, *B. anthracis* spores deposited on the tracked floor have the ability to reenter the air due to human-caused resuspension. The fate and transport of released *B. anthracis* particles is described by a set of ordinary differential equations (Equation 1), for which a detailed solution can be found in Hong [85]:

$$\frac{dM}{dt} = \begin{pmatrix} \dot{M}_{air} \\ \dot{M}_{tf} \\ \dot{M}_{utf} \\ \dot{M}_{w} \\ \dot{M}_{f} \\ \dot{M}_{ec} \\ \dot{M}_{ce} \\ \dot{M}_{n} \end{pmatrix} = \begin{pmatrix} [(1-e)p-1]\frac{Q}{V} - (\lambda_{tf} + \lambda_{utf} + \lambda_{w} + \lambda_{ce} + \frac{I\,e_n}{V}) & \mu_2 & 0 & 0 & 0 & 0 & 0 & 0 \\ \lambda_{tf} & -\mu_2 & 0 & 0 & 0 & 0 & 0 & 0 \\ \lambda_{utf} & 0 & 0 & 0 & 0 & 0 & 0 & 0 \\ \lambda_{w} & 0 & 0 & 0 & 0 & 0 & 0 & 0 \\ ep\frac{Q}{V} & 0 & 0 & 0 & 0 & 0 & 0 & 0 \\ (1-p)\frac{Q}{V} & 0 & 0 & 0 & 0 & 0 & 0 & 0 \\ \lambda_{ce} & 0 & 0 & 0 & 0 & 0 & 0 & 0 \\ \frac{I\,e_n}{V} & 0 & 0 & 0 & 0 & 0 & 0 & 0 \end{pmatrix} \begin{pmatrix} M_{air} \\ M_{tf} \\ M_{utf} \\ M_{w} \\ M_{f} \\ M_{ec} \\ M_{ce} \\ M_{n} \end{pmatrix} \quad (1)$$

where the numbers of spores in the different compartments are denoted by M_{air} (air), M_{tf} (tracked floor), M_{utf} (untracked floor), M_w (walls), M_f (filter), M_{ec} (external compartment) M_{ce} (ceiling), and M_n (nasal passages). The total air flow rate through the HVAC system is denoted by Q (m^3/min), p (dimensionless) is the fraction of total air flow that is recirculated into the building by the HVAC system, e (dimensionless) is the efficiency of the filter at removing particles, and V is the volume of the room (m^3). Removal to the

occupants' nasal passages is modeled with I (m^3/ min), denoting the breathing flow rate and e_n (dimensionless) the efficiency of the nasal passages at removing particles. Resuspension from the tracked floor due to occupants walking and other activities is modeled as a first order process with rate constant μ_2 (s^{-1}). Deposition from the air compartment is modeled as a first-order process with rate constants (s^{-1}) of λ_{tf} (deposition to tracked floor), λ_{utf} (untracked floor), λ_w (walls), and λ_{ce} (ceiling), which can be expressed by parameters representing the indoor air flow conditions [103, 130, 207]:

$$\lambda_{tf\,(utf)} = \frac{A_{tf\,(utf)}}{V} \times \frac{V_t}{1 - e^{-\frac{\pi V_t}{2\sqrt{Dk_e}}}} \tag{2}$$

$$\lambda_w = \frac{A_w}{V} \times \frac{2}{\pi} \sqrt{Dk_e} \tag{3}$$

$$\lambda_c = \frac{A_c}{V} \times \frac{V_t}{e^{\frac{\pi V_t}{2\sqrt{Dk_e}}} - 1} \tag{4}$$

where D (m^2/s) is the particle diffusivity, k_e (s^{-1}) is turbulence intensity, and V_t (m/s) is particle settling velocity, which is given in Equation 5 as a function of the particle's diameter (d), the viscosity of air (μ_{air}), the density of the particle (ρ_p), and the density of air (ρ_{air}).

$$V_t = \frac{gd^2(\rho_p - \rho_{air})}{18\mu_{air}} \tag{5}$$

The completely mixed assumption in the fate and transport model can miss localize areas of high concentrations. However, it is still true that, assuming first order processes, the average surface concentration of the room will be proportional to the

integral of the average air concentration over time. Thus, updating can be performed on average surface concentrations, but the error in the measured concentrations needs to reflect the sampling variability of the mean. In addition, sampling may not be representative of average conditions but may focus on or accidentally omit the area in the immediate vicinity of the release. This contributes an addition element of uncertainty to the analysis that cannot be readily quantified. In most cases, we believe that sampling will be biased toward more highly concentrated areas, resulting in over estimates of the release amount and conservative (health-protective) estimates of risk.

In addition to the fate and transport model described above, a risk assessment model is included to quantify the hazard posed by inhaling *B. anthracis* spores. An exponential dose-response model (Equation 6) is selected for particle sizes less than or equal to 5μM, while a beta-Possion dose-response model is used for 10μM particles (Equation 7) based on a study by Bartrand et al. [11]:

$$Risk(dose) = 1 - e^{-kdose} \tag{6}$$

$$Risk(dose) \approx 1 - (1 + \frac{dose}{\beta})^{-\alpha} \tag{7}$$

where *Risk (dose)* is the probability of positive response (death) corresponding to a certain exposure level, *k* is the parameter of an exponential dose-response model, and α, β are parameters of a beta distribution describing variability in survival probability [71]. The dose is estimated by integrating the concentration of *B. anthracis* over the exposure time (Equation 8).

$$dose = Inh \int_{t_1}^{t_2} C_{air}(t)dt \tag{8}$$

The details of the fate and transport model, including the ranges of inputs (parameters to be updated), are provided in Table A-1 of the supporting information.

2.2.2 Spore Concentration Data

The spore concentration data used in the updating process are based on sampling of the Hart Senate Office Building after a letter containing *B. anthracis* spores was opened as one of the 2001 series anthrax attacks [198, 199]. Three rounds of air sampling were conducted including two types of sampling schemes: semiquiescent sampling and active sampling. In the semiquiescent sampling scheme, one person placed and adjusted the sampler, but no one was present in the room during the subsequent sampling period. While in the active sampling scheme, three people set up the sampler and simulated daily office activities during the sampling period. The profiles of different sampling schemes are summarized in Table 2-1. Air concentrations were measured in each sampling scheme, and the differences were attributed to levels of human-caused resuspension. Besides air concentrations, fabric office dividers' concentrations were sampled from vertical surfaces, and horizontal concentrations were sampled from the carpet, as shown in Table 2-2 [198]. However, it is likely that measurements reported in Table 2 vary from the true values due to imperfect sample recovery efficiency [21, 61, 66]. Two parameters, R_air and R_surf are introduced to represent the recovery efficiencies for air and surface samples, respectively. Prior distribution for these parameters (given in Table A-1 of Supporting Information) were based on a review of the literature [22, 23, 42, 56, 60, 61, 66, 80].

Table 2-1 Information of different modeling stages

Stage name	Stage number	Description	Simulation duration	Number of people simulated	HVAC status	Simulated parameter
Initial release and quarantine period	1	Anthrax letter open period	15 mins	10	on	
		Vaccant period	1 week 6days 23 hours and 45 minutes	0	off	
Semiquiescent sampling period	2	Sampler setup	10 mins	1	off	
		Taking samples	10 mins	0	off	C_{air_semi}
Interval between sampling period	3		12 hours	0	off	
First round active sampling period	4	Sampler setup	10 mins	3	off	
		Taking samples	10 mins	3	off	C_{air_act1}
Interval between sampling period	5		12 hours	0	off	
Second round active sampling period	6	Sampler setup	10 mins	3	off	
		Taking samples	10 mins	3	off	C_{air_act2} C_{fod_act2} C_{cap_act2}

Table 2-2 Surface sample types and concentrations

Location	Sampling period	Symbol	Concentration (CFUs/m^3)	Log concentration	Mean concentration	Mean of the log transformed concentration	Standard error of the concentration	Standard error of the log transformed concentration
Air	Semiquiescent	C_{air_semi}	14.1	2.7	7.3	1.7	6.1	1.0
			2.0	0.7				
			6.0	1.8				
Air	Active period 1	C_{air_act1}	85.6	4.5	35.2	2.8	44.2	1.6
			16.7	2.8				
			3.3	1.2				
Air	Active period 2	C_{air_act2}	49.1	3.9	41.7	3.7	12.8	0.4
			26.9	3.3				
			49.1	3.9				
Fabric office dividers	Active period 2	C_{fod_act2}	1.0	0.0	100.3	3.3	99.5	2.9
			200.0	5.3				
			100.0	4.6				
Carpet	Active period 2	C_{cap_act2}	1500.0	7.3	2200.0	7.5	1571.6	0.7
			4000.0	8.3				
			1100.0	7.0				
			4600.0	8.4				

*Simulated spore concentrations on the HVAC filter of Stage 1 (C_{HVAC}) is assumed to be log normally distributed with the mean 7.54 and standard error 0.67.

2.2.3 Modeling Approach

Based on the details obtained from Weis' paper [199] and personal communications [198], the modeling period is divided into 6 stages (Figure 2-2 and Table 2-1). The final concentration computed from each stage serves as the following stage's initial concentration. Human exposure occurred during the first hour of Stage 1. The HVAC system was shut down to prevent the dispersion of *B. anthracis* spores after the first two hours. After a nearly two-week quarantine period, a round of semi-quiescent sampling (Stage 2) was conducted followed by a settling period (Stage 3), a round of active sampling (Stage 4), another settling period (Stage 5), and a second round of active sampling period (Stage 6). In the active sampling period, the resuspended *B. anthracis* spores are modeled as being 1 micron in diameter, reflecting the observation of Weis et. al. [199] that resuspended spores were all of small diameter due to the resuspension process breaking the aggregated spores into small ones. Settling is allowed between the different sampling periods. Semiquiescent sampling is modeled by assuming 10 minutes of resuspension due to the activity of one person during sampler setup followed by 10 minutes of measurement during which no further resuspension occurs. Air concentrations used for the updating process are the average of the modeled values during the measurement phase. Active sampling is modeled by assuming 10 minutes of resuspension due to three persons' simulated daily office activities followed by 10 minutes of continued resuspension-causing activity during measurement. Again air concentrations used for the updating process are the average of the modeled values during the measurement phase.

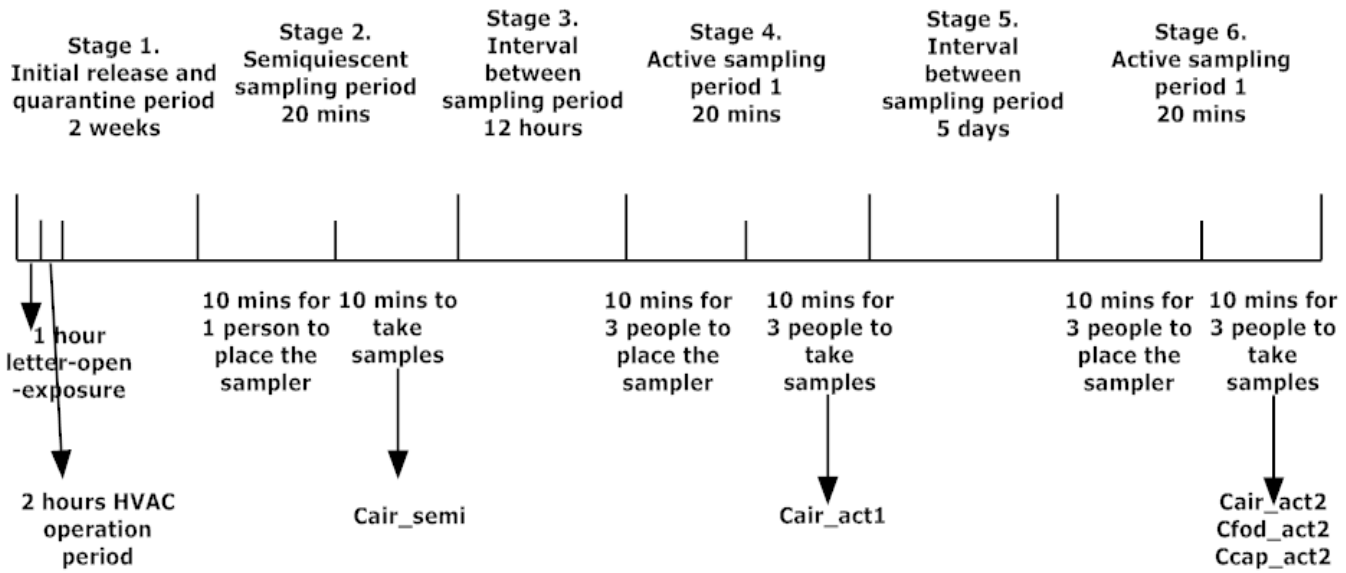

Figure 2-2 Time series of different model stages

A flow chart of the BMC updating process is shown in Figure 3. Monte Carlo simulation is used to develop a discrete distribution of model outputs using prior distributions of model parameters. Then the likelihood of each simulated output is evaluated by comparing to observations using Bayesian approach [128, 148]. Prior probability distributions are given in Table A-1. A truncated normal (log-normal) distribution is selected for parameters whose boundaries are available [139]. Correlations between inputs and the output of interest (i.e., the risk to an exposed person) are evaluated to identify the important uncertainties in input parameters. The absolute value of the input-output correlation coefficient indicates the importance of the contribution of the uncertainty in this input to the uncertainty in the output. The simulation results reported here are based on 150,000 iterations in MATLAB [114].

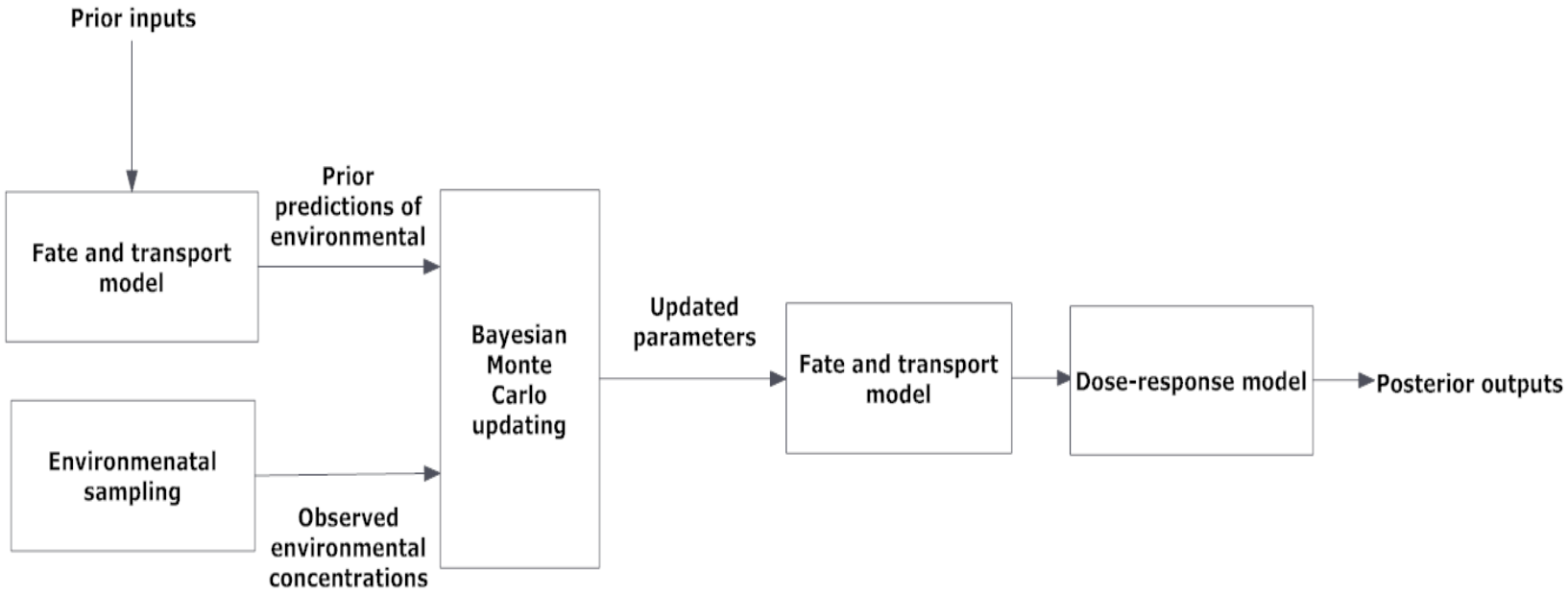

Figure 2-3 Flow chart of BMC updating

2.2.4 Bayesian updating

The posterior probability $P(\vec{\theta}\left|\overrightarrow{C_{\text{media}}}'\right)$ of modeled parameters is acquired by updating the parameters of the fate and transport model with the measured *B. anthracis* spore concentrations adjusted for recovery efficiency:

$$P(\vec{\theta}\left|\overrightarrow{C_{media}}'\right)=\frac{L_{overall}(\overrightarrow{C_{media}}'\left|\vec{\theta},\overrightarrow{C_{pred}}\right)\times P(\vec{\theta})}{\int_{\vec{\theta}} L_{overall}(\overrightarrow{C_{media}}'\left|\vec{\theta},\overrightarrow{C_{pred}}\right)\times P(\vec{\theta})\,d\vec{\theta}} \tag{9}$$

where P($\vec{\theta}$) is the joint prior probability of the model parameters, $\overrightarrow{C_{\text{media}}}'$ is the mean measurement adjusted for recovery which equals sampling results ($\overrightarrow{C_{media}}$) divided by the associated sample recovery efficiency (R_air or R_surf), and $\overrightarrow{C_{pred}}$ represents concentrations predicted by the fate and transport model as a function of model parameters $\vec{\theta}$. $L_{overall}(\overrightarrow{C_{media}}'\left|\vec{\theta},\overrightarrow{C_{pred}}\right)$ is the likelihood of obtaining a set of adjusted concentration observations ($\overrightarrow{C_{\text{media}}}'$) given model predictions ($\overrightarrow{C_{pred}}$), which are conditional on model parameters $\vec{\theta}$. The likelihood is the joint probability of acquiring the observed mean *B. anthracis* concentrations from the 5 types of samples (Table 2-2). Thus the likelihood can be rewritten as a function of the t-distribution:

$$L_{overall}(\overrightarrow{C_{media}}'\left|\vec{\theta},\overrightarrow{C_{pred}}\right)=\prod_{\substack{media=\text{air\_semi},\\ \text{air\_act1, air\_act2,}\\ \text{fod\_act2, cap\_act2}}} L(\overline{C}_{media}'\left|\vec{\theta},\overline{C}_{pred}\right)=\prod_{\substack{media=\text{air\_semi},\\ \text{air\_act1, air\_act2,}\\ \text{fod\_act2, cap\_act2}}} \frac{\Gamma(\frac{\nu_{media}+1}{2})}{\sqrt{\nu_{media}}\pi\Gamma(\frac{\nu_{media}}{2})}(1+\frac{t_{media}^{\,2}}{\nu})^{-(\frac{\nu_{media}+1}{2})} \tag{10}$$

where subscript media indexes the types of samples: samples are taken from the carpet, fabric office dividers, semi-quiescent air, active air sampling period 1, and active air

sampling period 2. ν_{media} is the number of degrees of freedom of the estimated mean of a particular observation, Γ is the Gamma function, and t_{media} is computed as:

$$t_{media} = \frac{\overline{C}_{media}' - \overline{C}_{pred}}{S_{C_{media}} / \sqrt{n}} \quad (11)$$

Usually differences between measurements and model predictions are assumed to follow a normal distribution with a mean of zero [18, 148, 172], but the normal distribution is replaced by a student's t distribution in this study, since the true standard deviation of the sampled values (measurements) is unavailable and only an estimated standard deviation ($S_{C_{media},media}$) is available. Concentration values are log transformed to reflect the standard assumption in environmental engineering of multiple dilutions yielding a log normal distribution [139].

2.2.5 Modeling Scenarios

The fractions of released *B. anthracis* in the letter opened in 2001 were analyzed by Battelle Memorial Institute, and the percentages of released spores with diameter 1 μm, 3 μm, 5 μm, and 10 μm were found to be 0.14%, 1.46%, 8.40%, and 90%, which are used as constants during the updating [102]. In addition to updating with the data available from the Weis study [199] (Scenario 1), hypothetical scenarios are created to explore what could be learned if different information were available (Table 2-3). Scenario 2 tests how the outcomes of BMC updating would be changed if 100% sample recovery efficiency is assumed. Thus, Scenario 2 inherits most of the prior information

from Scenario 1 except that two sample recovery efficiencies (R_air, R_surf) are set as 1. Scenario 3 evaluates how the performance of BMC updating would change if reaerosolization sampling is not conducted. In this scenario only concentrations sampled from fabric office dividers and carpet are used in the updating, and the air concentration information is ignored. Scenario 4 is designed to test whether or not the performance of the Bayesian updating approach could be enhanced if additional samples had been taken (it is assumed that these additional samples yielded similar results to the existing samples). The sample mean remains unchanged from Scenario 1, but the standard errors of the measurements are reduced by 50%, which roughly corresponds to the availability of 4 times more data. Scenario 5 examines how incorporating information from an additional sampling location, the HVAC system filter, affects the updating results (additional simulated data on the HVAC filter mean concentration and standard deviation are used in the updating process).

Table 2-3 Summary of updating scenarios

Symbol	Scenario	Feature
0	Prior	Monte Carlo Simulation based on prior information.
1	Scenario 1	BMC updating with default settings.
2	Scenario 2	BMC updating similar to Scenario 1 except 100% sample recovery efficiency is given.
3	Scenario 3	BMC updating without observations from reaerosolization.
4	Scenario 4	BMC updating with 50% less standard errors of the observations.
5	Scenario 5	BMC updating with simulated observations from HVAC.

2.3 Results and Discussion

Figures 2-4, 2-5, S1, and S2 summarize the probability distributions before and after Bayesian updating from different scenarios for 19 parameters. Uncertainties in the risk to the occupants via inhalation during the first hour of the release (i.e. before the room was evacuated), the total release quantity (successfully aerosolized), and the amount of spores that exit the room are substantially reduced by updating with the available data (Scenario 1). While the 5^{th} to 95^{th} percentile range for the estimated risk before BMC updating extends over roughly 5 orders of magnitude (9.35×10^{-6} to 1), the posterior range is around 1 order of magnitude (4.70×10^{-3} to 2.15×10^{-2}). Similarly, the 5^{th} to 95^{th} percentile range for the release quantity prior to the BMC updating extends over roughly 9 orders of magnitude (1.06×10^{4} to 1.01×10^{12}), but the posterior range is reduced to 1 order of magnitude (5.20×10^{6} to 2.40×10^{7}). The estimate of the amount of spores exiting the room ranges over roughly an order of magnitude from 1.34×10^{6} to 4.39×10^{7} (Table A-2).

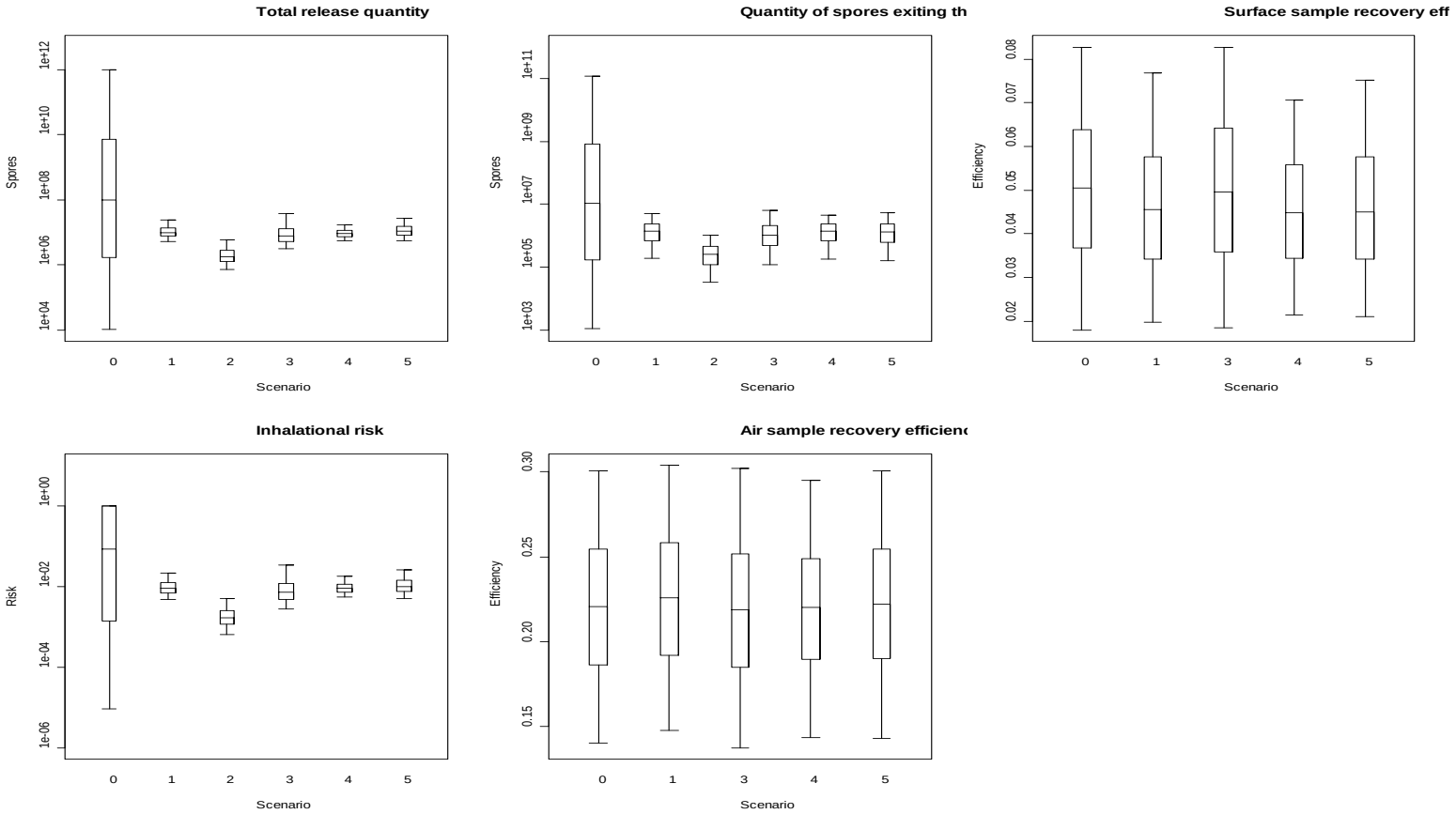

Figure 2-4 Prior and posterior CDF for the total released quantity, risk of exposed people, and the quantity of spores exit the room.
(The bottom and top of the box are 25th and 75th percentile, the band inside the box is the 50th percentile, and the upper and lower whiskers represent the 5th and 95th percentile, respectively. The number 1 to 5 represent BMC updating scenarios, while 0 represents the prior scenario.)

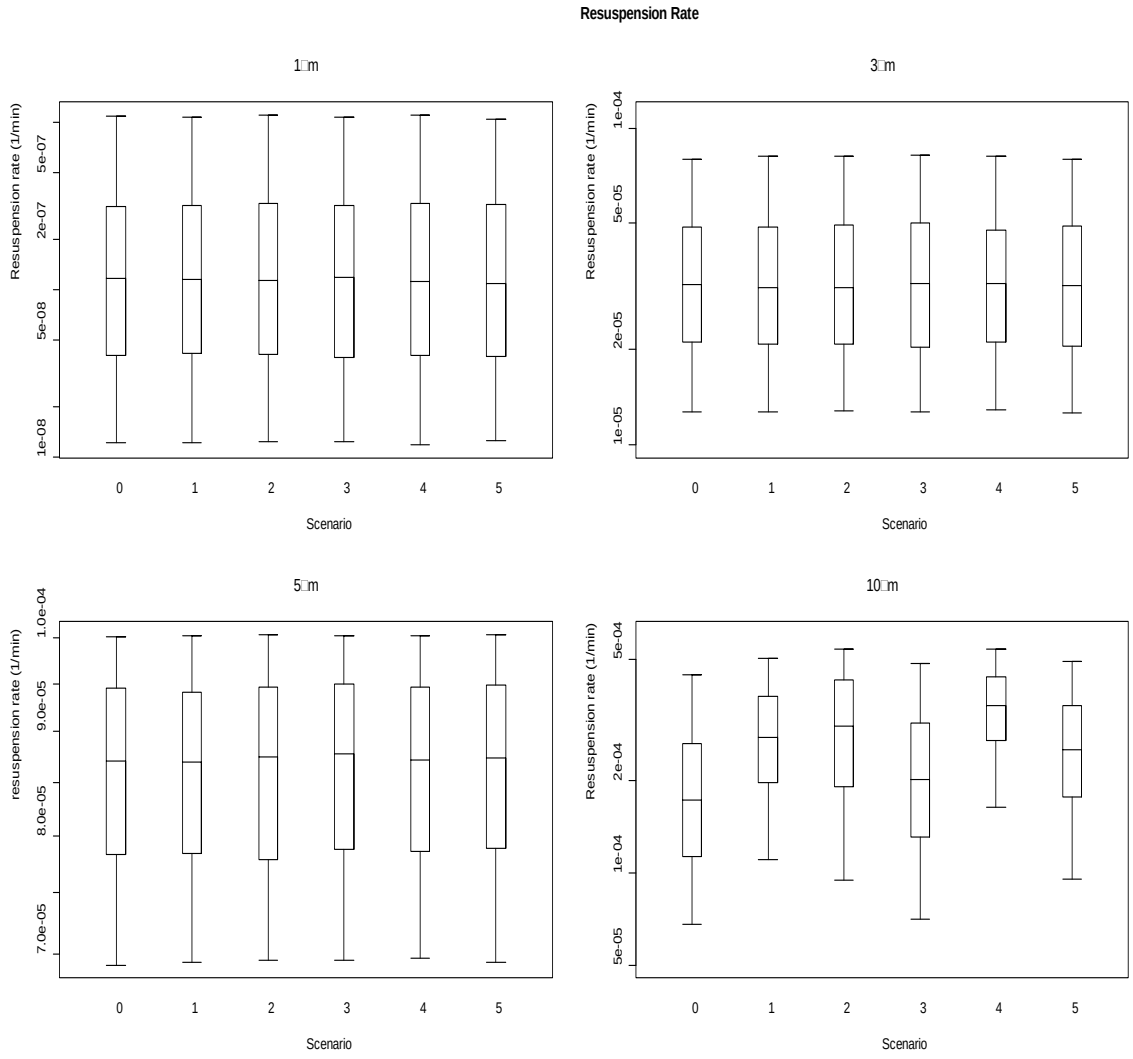

Figure 2-5 Prior and posterior CDF for the resuspension rate

(The bottom and top of the box are 25th and 75th percentile, the band inside the box is the 50th percentile, and the upper and lower whiskers represent the 5th and 95th percentile, respectively. The number 1 to 5 represent BMC updating scenarios, while 0 represents the prior scenario.)

Figure 2-5 shows the uncertainty bounds for resuspension rates are not greatly changed by the updating process. Only the resuspension rate for spores with a diameter of 10 micron is affected, and even this parameter is changed only modestly (the prior mean value of 2.02×10^{-4} shifts to a posterior mean of 2.90×10^{-4}). In general, uncertainties in other fate and transport model parameters as well as the sample recovery efficiencies are not substantially reduced by the updating process (see Supporting Information for details). While the data cannot be used to improve estimates of parameters describing the fate and transport of weaponized *B. anthracis*, the updating process does indicate that there is not a demonstrable conflict between the parameter estimates obtained from surrogates, such as house dust, and the observed behavior of *B. anthracis* spores.

The only difference between Scenarios 1 and 2 is the sample recovery efficiency, where the later one assumes that all the sampled *B. anthracis* are correctly measured, indicating that samples taken from the air and surface are unbiased. As a result, parameters like the total release quantity, risk and the amount exiting the room from Scenario 2 are lower than those from other scenarios, because one believes the sampling results represent the true deposited quantity. Scenario 3 (without reaerosolization sampling) has only modestly larger credible bounds for release quantity, risk and amount exiting the room across all the five BMC updating scenarios. This suggests that simple surface concentration measurements do almost as good a job of characterizing an attack as a more involved procedure that involves resuspension and air sampling. Due to the exclusion of air sampling, posterior distributions for spore's resuspension rate and air sample recovery efficiency are not successfully updated.

Comparing to Scenario 1, Scenario 4 quadruples the number of observations, which greatly reduces uncertainty in the release amount (90% CI: 5.64×10^{6} to 1.75×10^{7}) and in the risk estimates (90% CI: 5.50×10^{-3} to 1.80×10^{-2}), although little improvement is obtained for the estimate of the amount of spores exiting the room. The additional data does not improve the estimates of resuspension rate for all particle sizes, but the distribution of the resuspension rate of the 10 μm particles is shifted to somewhat higher values and has the smallest uncertainty bound. The 10 μm particles account for the majority of the release on a mass basis. Hence it is easiest to identify parameters for this size fraction. The posterior estimates for density and settling velocity of released particles also decrease; the latter one is a function of the former one (Equation 5), suggesting that increasing the number of samples can better identify particles' aerodynamic properties. Obtaining concentration information on the HVAC filter (Scenario 5) did not substantially reduce the uncertainty in parameter estimates in comparison to Scenario 1, except for the fraction of recirculated air (see Figure A-1 in Supporting Information).

Comparing across the default scenario and four additional scenarios, one finds that 1) having additional samples (N=12 from each surface in Scenario 3 rather than N=3 from Scenario 1) can greatly improve characterization of the release; 2) assuming a 100% sample recovery efficiency (Scenario 2) would lead one to underestimate the extent of a release; 3) the characterization is not greatly improved by measuring the concentration on the HVAC filter; 4) the samples taken from reaerosolization do not appear to greatly aid characterization of the release; and 5) the updating process does not greatly improve

estimates of fate and transport parameters, but in general parameters based on surrogates such as hose dust are not in conflict with the observed behavior of *B. anthracis* spores.

Table2-4 shows Spearman's rank correlations between parameter values and the output of interest, risk, via inhalation during the first hour of Stage 1. Correlations are shown for the prior distribution of parameter input values and the posterior values from different scenarios. When the updating process reduces a correlation coefficient, this input's uncertainty has been successfully reduced and the remaining uncertainty is less important. While the correlation coefficient increases, this indicates that because the uncertainties in other inputs have been reduced, the uncertainty in this input is now relatively more important [148]. In Table 2-4, a significantly increased correlation is found for the resuspension rate of 10 micron spores, particle density and the two sample recovery efficiencies (except Scenario 2 with 100% sample recovery), while the correlation for mass released decreases from its prior value. The mass of released spores constitutes the major prior uncertainty, but this uncertainty can be updated with considerable success (resulting in a lower posterior correlation coefficient). In fact, if a larger sample size were available (Scenario 4), the mass released would no longer be the dominant source of uncertainty. As more information is obtained on mass released (Scenario 4), learning more about fate and transport parameters, such as the reaerosolization rates, and particle settling velocity, becomes relatively more important. Unfortunately, these parameters were not readily updated through this process.

Table 2-4 Spearman's rank correlation between risk and inputs

Parameter	Meaning	Diameter (μm)	Prior	Posterior				
				Scenario 1	Scenario 2	Scenario 3	Scenario 4	Scenario 5
μ_2	Resuspension rate	1	5.70×10^{-3}	1.10×10^{-3}	4.30×10^{-3}	-1.03×10^{-2}	1.01×10^{-2}	2.01×10^{-2}
		3	-7.60×10^{-3}	1.75×10^{-2}	-1.19×10^{-4}	-8.30×10^{-3}	1.38×10^{-2}	6.10×10^{-3}
		5	-2.80×10^{-3}	-2.80×10^{-3}	-2.10×10^{-3}	-1.48×10^{-2}	1.31×10^{-2}	2.04×10^{-2}
		10	-6.40×10^{-3}	**-6.38×10^{-1}**	**-8.16×10^{-1}**	6.34×10^{-2}	**-6.55×10^{-1}**	**-6.86×10^{-1}**
P	The fraction of recirculated air		-6.03×10^{-4}	3.30×10^{-2}	3.52×10^{-2}	4.09×10^{-2}	5.53×10^{-2}	1.33×10^{-2}
Vt (ρ_p)	Particle settling velocity (Density)		-1.99×10^{-2}	*-3.50×10^{-1}*	*-1.63×10^{-1}*	*-2.75×10^{-1}*	*-4.35×10^{-1}*	*-3.56×10^{-1}*
Ke	Turbulence intensity of the exposure stage		-5.03×10^{-4}	4.15×10^{-2}	2.93×10^{-2}	2.20×10^{-2}	4.42×10^{-2}	1.53×10^{-2}
ACH	Air change rate		-2.94×10^{-2}	-9.52×10^{-2}	-5.27×10^{-2}	-3.28×10^{-2}	-1.04×10^{-1}	-5.24×10^{-2}
R_air	Air sample recovery efficiency		1.60×10^{-3}	*-2.69×10^{-1}*	NA	NA	-3.70×10^{-1}	*-2.80×10^{-1}*
R_surf	Surface sample recovery efficiency		1.60×10^{-3}	*-4.56×10^{-1}*	NA	**-6.00×10^{-1}**	**-7.18×10^{-1}**	*-4.10×10^{-1}*
Mass_t	Total release quantity		**9.99×10^{-1}**	**8.93×10^{-1}**	**9.37×10^{-1}**	**9.54×10^{-1}**	**8.27×10^{-1}**	**9.07×10^{-1}**

Moderate and strong correlation coefficients (value greater than 0.5) are present in bold, while weak ones (between 0.1 and 0.5) are shown in Italic.

Correlations from Table 2-4 are only based on a bivariate analysis. Complex multivariate relationships may exist in which the value of knowing one parameter is dependent on the amount of uncertainty in other variables. For example, in Scenario 5 information on the HVAC filter concentration was observed to provide little reduction in uncertainty. However, an exploratory analysis revealed that when the HVAC filter concentration was known, the fraction of recirculated air became closely correlated with risk. Thus, HVAC filter concentration was of little use on its own, but when coupled with knowledge of the air circulated through the filter, it became valuable in characterizing the release. To identity these types of multivariate relationships, regression analyses were conducted in which risk estimated by the model was regressed on model input values for the amount of spores measured from three different surfaces (i.e., carpet, fabric office dividers, and the HVAC filter), and 3 particulate fate and transport parameters (i.e., the HVAC air change rate, the HVAC air recirculation rate, and the density of weaponized *B. anthracis*).

Table 2-5 presents the regression models with the highest coefficient of determinations (R^2) for different number of regressors when the particulate size fractions of released *B. anthracis* are fixed at values observed in the 2001 attacks [102]. Results indicate that the amount of spores measured from the untracked floor provides the most information on the risk, if only one parameter can be measured. The second, third, and fourth parameters to enter the regression are not spore concentrations but rather are particulate and building air circulation parameters: particle density, air exchange rate, and the HVAC air recirculation rate. Note that in Regression 4, HVAC filter replaces

untracked floor as the most informative sampling location. This supports the observation during the exploratory analysis that HVAC filter becomes more informative as air circulation parameters are better specified. The amount of spores measured on the wall is the last parameter entering the regression. Table 2-6 shows the best regression models when the fractions of released spores are treated as random variables, reflecting a situation in which the size fractions of released *B. anthracis* spores are not known. This reflects the situation when a sample of the released agent cannot be recovered in sufficient quantity to allow its size distribution to be identified. In this case spores concentrations on the HVAC filter enter the regression first, indicating it is a good sample location. The remaining variables to enter are air recirculation fraction, air change rate, particle density, untracked floor, and walls. As with the previous case, characterizing the particulate and air circulation may be as important as charactering spore concentrations.

Table 2-5 Models with highest coefficient of determinations (R^2) for different numbers of regressores and size fractions based on pre-BMC data

Model Number	Function	Parameter	Coefficients	Std. Error	Residual Standard Deviation	R^2
1	Risk~f(Untracked floor)+Const.	Untracked floor	1.70×10^{-3}	1.15×10^{-5}	1.53×10^{-5}	7.54×10^{-1}
		Const.	-1.89×10^{-2}	1.46×10^{-4}		
2	Risk~f(Untracked floor, Particle density)+Const.	Untracked floor	1.70×10^{-3}	1.12×10^{-5}	1.48×10^{-5}	7.69×10^{-1}
		Particle density	-1.30×10^{-3}	5.86×10^{-5}		
		Const.	-9.60×10^{-3}	4.51×10^{-4}		
3	Risk~f(Untracked floor, Air change rate, Particle density)+Const.	Untracked floor	1.70×10^{-3}	1.12×10^{-5}	1.48×10^{-5}	7.70×10^{-1}
		Air change rate	-1.03×10^{-4}	2.49×10^{-5}		
		Particle density	-1.30×10^{-3}	5.86×10^{-5}		
		Const.	-9.60×10^{-3}	4.51×10^{-4}		
4	Risk~f(HVAC filter, Air change rate, Air recirculation fraction, Particle density)+Const.	HVAC filter	1.70×10^{-3}	1.12×10^{-5}	1.48×10^{-5}	7.71×10^{-1}
		Air change rate	-1.80×10^{-3}	2.73×10^{-5}		
		Air recirculation fraction	-1.70×10^{-3}	2.29×10^{-5}		
		Particle density	3.72×10^{-4}	5.83×10^{-5}		
		Const.	-2.16×10^{-2}	4.72×10^{-4}		
5	Risk~f(HVAC filter, Untracked floor, Air change rate, Air recirculation fraction, Particle density)+Const.	HVAC filter	9.50×10^{-3}	1.09×10^{-3}	1.47×10^{-5}	7.72×10^{-1}
		Untracked floor	-7.80×10^{-3}	1.10×10^{-3}		
		Air change rate	-9.40×10^{-3}	1.07×10^{-3}		
		Air recirculation fraction	-9.50×10^{-3}	1.10×10^{-3}		
		Particle density	7.80×10^{-3}	1.04×10^{-3}		
		Const.	-7.55×10^{-2}	7.60×10^{-3}		
6	Risk~f(HVAC filter, Untracked floor, Walls, Air change rate, Air recirculation fraction, Particle density)+Const.	HVAC filter	9.90×10^{-3}	1.30×10^{-3}	1.47×10^{-5}	7.72×10^{-1}
		Untracked floor	-8.20×10^{-3}	1.40×10^{-3}		
		Walls	3.04×10^{-5}	6.15×10^{-5}		
		Air change rate	-9.80×10^{-3}	1.30×10^{-3}		
		Air recirculation fraction	-9.90×10^{-3}	1.33×10^{-3}		
		Particle density	8.10×10^{-3}	1.28×10^{-3}		
		Const.	-7.80×10^{-2}	9.10×10^{-3}		

a. All the values are log-transformed before linear regression.
b. Parameters HVAC filter, Untracked floor, and Walls refer the amount of *B. anthracis* measured from those surfaces
c. Mean prediction is -6.76

Table 2-6 Models with highest coefficient of determinations (R^2) for different numbers of regressors and unknown size fractions based on pre-BMC data

Model Number	Function	Parameter	Coefficients	Std. Error	Residual Standard Deviation	R^2
7	Risk~f(HVAC filter)+Const.	HVAC filter	8.70×10^{-4}	5.13×10^{-5}	9.26×10^{-5}	3.05×10^{-1}
		Const.	-6.00×10^{-3}	6.09×10^{-4}		
8	Risk~f(HVAC filter, Air recirculation fraction)+Const.	HVAC filter	1.10×10^{-3}	5.56×10^{-5}	8.78×10^{-5}	3.77×10^{-1}
		Air recirculation fraction	-1.10×10^{-3}	1.29×10^{-4}		
		Const.	-9.70×10^{-3}	7.21×10^{-4}		
9	Risk~f(HVAC filter, Air change rate, Air recirculation fraction)+Const.	HVAC filter	1.30×10^{-3}	5.78×10^{-5}	8.50×10^{-5}	4.19×10^{-1}
		Air change rate	-1.10×10^{-3}	1.62×10^{-4}		
		Air recirculation fraction	-1.20×10^{-3}	1.25×10^{-4}		
		Const.	-1.11×10^{-2}	7.26×10^{-4}		
10	Risk~f(HVAC filter, Air change rate, Air recirculation fraction, Particle density)+Const.	HVAC filter	1.30×10^{-3}	5.76×10^{-5}	8.50×10^{-5}	4.22×10^{-1}
		Air change rate	-1.10×10^{-3}	1.62×10^{-4}		
		Air recirculation fraction	-1.20×10^{-3}	1.25×10^{-4}		
		Particle density	5.96×10^{-4}	3.28×10^{-4}		
		Const.	-1.57×10^{-2}	2.60×10^{-3}		
11	Risk~f(HVAC filter, Untracked floor, Air change rate, Air recirculation fraction, Particle density)+Const.	HVAC filter	1.30×10^{-3}	5.79×10^{-5}	8.50×10^{-5}	4.22×10^{-1}
		Untracked floor	-5.57×10^{-6}	8.81×10^{-6}		
		Air change rate	-1.10×10^{-3}	1.62×10^{-4}		
		Air recirculation fraction	-1.20×10^{-3}	1.25×10^{-4}		
		Particle density	4.85×10^{-4}	3.71×10^{-4}		
		Const.	-1.47×10^{-2}	3.00×10^{-3}		
12	Risk~f(HVAC filter, Untracked floor, Walls, Air change rate, Air recirculation fraction, Particle density)+Const.	HVAC filter	1.30×10^{-3}	5.79×10^{-5}	8.50×10^{-5}	4.23×10^{-1}
		Untracked floor	-2.69×10^{-4}	3.13×10^{-4}		
		Walls	-2.64×10^{-4}	3.14×10^{-4}		
		Air change rate	-1.10×10^{-3}	1.62×10^{-4}		
		Air recirculation fraction	-1.20×10^{-3}	1.25×10^{-4}		
		Particle density	7.36×10^{-4}	4.76×10^{-4}		
		Const.	-1.61×10^{-2}	3.40×10^{-3}		

a. All the values are log-transformed before linear regression.
b. Parameters HVAC filter, Untracked floor, and Walls refer the amount of *B. anthracis* measured from those surfaces
c. Mean prediction is -5.74.

It is notable that when the size fractions of released spores are provided (Table 2-5), the regression model can generate more reliable risk prediction (lower residual standard deviation) than the situation where size fraction is unknown (Table 2-6). In fact, when the size distribution is known, accurate knowledge of average concentrations on even a single surface provides sufficient information such that further characterization of the transport parameters of the room reduces the residual standard deviation only a little (from 1.53×10^{-5} in Regression 1 to 1.47×10^{-5} in Regression 6). In contrast, when the size distribution is not known, having more information becomes more important in characterizing the human risk (R^2 from 9.26×10^{-5} in Regression 7 to 8.50×10^{-5} in Regression 12). Even when all 6 parameters are measured accurately there is still more uncertainty than when only floor concentration is measured and the size distribution is known (i.e., the residual standard deviation is higher for Regression 12 than for Regression 1).

Based on the posterior risk estimates calculated here for the people in the building, the decision to provide prophylactic antibiotic treatment in the 2001 anthrax letter attacks is justified [36, 121]. The best estimate for risk to occupants of the room where the spores were released is roughly 1 in 100 (based on Scenario 1). Costs and side effects of antibiotic treatment are modest and may be justified for exposures much lower than this. For example the analysis of Mitchell-Blackwood et al. suggests that benefits would exceed costs for risk levels exceeding 1 in 6,547 [121].

The model also provides an estimate of the number of spores leaving the room. It is complex and difficult to predict the fate and transport of *B. anthracis* spores in the outdoor environment since a significant amount of uncertainties can be found from many factors, such as the weather, surrounding topography, etc. To roughly assess the scale of possible impacts, extrapolations are conducted based on a previous assessment carried out by the World Health Organization (WHO) in 1970, and a recent investigation carried by Wein and Craft on the human health adverse impacts from an outdoor release of *B. anthracis* spores [94, 197]. The WHO's report estimated that the number of casualties would be around 25, 000, if 50 kg of *B. anthracis* spores were released by aircraft over an area with a population of 5 million, corresponding to an expected mortality of 5×10^{-12} per spore released [94]. This rate is then computed as the ratio between the number deaths divided by the amount of total released spores. Wein et. al. indicated that if the released amount of *B. anthracis* spores were reduced to 1 kg with 50% dissemination efficiency over a large U.S. city with 1.39 million people, the most conservative mortality is linked to the people who only receive post- attack antibiotic, which could as much as 146,269, corresponding to mortality rate of 1.5×10^{-9} per spore released [197]. In our study, around 10^{7} spores (10^{-8} kg) are estimate as exiting the release location. If such amount of spores were dispersed in the settings of WHO's study, the expected mortality would be around the level of 10^{-5}, while if such a release happed in the scenarios of Wein's study, a mortality of 1.5×10^{-2} would be expected. The previous two extrapolations are made under ideal situations, and these results should be further analyzed in the future. The WHO-based figure would suggest expected mortality was minimal. The figure based on the study of Wein and Craft would suggest that there was a non-negligible risk of infection outside the room. Since much of the risk would be contained within the building this supports the decision to

widely administer prophylactic antibiotics to occupants of the building even if they were not in the room where the release occurred. Whether risk outside the building could reach actionable thresholds is not clear from this analysis, but it does suggest that in the event of a future release, site-specific modeling would be justified to identify any potentially problematic exposures outside the building.

This paper presents an application of the BMC method in updating uncertainty for an integrated fate, transport, and risk assessment model. While substantive reductions in the uncertainties of model fate and transport parameters were not achieved by the BMC updating process, neither did the data exclude the parameter estimates obtained from literature information on surrogates for *B. anthracis*. Four hypothetical scenarios were included to test the performance of the BMC updating given different types of data. Results suggest that a larger sample size would help to reduce input uncertainties, that assuming a perfect sample recovery would cause risk underestimation, and that measurements from the HVAC filter and air after resuspension activities did not greatly improve model posterior estimates, unless a variety of other parameters can also be measured. In addition, multivariate regressions based on different types of data indicate that measurements of different surface concentrations and particulate and air circulation parameters are necessary when the particulate size distribution is unknown. When the size distribution is known then measuring a single surface provides most of the information on the release quantity. This study provides a general framework for applying the Bayesian Monte Carlo approach to characterize a biological attack. In the future, the Bayesian approach can be applied to other phases of the response management framework, such as guidance on remediation of contaminated buildings [111]. To make

the approach more readily applicable, the MATLAB code developed here could be programmed into a software package to perform the updating which would enable the approach to be employed after an incident by individuals without specialized computer knowledge. In addition, the speed of BMC updating could be improved by conducting most of the computations using a parallel computing approach, such as using a GPU instead of a CPU [137].

2.4 Appendix A

Table A-1. Model Inputs

Parameter	Unit	Meaning	Diameter	Distribution	Mean	Standard deviation	Boundary
Mass_t	spores	Total release quantity		Truncated log-normal	8	2.41	$[3.0\text{-}1.3\times10^{1}]$
R_air		Air sample recovery efficiency			0.22	0.05	[0.0-1.0]
R_surf		Surface sample recovery efficiency		Truncated normal	0.05	0.02	[0.0-1.0]
ρ_p	g/cm^3	Particle density			1000	607	$[1.0\times10^{3}\text{-}3.0\times10^{3}]$
ACH		Air change rate			1.55	0.88	$[1.0\times10^{-1}\text{-}3.0]$
P		The fraction of recirculated air			0.50	0.3	[0.0-1.0]
Ke		Turbulence intensity of exposure stage			0.23	0.14	$[1.0\times10^{-5}\text{-}4.5\times10^{-1}]$
Ke1		Turbulence intensity of stage i		Truncated normal	0.34	0.07	$[2.3\times10^{-1}\text{-}4.5\times10^{-1}]$
Ke2					0.12		$[1.0\times10^{-5}\text{-}2.3\times10^{-1}]$
Ke3,5					0.12		$[1.0\times10^{-5}\text{-}2.3\times10^{-1}]$
Ke4,6					0.34		$[2.3\times10^{-1}\text{-}4.5\times10^{-1}]$
μ_2	m/min	Resuspension rate	1	Truncated log-normal	-11.90	1.71	$[-1.5\times10^{1}\text{- }-9.0]$
			3		-6.25	0.70	[-7.4- -5.1]
			5		-4.98	0.33	[-5.5- -4.4]
			10		-4.57	0.72	[-5.8- -3.4]
e_n		Efficiency of the nasal passages at removing particles	1	Truncated normal	0.14	0.07	$[2.0\times10^{-2}\text{-}2.5\times10^{-1}]$
			3		0.45	0.14	$[2.2\times10^{-1}\text{-}6.8\times10^{-1}]$
			5		0.62	0.12	$[4.2\times10^{-1}\text{-}8.1\times10^{-1}]$
			10		0.77	0.09	$[6.2\times10^{-1}\text{-}9.1\times10^{-1}]$
Mass_f		Size fraction of released spores	1	Constant	0.14%	NA	NA
			3		1.46%		
			5		8.40%		
			10		90%		

Table A-2 Prior and posterior distributions for model inputs

Parameter	Meaning	Prior Mean Mean (90% CI)	Posterior Mean (90% CI)				
			Scenario 1 Mean (90% CI)	Scenario 2 Mean (90% CI)	Scenario 3 Mean (90% CI)	Scenario 4 Mean (90% CI)	Scenario 5 Mean (90% CI)
Risk	Inhalational risk	3.85×10^{-1} (9.35×10^{-6}-1)	1.05×10^{-2} (4.70×10^{-3}-2.15×10^{-2})	2.10×10^{-3} (6.40×10^{-4}-4.90×10^{-3})	1.34×10^{-2} (2.70×10^{-3}-3.42×10^{-2})	1.00×10^{-2} (5.50×10^{-3}-1.80×10^{-2})	1.19×10^{-2} (5.00×10^{-3}-2.53×10^{-2})
Mass_t	Total release quantity	2.12×10^{11} (1.06×10^{4}-1.01×10^{12})	1.16×10^{7} (5.20×10^{6}-2.40×10^{7})	2.28×10^{6} (7.02×10^{5}-5.87×10^{6})	2.03×10^{7} (3.15×10^{6}-3.77×10^{7})	1.02×10^{7} (5.64×10^{6}-1.75×10^{7})	1.29×10^{7} (5.53×10^{6}-2.69×10^{7})
R_air	Air sample recovery efficiency	2.20×10^{-1} (1.39×10^{-1}-3.02×10^{-1})	2.26×10^{-1} (1.48×10^{-1}-3.04×10^{-1})	NA	2.19×10^{-1} (1.37×10^{-1}-3.02×10^{-1})	2.19×10^{-1} (1.43×10^{-1}-2.95×10^{-1})	2.22×10^{-1} (1.43×10^{-1}-3.00×10^{-1})
R_surf	Surface sample recovery efficiency	5.03×10^{-2} (1.82×10^{-2}-8.26×10^{-2})	4.64×10^{-2} (1.97×10^{-2}-7.68×10^{-2})	NA	5.00×10^{-2} (1.85×10^{-2}-8.28×10^{-2})	4.53×10^{-2} (2.15×10^{-2}-7.07×10^{-2})	4.63×10^{-2} (2.11×10^{-2}-7.51×10^{-2})
ρ_p	Particle density	2.00×10^{3} (1.20×10^{3}- 2.79×10^{3})	1.87×10^{3} (1.12×10^{3}-2.69×10^{3})	1.86×10^{3} (1.14×10^{3}-2.70×10^{3})	1.94×10^{3} (1.15×10^{3}-2.77×10^{3})	1.58×10^{3} (1.04×10^{3}-2.44×10^{3})	1.84×10^{3} (1.11×10^{3}-2.72×10^{3})
ACH	Air change rate	1.55 (3.94×10^{-1}- 2.70)	1.55 (4.32×10^{-1}-2.71)	1.57 (4.25×10^{-1}-2.71)	1.54 (3.69×10^{-1}-2.70)	1.54 (3.76×10^{-1}-2.65)	1.51 (3.81×10^{-1}-2.68)
P	The fraction of recirculated air	5.03×10^{-1} (1.05×10^{-1}-8.99×10^{-1})	5.06×10^{-1} (1.14×10^{-1}-8.99×10^{-1})	5.01×10^{-1} (9.35×10^{-2}-9.00×10^{-1})	5.10×10^{-1} (1.13×10^{-2}-8.88×10^{-1})	5.21×10^{-1} (1.03×10^{-1}-9.14×10^{-1})	5.49×10^{-1} (1.65×10^{-1}-9.12×10^{-1})
Ke	Turbulence intensity of exposure stage	2.28×10^{-1} (4.61×10^{-2}-4.10×10^{-1})	2.42×10^{-1} (5.99×10^{-2}-4.10×10^{-1})	2.39×10^{-1} (5.56×10^{-2}-4.15×10^{-1})	2.42×10^{-1} (6.11×10^{-2}-4.14×10^{-1})	2.66×10^{-1} (8.40×10^{-2}-4.20×10^{-1})	2.39×10^{-1} (5.61×10^{-2}-4.14×10^{-1})
Ke1	Turbulence intensity of stage i	3.40×10^{-1} (2.51×10^{-1}-4.29×10^{-1})	3.41×10^{-1} (2.50×10^{-1}-4.30×10^{-1})	3.40×10^{-1} (2.52×10^{-1}-4.29×10^{-1})	3.42×10^{-1} (2.51×10^{-1}-4.30×10^{-1})	3.39×10^{-1} (2.51×10^{-1}-4.26×10^{-1})	3.41×10^{-1} (2.51×10^{-1}-4.30×10^{-1})
Ke2		1.18×10^{-1} (2.60×10^{-2}-2.08×10^{-1})	1.18×10^{-1} (2.55×10^{-2}-2.10×10^{-1})	1.19×10^{-1} (2.42×10^{-2}-2.09×10^{-1})	1.17×10^{-1} (2.53×10^{-2}-2.09×10^{-1})	1.18×10^{-1} (2.24×10^{-2}-2.09×10^{-1})	1.19×10^{-1} (2.63×10^{-2}-4.28×10^{-1})
Ke3,5		1.18×10^{-1} (2.49×10^{-2}-2.08×10^{-1})	1.24×10^{-1} (3.25×10^{-2}-2.11×10^{-1})	1.22×10^{-1} (3.04×10^{-2}-2.11×10^{-1})	1.22×10^{-1} (2.99×10^{-2}-2.10×10^{-1})	1.36×10^{-1} (4.58×10^{-2}-2.16×10^{-1})	1.24×10^{-1} (3.23×10^{-2}-2.10×10^{-1})
Ke4,6		3.41×10^{-1} (2.52×10^{-1}-4.30×10^{-1})	3.39×10^{-1} (2.52×10^{-1}-4.30×10^{-1})	3.40×10^{-1} (2.52×10^{-1}-4.28×10^{-1})	3.39×10^{-1} (2.51×10^{-1}-4.27×10^{-1})	3.40×10^{-1} (2.52×10^{-1}-4.30×10^{-1})	3.40×10^{-1} (2.53×10^{-1}-4.29×10^{-1})
Vt (m/s)	Particle settling velocity	6.00×10^{-5} (3.59×10^{-5}-8.39×10^{-5})	5.62×10^{-5} (3.36×10^{-5}-8.10×10^{-5})	5.60×10^{-5} (3.43×10^{-5}-8.11×10^{-5})	5.82×10^{-5} (3.47×10^{-5}-8.32×10^{-5})	4.76×10^{-5} (3.12×10^{-5}-7.33×10^{-5})	5.53×10^{-5} (3.33×10^{-5}-8.18×10^{-5})
		5.40×10^{-4} (3.23×10^{-4}-7.55×10^{-4})	5.06×10^{-4} (3.03×10^{-4}-7.29×10^{-4})	5.04×10^{-4} (3.09×10^{-4}-7.30×10^{-4})	5.24×10^{-4} (3.12×10^{-4}-7.49×10^{-4})	4.28×10^{-4} (2.81×10^{-4}-6.59×10^{-4})	4.97×10^{-4} (3.00×10^{-4}-7.37×10^{-4})
		1.50×10^{-3} (8.98×10^{-4}-2.10×10^{-3})	1.40×10^{-3} (8.41×10^{-4}-2.00×10^{-3})	1.40×10^{-3} (8.58×10^{-4}-2.00×10^{-3})	1.50×10^{-3} (8.67×10^{-4}-2.10×10^{-3})	1.20×10^{-3} (7.81×10^{-4}-1.80×10^{-3})	1.40×10^{-3} (8.32×10^{-4}-2.00×10^{-3})
		6.00×10^{-3} (3.60×10^{-3}-8.40×10^{-3})	5.60×10^{-3} (3.40×10^{-3}-8.10×10^{-3})	5.60×10^{-3} (3.40×10^{-3}-8.10×10^{-3})	5.80×10^{-3} (3.50×10^{-3}-8.30×10^{-3})	4.80×10^{-3} (3.10×10^{-3}-7.30×10^{-3})	5.50×10^{-3} (3.30×10^{-3}-8.20×10^{-3})

a. 0-Semiquiescent sampling period first stage place the sampler 1-Semiquiescent sampling period second stage sample 2,4-Period between Semiquiescent and Active Period 3,5-Active Sampling period

b. The number 1 to 4 represent BMC updating scenario, while 0 represents the prior scenario.

Table A-2 Prior and posterior distributions for model inputs (continued)

Parameter	Meaning	Diameter	Prior Mean Mean (90% CI)	Posterior Mean (90% CI)				
				Scenario 1 Mean (90% CI)	Scenario 2 Mean (90% CI)	Scenario 3 Mean (90% CI)	Scenario 4 Mean (90% CI)	Scenario 5 Mean (90% CI)
μ_2 (m/min)	Resuspension rate	1	2.63×10^{-7} (1.22×10^{-8}-1.09×10^{-6})	2.63×10^{-7} (1.23×10^{-8}-1.08×10^{-6})	2.69×10^{-7} (1.24×10^{-8}-1.11×10^{-6})	2.60×10^{-7} (1.25×10^{-8}-1.07×10^{-6})	2.61×10^{-7} (1.19×10^{-8}-1.10×10^{-6})	2.56×10^{-7} (1.26×10^{-8}-1.05×10^{-6})
		3	3.74×10^{-5} (1.29×10^{-5}-8.09×10^{-5})	3.71×10^{-5} (1.27×10^{-5}-8.16×10^{-5})	3.72×10^{-5} (1.28×10^{-5}-8.12×10^{-5})	3.73×10^{-5} (1.27×10^{-5}-8.18×10^{-5})	3.71×10^{-5} (1.29×10^{-5}-8.18×10^{-5})	3.69×10^{-5} (1.26×10^{-5}-7.95×10^{-5})
		5	8.62×10^{-5} (6.92×10^{-5}-1.00×10^{-4})	8.60×10^{-5} (6.93×10^{-5}-1.00×10^{-4})	8.62×10^{-5} (6.95×10^{-5}-1.00×10^{-4})	8.66×10^{-5} (6.95×10^{-5}-1.00×10^{-4})	8.63×10^{-5} (6.96×10^{-5}-1.00×10^{-4})	8.64×10^{-5} (6.94×10^{-5}-1.00×10^{-4})
		10	2.02×10^{-4} (6.76×10^{-5}-4.42×10^{-4})	2.90×10^{-4} (1.10×10^{-4}-5.04×10^{-4})	3.09×10^{-4} (9.48×10^{-5}-5.36×10^{-4})	2.29×10^{-4} (7.05×10^{-5}-4.84×10^{-4})	3.51×10^{-4} (1.64×10^{-4}-5.37×10^{-4})	2.69×10^{-4} (9.51×10^{-5}-4.91×10^{-4})
e_n	Efficiency of the nasal passages at removing particles	1	1.38×10^{-1} (4.57×10^{-2}-2.28×10^{-1})	1.38×10^{-1} (4.83×10^{-2}-2.29×10^{-1})	1.38×10^{-1} (4.39×10^{-2}-2.32×10^{-1})	1.37×10^{-1} (4.41×10^{-2}-2.29×10^{-1})	1.37×10^{-1} (4.52×10^{-2}-2.29×10^{-1})	1.38×10^{-1} (4.59×10^{-2}-2.29×10^{-1})
		3	4.50×10^{-1} (2.68×10^{-1}-6.33×10^{-1})	4.51×10^{-1} (2.66×10^{-1}-6.33×10^{-1})	4.52×10^{-1} (2.66×10^{-1}-6.34×10^{-1})	4.46×10^{-1} (2.62×10^{-1}-6.30×10^{-1})	4.51×10^{-1} (2.64×10^{-1}-6.35×10^{-1})	4.54×10^{-1} (2.64×10^{-1}-6.38×10^{-1})
		5	6.18×10^{-1} (4.61×10^{-1}-7.72×10^{-1})	6.22×10^{-1} (4.64×10^{-1}-7.74×10^{-1})	6.21×10^{-1} (4.61×10^{-1}-7.74×10^{-1})	6.19×10^{-1} (4.63×10^{-1}-7.73×10^{-1})	6.22×10^{-1} (4.60×10^{-1}-7.75×10^{-1})	6.18×10^{-1} (4.63×10^{-1}-7.71×10^{-1})
		10	7.67×10^{-1} (6.51×10^{-1}-8.83×10^{-1})	7.66×10^{-1} (6.52×10^{-1}-8.78×10^{-1})	7.68×10^{-1} (6.52×10^{-1}-8.83×10^{-1})	7.66×10^{-1} (6.48×10^{-1}-8.77×10^{-1})	7.63×10^{-1} (6.48×10^{-1}-8.83×10^{-1})	7.67×10^{-1} (6.49×10^{-1}-8.82×10^{-1})
Dose/ Mass_t	Fraction of inhaled spores and total released	1	1.60×10^{-3} (1.00×10^{-3}-2.10×10^{-3})	1.60×10^{-3} (1.00×10^{-3}-2.00×10^{-3})	1.60×10^{-3} (1.00×10^{-3}-2.00×10^{-3})	1.60×10^{-3} (1.00×10^{-3}-2.10×10^{-3})	1.60×10^{-3} (1.00×10^{-3}-2.10×10^{-3})	1.60×10^{-3} (1.10×10^{-3}-2.10×10^{-3})
		3	1.20×10^{-3} (8.15×10^{-4}-1.60×10^{-3})	1.20×10^{-3} (8.17×10^{-4}-1.60×10^{-3})	1.20×10^{-3} (8.18×10^{-4}-1.60×10^{-3})	1.20×10^{-3} (8.24×10^{-4}-1.60×10^{-3})	1.20×10^{-3} (8.46×10^{-4}-1.70×10^{-3})	1.20×10^{-3} (8.40×10^{-4}-1.60×10^{-3})
		5	8.30×10^{-4} (5.95×10^{-4}-1.20×10^{-3})	8.51×10^{-4} (6.09×10^{-4}-1.20×10^{-3})	8.53×10^{-4} (6.09×10^{-4}-1.20×10^{-3})	8.44×10^{-4} (6.05×10^{-4}-1.20×10^{-3})	9.05×10^{-4} (6.42×10^{-4}-1.30×10^{-3})	8.70×10^{-4} (6.14×10^{-4}-1.20×10^{-3})
		10	3.79×10^{-4} (2.75×10^{-4}-5.38×10^{-4})	4.05×10^{-4} (2.90×10^{-4}-5.72×10^{-4})	4.08×10^{-4} (2.89×10^{-4}-5.78×10^{-4})	3.90×10^{-4} (2.81×10^{-4}-5.51×10^{-4})	4.59×10^{-4} (3.18×10^{-4}-6.32×10^{-4})	4.12×10^{-4} (2.91×10^{-4}-5.90×10^{-4})
		Total	4.30×10^{-4} (3.15×10^{-4}-6.00×10^{-4})	4.55×10^{-4} (3.30×10^{-4}-6.34×10^{-4})	4.58×10^{-4} (3.29×10^{-4}-6.41×10^{-4})	4.42×10^{-4} (3.21×10^{-4}-6.15×10^{-4})	5.09×10^{-4} (3.61×10^{-4}-6.98×10^{-4})	4.34×10^{-4} (3.32×10^{-4}-6.54×10^{-4})
Mass_ex	Total pathogen exit the release room	1	1.32×10^{11} (5.60×10^{3}-5.71×10^{11})	7.30×10^{6} (1.24×10^{6}-1.75×10^{7})	1.45×10^{6} (2.00×10^{5}-3.97×10^{6})	1.35×10^{7} (8.07×10^{5}-2.51×10^{7})	6.23×10^{6} (1.00×10^{6}-1.29×10^{7})	7.60×10^{6} (1.05×10^{6}-1.90×10^{7})
		3	8.74×10^{10} (3.46×10^{3}-3.71×10^{11})	4.92×10^{6} (6.74×10^{5}-1.26×10^{7})	9.76×10^{5} (1.14×10^{5}-2.74×10^{6})	8.85×10^{6} (4.58×10^{5}-1.66×10^{7})	4.30×10^{6} (5.80×10^{5}-9.72×10^{6})	5.02×10^{6} (5.85×10^{5}-1.34×10^{7})
		5	5.84×10^{10} (2.18×10^{3}-2.40×10^{11})	3.36×10^{6} (3.90×10^{5}-9.16×10^{6})	6.65×10^{5} (6.59×10^{4}-1.93×10^{6})	6.00×10^{6} (2.64×10^{5}-1.14×10^{7})	3.02×10^{6} (3.47×10^{5}-7.23×10^{6})	3.40×10^{6} (3.34×10^{5}-9.65×10^{6})
		10	2.65×10^{10} (9.14×10^{2}-1.04×10^{11})	1.62×10^{6} (1.55×10^{5}-4.66×10^{6})	3.18×10^{5} (2.70×10^{4}-9.33×10^{5})	2.91×10^{6} (9.78×10^{4}-5.67×10^{6})	1.56×10^{6} (1.48×10^{5}-4.13×10^{6})	1.62×10^{6} (1.32×10^{5}-4.81×10^{6})

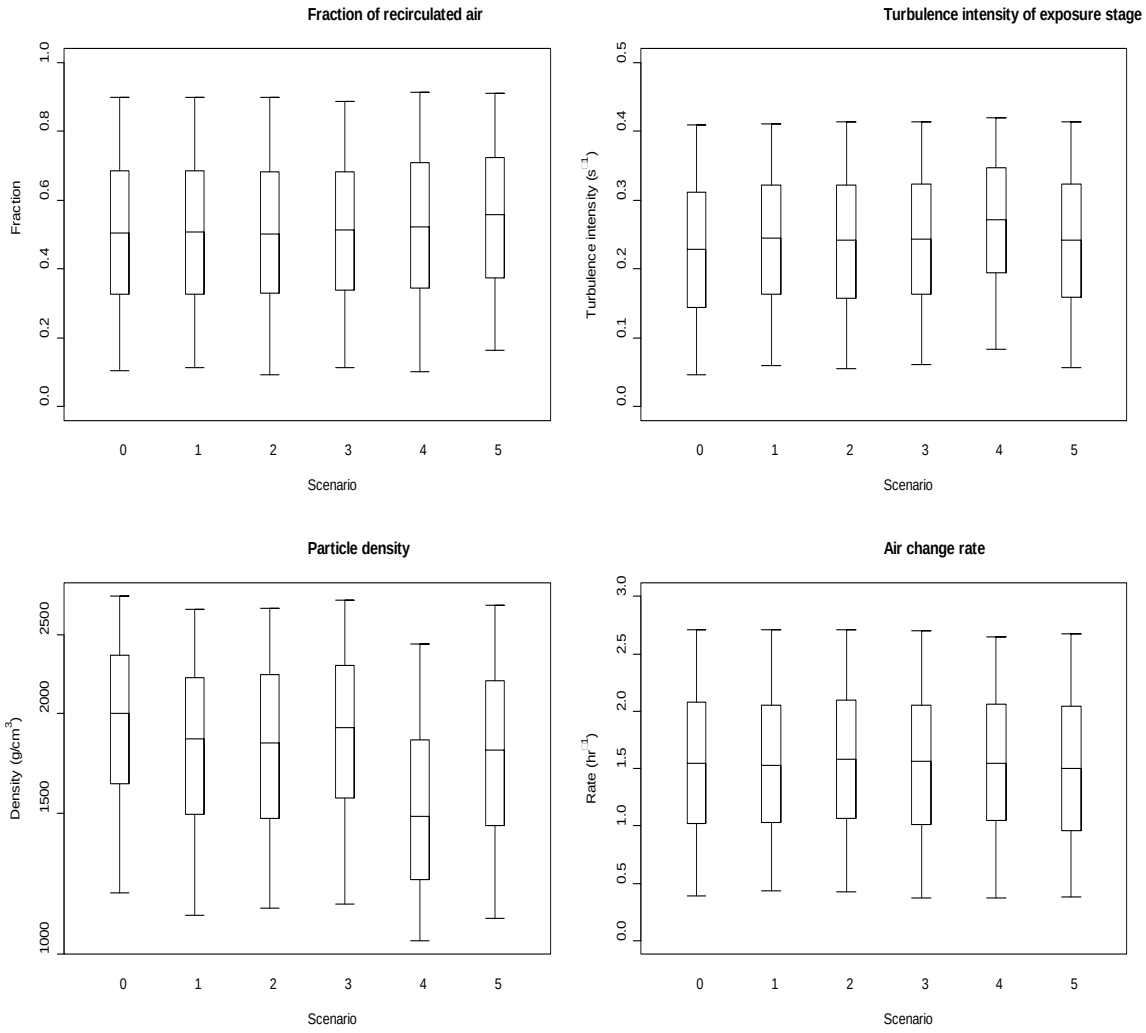

Figure A-1 Prior and posterior CDF for particle transport parameters

(The bottom and top of the box are 25th and 75th percentile, the band inside the box is the 50th percentile, and the upper and lower whiskers represent the 5th and 95th percentile, respectively. The number 1 to 4 represent BMC updating scenarios, while 0 represents the prior scenario.)

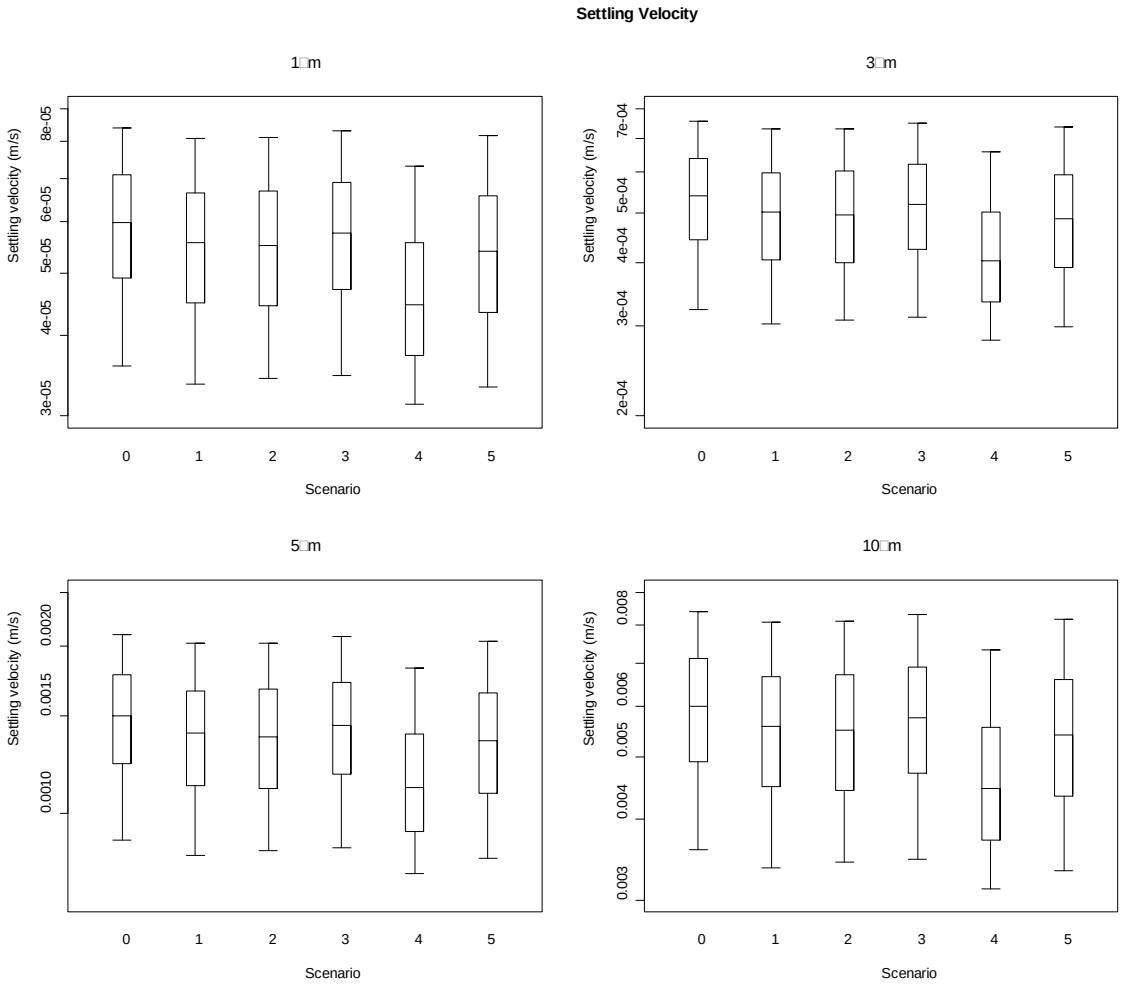

Figure A-2 Prior and posterior CDF for the settling velocities

(The bottom and top of the box are 25th and 75th percentile, the band inside the box is the 50th percentile, and the upper and lower whiskers represent the 5th and 95th percentile, respectively. The number 1 to 4 represent BMC updating scenarios, while 0 represents the prior scenario.)

CHAPTER 3: CHARACTERIZING BIOAEROSOL RISK FROM ENVIRONMENTAL SAMPLING

Abstract

In the aftermath of a release of microbiological agents, environmental sampling must be conducted to characterize the release sufficiently so that mathematical models can then be used to predict the subsequent dispersion and human health risks. Because both the dose-response and environmental transport of aerosolized microbiological agents are functions of the effective aerodynamic diameter of the particles, environmental assessments should consider not only the total amount of agent but also the size distributions of the aerosolized particles. This chapter evaluates different approaches to estimating risk from measurements of microorganisms deposited on surfaces after an aerosol release. For a various combinations of sampling surfaces, size fractions, HVAC operating conditions, size distributions of release spores, and uncertainties in surface measurements, the accuracy of model predictions are tested in order to assess how much detail can realistically be identified from surface sampling results. The recommended modeling and sampling scheme is one choosing 3, 5 and 10μm diameter particles as identification targets and taking samples from untracked floor, wall and the HVAC filter. This scheme provides reasonably accurate, but somewhat conservative, estimates of risk across a range of different scenarios. Performance of the recommended sampling scheme is tested by using data from a large scale field test as a case study. Sample sizes of 10-25 are sufficient to develop order of magnitude estimates of risk. Larger sample sizes have little benefit unless uncertainties in sample recoveries can be reduced.

3.1 Introduction

After the 2001 anthrax attacks, many researchers have focused on how to effectively estimate human health risk during a bio-terrorist attack, so that appropriate response actions can be taken [16, 17, 19, 20, 37, 46, 52, 55, 88, 93, 94, 121, 146, 158, 196, 199]. Thus, many models have been developed, including pathogen dose-response models [11, 90] and environmental transport models [152, 162, 174, 175, 189]. These previous modeling efforts have recognized that the size distribution of the particulates has a substantial impact on the risk. For example, a previous study [85] estimated that a *B. anthracis* spore concentration of $100/m^2$ on a floor would correspond to a risk of one in a thousand if the spores were finely aerosolized, 1μm diameter particles, but one in a million if the spores were present as 10μm diameter clumps. Smaller particles settle more slowly and are less readily removed by HVAC system filters [162]. These properties allow them to disperse over larger areas and persist longer in the air than larger particles. In addition, fine particulates are more respirable, and thus present greater risks when inhaled than larger particles [11].

Previous modeling efforts have generally accounted for these aerosol size effects by modeling a number of discrete particle sizes [11, 85, 149, 162]. However, little previous research has examined how to conduct sampling in order to effectively parameterize these models. While some aerosol samplers can provide information on particulate sizes, aerosol concentrations decline rapidly after a release making it unlikely that response will be rapid enough to characterize a release based on aerosol

concentrations. The material used in the attack may not be recovered in sufficient quantity for a size distribution analysis to be conducted. Surface sampling techniques generally provide information on only the total number of organisms or gene copies present, not the size fractions of particulates that organisms are associated with. Because different size particles partition into various environmental compartments at different rates, the concentrations found in different environmental compartments may allow the size distribution of the release to be identified.

This study addresses the question of how much can be learned from simple aggregate concentration measurements, such as could reasonably be made after an actual release. In order to assess how size distributions can realistically be identified from surface sampling results, a variety of alternative model formulations and sampling schemes are evaluated following a 7-step framework. The recommended modeling and sampling scheme is then applied to a case study using parameter estimates from a large scale field test, which aims to provide insights between a sampling scheme's reliability and its required sample size.

3.2 Methodology

The method has two components. First, forward modeling is conducted, in which characteristics of a release are assumed and a fate and transport model is used to estimate spore concentrations in different environmental compartments. The *B. anthracis* spore concentrations predicted by the fate and transport model then serve as inputs for different

inverse modeling approaches, which are evaluated on their ability to match the forward modeling results. The overall goal of this analysis is to identify sampling and modeling schemes, specifically as a combination of sampling locations and modeled particle sizes, which allow the release quantities for different spore sizes, their associated risks, and the amount exiting the release room to be characterized with the least error.

3.2.1 Fate and transport model (forward modeling)

The general fate and transport model for a simple office with a HVAC system is expressed as:

$$\frac{d\overrightarrow{M(t)}}{dt} = \vec{T}\overrightarrow{M(t)}$$

where $\overrightarrow{M(t)}$ is the quantity of spores in different compartments, and $\vec{T}$ is a matrix of transfer coefficients. Based on Figure 3-1, the modeled office is divide into 7 internal compartments: air, tracked floor, untracked floor, walls, ceiling, HVAC, and the nasal passages of an occupant of the office, and an eighth compartment that consists of all areas external to the room.

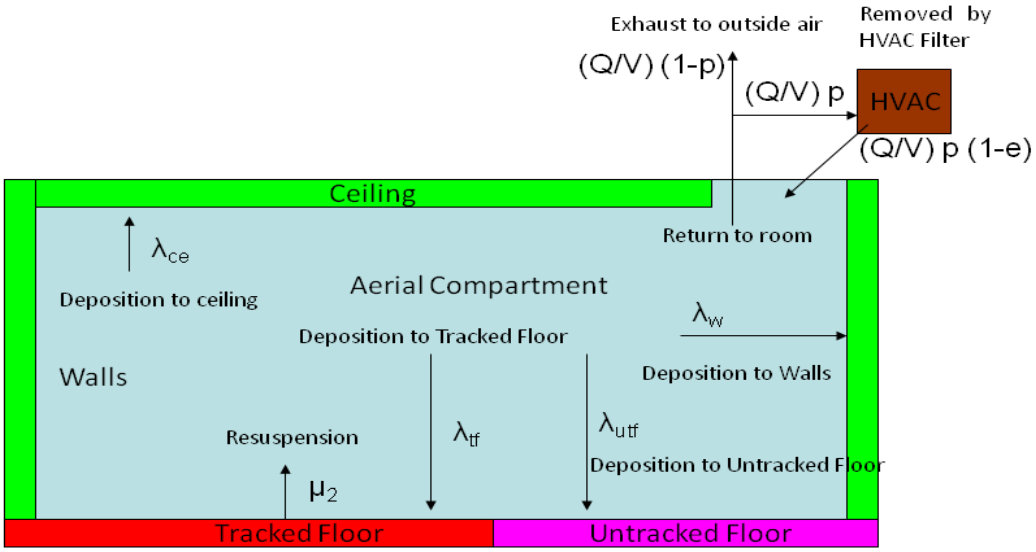

Figure 3-1 Schematic of single room office suite

Thus the general fate and transport model can be written as:

$$\frac{dM}{dt} = \begin{pmatrix} \dot{M}_{air} \\ \dot{M}_{tf} \\ \dot{M}_{utf} \\ \dot{M}_{w} \\ \dot{M}_{f} \\ \dot{M}_{ec} \\ \dot{M}_{ce} \\ \dot{M}_{n} \end{pmatrix} = \begin{pmatrix} [(1-e)p-1]\frac{Q}{V} - (\lambda_{tf} + \lambda_{utf} + \lambda_{w} + \lambda_{ce} + \frac{I\,e_n}{V}) & \mu_2 & 0 & 0 & 0 & 0 & 0 & 0 \\ \lambda_{tf} & -\mu_2 & 0 & 0 & 0 & 0 & 0 & 0 \\ \lambda_{utf} & 0 & 0 & 0 & 0 & 0 & 0 & 0 \\ \lambda_{w} & 0 & 0 & 0 & 0 & 0 & 0 & 0 \\ ep\frac{Q}{V} & 0 & 0 & 0 & 0 & 0 & 0 & 0 \\ (1-p)\frac{Q}{V} & 0 & 0 & 0 & 0 & 0 & 0 & 0 \\ \lambda_{ce} & 0 & 0 & 0 & 0 & 0 & 0 & 0 \\ \frac{I\,e_n}{V} & 0 & 0 & 0 & 0 & 0 & 0 & 0 \end{pmatrix} \begin{pmatrix} M_{air} \\ M_{tf} \\ M_{utf} \\ M_{w} \\ M_{f} \\ M_{ec} \\ M_{ce} \\ M_{n} \end{pmatrix} \quad (1)$$

where $M_{air}(t)$ is the number of spores in the air compartment, $M_{tf}(t)$ is the number of spores on the tracked surface of the floor, $M_{utf}(t)$ is the number of spores on the untracked surface of the floor, $M_w(t)$ is the number of spores on the walls, $M_f(t)$ is the number of spores on the filter, $M_{ec}(t)$ is the number of spores in the external compartment, $M_{ce}(t)$ is the number of spores on the ceiling, $M_n(t)$ is the number of spores in the occupant's nasal passages. M_{air}, M_{tf}, M_{utf}, M_w, M_f, M_{ec}, M_{ce} and M_n are all given in units of spores (number of organisms). Next we define the following parameters: Q is the discharge from the air compartment (units of m^3/s), μ_2 is the resuspension rate from the tracked surface into the air compartment (units of s^{-1}), p is the fraction of air recirculated into the building by the HVAC system, e is the efficiency of the filter at removing particles, e_n is the efficiency of the nasal passages at removing particles, I is the inhalation rate of the occupant (units of m^3/s), and V is the volume of the room (units of m^3). λ_{tf}, λ_{utf}, λ_w and λ_{ce} are the deposition rates for aerosolized pathogens onto the tracked surface, the untracked surface and the floors, walls, and ceiling respectively (units of s^{-1}), which can be expressed by parameters representing the indoor air flow conditions:

$$\lambda_{tf\,(utf)} = \frac{A_{tf\,(utf)}}{Vol} \times \frac{v}{1 - e^{-\frac{\pi v}{2\sqrt{Dk_e}}}} \tag{2}$$

$$\lambda_w = \frac{A_w}{Vol} \times \frac{2}{\pi} \sqrt{Dk_e} \tag{3}$$

$$\lambda_c = \frac{A_c}{Vol} \times \frac{v}{e^{\frac{\pi v}{2\sqrt{Dk_e}}} - 1} \tag{4}$$

where D (m^2/s) is the particle diffusivity, k_e (s^{-1}) is turbulence intensity, and v (m/s) is particle settling velocity, which is given in Equation 5 as a function of the particle's diameter (d, units of m), the viscosity of air (μ_{air}, units of kg/(m×s)), the density of the particle (ρ_p, units of kg/m^3), and the density of air (ρ_{air}, units of kg/m^3).

$$V_t = \frac{gd^2(\rho_p - \rho_{air})}{18\mu_{air}} \tag{5}$$

For the details of the solution to Equation 1, please refer to Hong et. al. [85]. Parameter values are provided as Supplementary Information.

Such compartment modeling approaches are widely used, although their limitations must be acknowledged. This modeling approach assumes that each compartment is completely mixed, which is not accurate at the immediate time of a release but becomes much more accurate as the release disperses over time. Thus, the methodology presented here is intended for use in areas somewhat removed from the initial release such that concentrations on different surfaces (walls, untracked floor, and HVAC filter) can be considered reflective of more or less the same time-averaged air concentration. The model used here is based on literature studies of how particulates

behave in the indoor environmental [129, 131, 146, 162, 171, 173, 184, 183]. In the case of *B.anthracis* spores, a verification of the above mentioned fate and transport model has been undertaken [87] by comparing the results of a completely mixed compartment model with observations of *B.anthracis* spore concentrations from the Hart Senate Office Building reported by Weis et. al. [199]. The observed behavior of the spores was generally consistent with model predictions, allowing the model to be used to generate order of magnitude estimates of risk [87]. This verification analysis used a Bayesian Monte Carlo approach to identify release parameters. While the Bayesian Monte Carlo approach has promise, it does require the identification of prior distributions for parameters and thousands of model runs to characterize posterior distributions, which is complicated and computationally intensive. In the following section, the potential of a more straightforward and rapid classical approach to identifying release characteristics is evaluated.

3.2.2 Particle identification (inverse modeling)

Because all of the processes in Equation 1 are first order, the release quantity ($\overrightarrow{\mathrm{M_r}}$) can be expressed as the product of a matrix, commonly termed the inverse transfer matrix ($\overrightarrow{\mathrm{T^{-1}}}$) and the mass of deposited *B. anthracis* spores in each environmental compartment ($\overrightarrow{\mathrm{M_s}}$) [148]:

$$\overrightarrow{\mathrm{M_r}} = \overrightarrow{\mathrm{T^{-1}}}\overrightarrow{\mathrm{M_s}} \tag{6}$$

The inverse transfer matrix ($\overrightarrow{\mathrm{T^{-1}}}$) in Equation 6 is a function of time, as specified by the transfer matrix ($\vec{T}$) of the fate and transport model. This matrix goes through an

initial period of rapid change, when deposition from the air compartment is the dominant process. Then resuspension, a much slower process, becomes the rate controlling process. This is illustrated in Figure 3-2 which shows the mass in different compartments over time for the four different particle sizes considered. The mass in each compartment varies in the first few minutes and then stabilizes within several hours of the release. This stabilization is not a true steady state, as eventually resuspension will deplete concentrations on tracked surfaces (and in fact a gradual decline in tracked floor concentration can be seen over several hours for the 10μm fraction, as this fraction is most readily resuspended). However, this period after the initial deposition phase is termed "quasi-steady state" because surface concentrations are roughly stable over the time period during which initial release characterization would be expected to occur (days). The $\overrightarrow{T^{-1}}$ matrix can be considered roughly constant in this period.

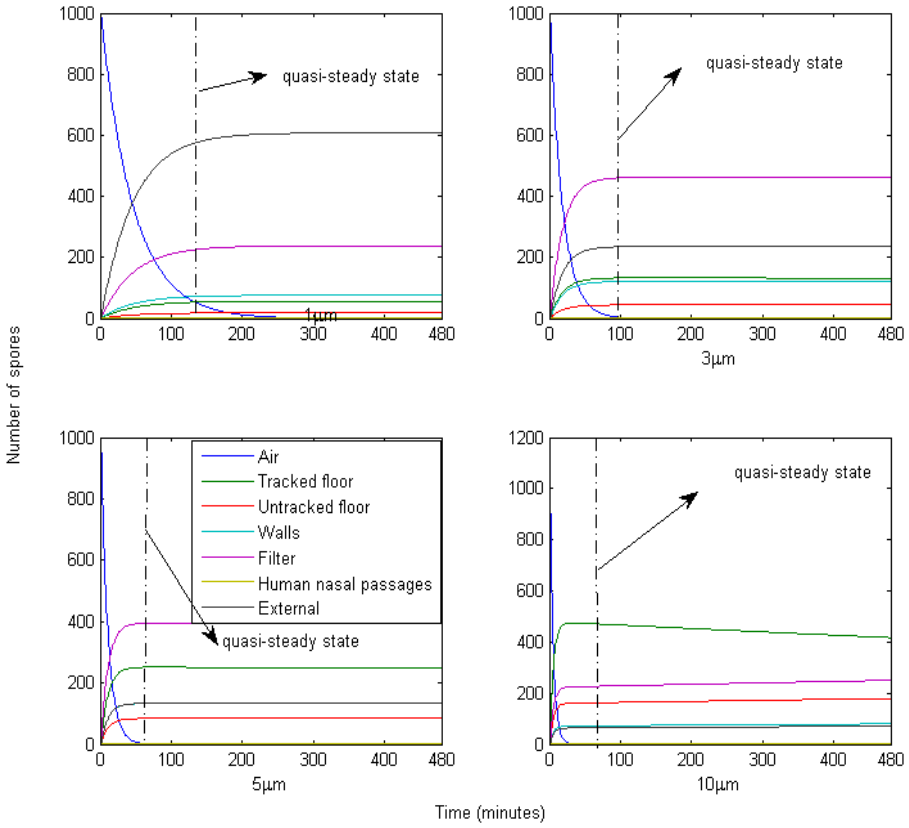

Figure 3-2 Number of spores in different environmental compartments over time for a single room model.

The approximate transition from the phase of initial deposition of the aerosol to a quasi-steady state (see text) is indicated by a vertical line in each plot.

At quasi-steady state, if the diameter of spores are divided into four groups: 1μm, 3μm, 5μm, and 10μm [88], Equation 6 can be expanded to give:

$$\begin{bmatrix} M_{r1} \\ M_{r3} \\ M_{r5} \\ M_{r10} \end{bmatrix} = \begin{bmatrix} K_{surfA\_1} & K_{surfA\_3} & K_{surfA\_5} & K_{surfA\_10} \\ K_{surfB\_1} & K_{surfB\_3} & K_{surfB\_5} & K_{surfB\_10} \\ K_{surfC\_1} & K_{surfC\_3} & K_{surfC\_5} & K_{surfC\_10} \\ K_{surfD\_1} & K_{surfD\_3} & K_{surfD\_5} & K_{surfD\_10} \end{bmatrix}^{-1} \begin{bmatrix} M_{s\_surfA} \\ M_{s\_surfB} \\ M_{s\_surfC} \\ M_{s\_surfD} \end{bmatrix} \quad (7)$$

Where K_{surfi_j} is the distribution coefficient for spores with diameter of j on surface i, M_{s_surfi} is the unbiased mass measurements of the total spores on surface i, and M_{rj} is the initial release quantity for spores whose diameters are j μm. It is the M_{rj}values which need to be identified from sampling so that the impacts of the release can be modeled.

Because of the difficulties associated with recovering samples from surfaces [21, 61, 66], leading to potential errors in the sampling and analysis steps, measurements from the surfaces vary from their true values. Thus, it is necessary to evaluate the impacts of such errors in measurements of $\overrightarrow{M_s}$ on the characterized release quantity, $\widehat{\overrightarrow{M_r}}$. Simulated measurement errors are constructed by Hadamard multiplying (element by element product, symbol ○) $\overrightarrow{M_s}$, the environmental compartment concentration values from the fate and transport model, by a coefficient ($\vec{Z}$), whose elements are assumed to be normally distributed with mean of 1 and standard deviation of 0.3. Thus equation (8) links the estimated release quantity $\widehat{\overrightarrow{M_r}}$, with measured values subject to random errors:

$$\widehat{\overrightarrow{M_r}} = \overrightarrow{T^{-1}}\left(\overrightarrow{M_s} \circ \vec{Z}\right) \quad (8)$$

3.2.3 Modeled scenarios

Three sets of size distributions of released *B. anthracis* spores are employed to test the robustness of candidate modeling and sampling schemes. The nominal size distribution is based on the lab analysis of the 2001 anthrax letter attack: the fractions of 1, 3, 5, and 10μm are 0.14%, 1.46%, 8.40%, and 90%, respectively [102]. The second set doubles the quantity of spores with diameters of 1, 3, and 5μm, and reduces the amount of 10μm; thus the new fractions are 0.28%, 2.92%, 16.80%, and 80%, respectively. This size fraction represents the situation where more fine particles are released, which is termed "light". While the third size fraction, termed "heavy", has half the number of 1, 3, and 5μm spores (size fractions are 0.07%, 0.73%, 4.20%, and 95%) as compared to the nominal situation. Since different HVAC operation situations might change the fate and transport properties of released spores and impact human exposure, three HVAC operating conditions are considered, representing low, medium, and high air recirculation rates (p=0.5, 0.75, 0.95) for each set of size distributions considered. In addition, surface concentration measurements with errors (model predictions multiplied by a matrix **Z**) and without errors are considered. Since the impacts of measurement error are modeled by a matrix $\vec{Z}$ whose elements are random numbers, it is necessary to propagate this uncertainty. Thus medians and 90% confidence intervals from Monte Carlo simulations with 1000 iterations are included. In total each candidate scheme is evaluated under 18 conditions (3 HVAC operational conditions × 3 size fraction distributions × with and without measurement errors).

3.2.4 Evaluation framework

Only 3 out of 8 modeled locations (wall, untracked floor, and HVAC filter) are considered feasible for sampling in this study. The indoor air, external air, ceiling, and human nasal passage compartments in the fate and transport model (Equation 1) are excluded due to the relatively low concentration values that would be expected in these compartments several hours after a release, which could not be measured accurately. The tracked floor is excluded because it provides essentially the same information as the untracked floor but with less reliability as it is less stable over time. This indicates that no more than three size fractions can be identified from the release quantity, while the full model includes four size fractions.

The steps of the model evaluation framework used in this study are illustrated in Figure 3-3: 1) the full model, consisting of all 4 size fractions is run and concentrations in the different environmental compartments at quasi-steady state are simulated, as well as the risk to the occupants of the room and the amount of spores exiting the room; 2) a set of compartments is chosen for measuring *B. anthracis* spore concentrations; 3) particle sizes are selected to be modeled; given that only 3 environmental compartments are considered suitable for measurement and that the full model has 4 particle sizes, the number of size fractions to be modeled based on available measurements must be reduced from the number in the full model, hence this is termed the reduced model; 4) the inverse transfer matrix at quasi-steady for the reduced model is computed, and the matrix ($\vec{Z}$), representing measurement error, is generated; 5) Monte Carlo simulations are conducted, and the release quantities are calculated with Equation 6. When simulated

measurement errors are included in the environmental concentrations, then Equation 8 is used. When measurement errors are present, it is possible to obtain negative estimates of mass. Zeros are substituted for any negative estimates; 6) using the release quantities estimated from the reduced model, the risk to occupants of the room and the number of spores exiting this room are calculated; and 7) the ratios of the reduced model and full model are determined for the risk to occupants and amount of spores exiting the room.

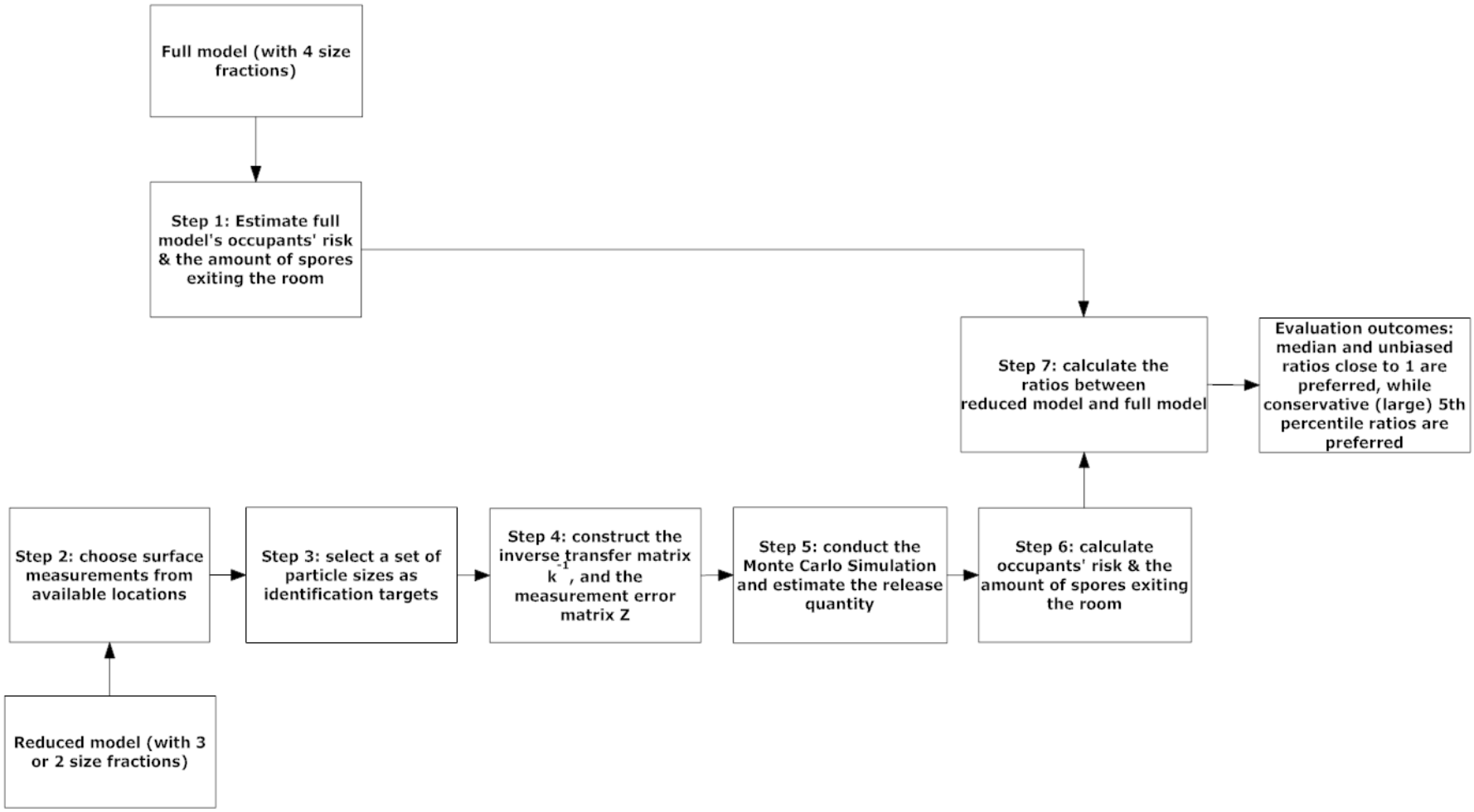

Figure 3-3 Evaluation framework used in this study

For an identification approach to be effective, the ratios of quantities such as human risk and the amount of spores exiting the room between the reduced form and the full model (based on four size fractions) should be close to one but should not have much risk of falling substantially below one. Ratios greater than one represent conservative models, meaning that a model that overestimates risk to the occupants of the room, which in most cases would be preferred to an approach that underestimates risk. Likewise an approach that overestimates the number of spores leaving the room (which would inform estimates of risk to those downwind of the release) would generally be preferred over an approach that underestimates the number of spores leaving the room. However, in order to provide a reasonable prediction, these ratios should not be too far away from one.

3.3 Results

The first modeling and sampling schemes considered are those ones with three different size fractions. The fraction of spores with the diameter of 10μm is always identified because it constitutes the vast majority of the release, while the other two identification targets are selected from the remaining three candidate particle sizes. Table 3-1 presents results for identification approaches for three particle sizes. If the surface sampling results are perfect (no errors), ratios for the occupants' risk, and the amount of spores exiting the room are very close to 1, indicating that these approaches closely match the full model. However, once sampling inefficiency and potential errors are considered. The median ratios from some sampling schemes overestimate risk by a factor of 2 or 3. This indicates that predictions for the release quantity and ratios are sensitive to

measurement errors. Across the different size fraction identification schemes, the ones using 3, 5 and 10μms as the identification targets outperform others, because the 5th percentiles for the ratios of human health risk and the amount of spores exiting the room are closer to 1, which means adopting this sampling schemes reduces the potential extent of underestimation due to sampling error.

Table 3-1 Results for approaches to identify three size fractions

Selected compartments	Size fractions to be identified (μm)	Set of size distribution	HVAC operation condition	Ratio of occupants' risk				Ratio of spores exiting the room			
				No measurement error	Measurement error			No measurement error	Measurement error		
					50%	5%	95%		50%	5%	95%
Untracked floor Walls HVAC filter	1,3,10	Nominal	0.50	1.15	1.83	0.68	5.02	1.06	1.34	0.88	2.12
			0.75	1.14	1.92	0.73	4.90	1.06	1.38	0.90	2.14
			0.95	1.11	1.68	0.69	4.61	1.05	1.31	0.89	2.10
		Light	0.50	1.20	1.37	0.59	3.48	1.12	1.26	0.85	1.99
			0.75	1.18	1.31	0.57	3.38	1.11	1.25	0.86	1.94
			0.95	1.14	1.27	0.55	3.18	1.09	1.21	0.85	1.91
		Heavy	0.50	1.11	2.47	0.88	6.56	1.03	1.41	0.91	2.32
			0.75	1.10	2.56	0.88	6.63	1.03	1.45	0.94	2.35
			0.95	1.08	2.32	0.89	6.45	1.03	1.42	0.91	2.30
		Overall				0.57	6.63			0.85	2.35
	1,5,10	Nominal	0.50	1.00	1.40	0.61	3.70	1.00	1.19	0.85	1.70
			0.75	1.00	1.44	0.65	3.58	1.00	1.20	0.87	1.70
			0.95	1.00	1.31	0.63	3.35	1.00	1.16	0.86	1.68
		Light	0.50	1.00	1.12	0.55	2.53	0.99	1.10	0.81	1.53
			0.75	1.00	1.08	0.53	2.47	0.99	1.10	0.83	1.51
			0.95	1.00	1.07	0.54	2.33	0.99	1.07	0.82	1.46
		Heavy	0.50	1.00	1.82	0.80	4.76	1.00	1.24	0.87	1.91
			0.75	1.00	1.88	0.81	4.80	1.00	1.28	0.89	1.91
			0.95	1.00	1.77	0.77	4.69	1.00	1.25	0.86	1.88
		Overall				0.53	4.80			0.81	1.91

Table 3-1. Results for approaches to identify three size fractions (continued)

Selected compartments	Size fractions to be identified (µm)	Set of size distribution	HVAC operation condition	Ratio of occupants' risk				Ratio of spores exiting the room			
				No measurement error	Measurement error			No measurement error	Measurement error		
					50%	5%	95%		50%	5%	95%
Untracked floor Walls HVAC filter	**3,5,10**	**Nominal**	**0.50**	**1.00**	**2.53**	**0.79**	**6.05**	**1.00**	**1.52**	**0.96**	**2.69**
			0.75	**1.00**	**2.58**	**0.89**	**6.05**	**1.00**	**1.54**	**0.95**	**2.71**
			0.95	**1.00**	**2.35**	**0.92**	**5.61**	**1.01**	**1.48**	**0.96**	**2.66**
		Light	**0.50**	**1.00**	**1.80**	**0.75**	**3.99**	**1.00**	**1.36**	**0.92**	**2.39**
			0.75	**1.00**	**1.71**	**0.78**	**3.75**	**1.01**	**1.35**	**0.91**	**2.37**
			0.95	**1.00**	**1.57**	**0.77**	**3.53**	**1.01**	**1.28**	**0.90**	**2.25**
		Heavy	**0.50**	**1.00**	**3.43**	**1.03**	**8.13**	**1.00**	**1.61**	**0.97**	**2.98**
			0.75	**1.00**	**3.48**	**1.02**	**8.47**	**1.00**	**1.65**	**1.00**	**3.02**
			0.95	**1.00**	**3.21**	**1.00**	**8.24**	**1.00**	**1.60**	**0.97**	**2.93**
		Overall				**0.75**	**8.47**			**0.90**	**3.02**

a.The size fractions of 1, 3, 5, and 10µm for the nominal scenario are 0.14%, 1.46%, 8.40%. and 90%, The size fractions of 1, 3, 5, and 10µm for the light scenario for the light scenario are 0.28%, 2.92%, 16.80%, and 80%. The size fractions of 1, 3, 5, and 10µm for the heavy scenario and 0.07%, 0.73%, 4.20%, and 95%.
b. If a negative release quantity is identified, it will be assumed 0.
c. Bold shows the qualified surface particle size combination.
d. Values in the 'Overall' row come from the lowest 5% and the highest 95% ratios.

If two size fractions are to be estimated, again the 10μm size fraction is always included in the model because it accounts for the majority of spores. The other identification target is selected from the 1, 3, and 5μm diameter size fractions, while two sampling surfaces are selected from untracked floor, wall, and the HVAC filter. Table 3-2 provides the results for the identification approaches based on two sampling surfaces. If measurement error is not considered, three candidate sampling schemes satisfy the evaluation criteria: 1) identifying 5 and 10μm particle sizes by sampling from the untracked floor, and the walls; 2) identifying 5 and 10μm particle sizes by sampling from the walls and the HVAC filter; and 3) identifying 3 and 10μm particle sizes by sampling the untracked floor and the HVAC filter. However, if the effect of measurement error is considered, the 5^{th} percentile ratios for the human risk are less than 0.5 for the selected combinations, indicating serious underestimations of risk are possible due to sampling error. As a result, none of the two particle size approaches are recommended.

Table 3-2 Results for approaches to identify two size fractions

Selected compartments	Size fractions to be identified (μm)	Set of size distribution	HVAC operation condition	Ratio of occupants' risk				Ratio of spores exiting the room			
				No measurement error	Measurement error			No measurement error	Measurement error		
					50%	5%	95%		50%	5%	95%
Untracked floor Walls	1,10	Nominal	0.50	0.68	0.69	0.45	1.12	0.93	0.93	0.60	1.28
			0.75	0.68	0.69	0.43	1.06	0.92	0.92	0.63	1.26
			0.95	0.68	0.68	0.42	1.08	0.92	0.92	0.62	1.23
		Light	0.50	0.58	0.59	0.35	0.84	0.86	0.86	0.62	1.14
			0.75	0.58	0.58	0.34	0.84	0.86	0.86	0.61	1.12
			0.95	0.60	0.59	0.36	0.82	0.86	0.86	0.61	1.09
		Heavy	0.50	0.78	0.85	0.55	1.35	0.96	0.98	0.64	1.36
			0.75	0.78	0.83	0.54	1.34	0.96	0.99	0.62	1.38
			0.95	0.77	0.82	0.54	1.32	0.96	0.97	0.63	1.34
		Overall				0.34	1.35			0.60	1.38
	3,10	Nominal	0.50	0.88	0.90	0.47	1.75	0.98	1.01	0.69	1.33
			0.75	0.90	0.91	0.45	1.68	0.99	0.99	0.72	1.32
			0.95	0.92	0.92	0.44	1.70	0.99	1.00	0.73	1.31
		Light	0.50	0.85	0.87	0.37	1.38	0.97	0.98	0.73	1.23
			0.75	0.87	0.86	0.37	1.37	0.97	0.97	0.73	1.22
			0.95	0.90	0.88	0.41	1.36	0.99	0.99	0.74	1.21
		Heavy	0.50	0.92	0.98	0.58	2.12	0.99	1.04	0.72	1.40
			0.75	0.93	0.94	0.57	2.08	0.99	1.04	0.71	1.40
			0.95	0.95	0.95	0.56	2.13	1.00	1.04	0.71	1.37
		Overall				0.37	2.13			0.69	1.40

Table 3-2 Results for approaches to identify two size fractions (continued)

Selected compartments	Size fractions to be identified (µm)	Set of size distribution	HVAC operation condition	Ratio of occupants' risk				Ratio of spores exiting the room			
				No measurement error	Measurement error			No measurement error	Measurement error		
					50%	5%	95%		50%	5%	95%
Untracked floor Walls	5,10	Nominal	0.50	1.08	1.11	0.49	2.39	1.02	1.05	0.74	1.39
			0.75	1.10	1.11	0.46	2.30	1.02	1.05	0.76	1.37
			0.95	1.15	1.14	0.45	2.30	1.03	1.05	0.77	1.36
		Light	0.50	1.11	1.14	0.39	1.90	1.03	1.04	0.77	1.30
			0.75	1.13	1.13	0.39	1.89	1.04	1.03	0.78	1.30
			0.95	1.19	1.16	0.46	1.86	1.06	1.06	0.80	1.30
		Heavy	0.50	1.06	1.10	0.59	2.88	1.01	1.08	0.75	1.48
			0.75	1.07	1.03	0.59	2.79	1.01	1.08	0.74	1.46
			0.95	1.11	1.10	0.58	2.89	1.02	1.09	0.75	1.42
		Overall				0.39	2.89			0.74	1.48
Untracked floor HVAC	1,10	Nominal	0.50	3.67	3.74	0.42	21.23	1.88	1.89	0.81	7.46
			0.75	3.71	3.68	0.40	21.04	1.92	1.92	0.79	7.67
			0.95	3.69	3.75	0.37	18.44	1.94	1.94	0.76	6.92
		Light	0.50	4.45	4.47	0.29	14.56	2.60	2.60	0.76	7.14
			0.75	4.46	4.59	0.29	14.02	2.64	2.63	0.80	6.91
			0.95	4.37	4.08	0.25	13.26	2.66	2.50	0.74	6.83
		Heavy	0.50	2.83	1.94	0.53	25.86	1.46	1.48	0.79	7.01
			0.75	2.88	2.03	0.54	25.25	1.49	1.51	0.82	6.99
			0.95	2.90	2.77	0.53	25.27	1.50	1.54	0.82	7.22
		Overall				0.25	25.86			0.74	7.67

Table 3-2 Results for approaches to identify two size fractions (continued)

Selected compartments	Size fractions to be identified (μm)	Set of size distribution	HVAC operation condition	Ratio of occupants' risk				Ratio of spores exiting the room			
				No measurement error	Measurement error			No measurement error	Measurement error		
					50%	5%	95%		50%	5%	95%
Untracked floor HVAC	3,10	Nominal	0.50	1.12	1.13	0.42	4.83	1.05	1.18	0.79	1.96
			0.75	1.11	1.12	0.40	4.83	1.05	1.19	0.75	1.99
			0.95	1.09	1.09	0.37	4.20	1.05	1.16	0.76	1.87
		Light	0.50	1.16	1.16	0.29	3.32	1.10	1.13	0.72	1.87
			0.75	1.15	1.14	0.29	3.15	1.10	1.12	0.74	1.81
			0.95	1.11	1.04	0.26	2.98	1.08	1.08	0.71	1.75
		Heavy	0.50	1.08	1.04	0.54	5.91	1.03	1.25	0.77	1.98
			0.75	1.08	1.04	0.55	5.75	1.03	1.23	0.78	1.95
			0.95	1.06	1.05	0.53	5.78	1.02	1.23	0.77	2.00
		Overall				0.29	5.91			0.71	2.00
	5,10	Nominal	0.50	0.96	0.96	0.43	3.74	0.98	1.12	0.77	1.59
			0.75	0.94	0.95	0.41	3.73	0.98	1.12	0.75	1.56
			0.95	0.92	0.92	0.38	3.24	0.97	1.08	0.74	1.53
		Light	0.50	0.94	0.94	0.29	2.57	0.97	1.02	0.68	1.44
			0.75	0.93	0.92	0.29	2.41	0.96	1.01	0.70	1.42
			0.95	0.90	0.84	0.26	2.28	0.94	0.98	0.70	1.36
		Heavy	0.50	0.97	1.07	0.55	4.57	0.99	1.19	0.77	1.68
			0.75	0.96	1.07	0.56	4.45	0.99	1.18	0.76	1.70
			0.95	0.94	1.03	0.54	4.46	0.98	1.18	0.76	1.67
		Overall				0.29	4.57			0.68	1.70

Table 3-2 Results for approaches to identify two size fractions (continued)

Selected compartments	Size fractions to be identified (μm)	Set of size distribution	HVAC operation condition	Ratio of occupants' risk				Ratio of spores exiting the room			
				No measurement error	Measurement error			No measurement error	Biased		
					50%	5%	95%		50%	5%	95%
Wall HVAC	1,10	Nominal	0.50	0.64	0.68	0.45	1.08	1.00	1.00	0.68	1.38
			0.75	0.63	0.67	0.45	1.04	1.00	1.01	0.69	1.36
			0.95	0.64	0.66	0.44	1.03	1.00	1.00	0.68	1.34
		Light	0.50	0.53	0.54	0.35	0.81	0.99	1.00	0.72	1.29
			0.75	0.53	0.53	0.35	0.79	0.99	0.99	0.73	1.25
			0.95	0.54	0.54	0.34	0.77	0.99	0.99	0.74	1.24
		Heavy	0.50	0.75	0.85	0.58	1.33	1.00	1.03	0.65	1.43
			0.75	0.75	0.84	0.57	1.30	1.00	1.02	0.65	1.42
			0.95	0.74	0.83	0.55	1.29	1.00	1.01	0.67	1.45
		Overall				0.34	1.33			0.65	1.45
	3,10	Nominal	0.50	0.83	0.85	0.48	1.98	1.01	1.04	0.73	1.50
			0.75	0.84	0.87	0.50	1.87	1.01	1.04	0.73	1.48
			0.95	0.88	0.90	0.48	1.92	1.01	1.03	0.72	1.45
		Light	0.50	0.77	0.78	0.38	1.51	1.01	1.03	0.76	1.36
			0.75	0.80	0.80	0.38	1.45	1.01	1.02	0.77	1.31
			0.95	0.85	0.85	0.37	1.42	1.02	1.02	0.77	1.27
		Heavy	0.50	0.88	1.03	0.63	2.41	1.00	1.07	0.69	1.57
			0.75	0.89	1.02	0.61	2.36	1.00	1.06	0.68	1.59
			0.95	0.92	0.99	0.59	2.37	1.01	1.04	0.70	1.58
		Overall				0.37	2.41			0.68	1.59

Table 3-2 Results for approaches to identify two size fractions (continued)

Selected compartments	Size fractions to be identified (μm)	Set of size distribution	HVAC operation condition	Ratio of occupants' risk				Ratio of spores exiting the room			
				No measurement error	Measurement error			No measurement error	Biased		
					50%	5%	95%		50%	5%	95%
Wall HVAC	5,10	Nominal	0.50	1.18	1.19	0.53	3.91	1.00	1.09	0.78	1.92
			0.75	1.23	1.28	0.55	3.69	1.00	1.10	0.76	1.91
			0.95	1.34	1.35	0.52	3.75	1.00	1.09	0.77	1.82
		Light	0.50	1.24	1.27	0.41	3.05	0.99	1.07	0.80	1.63
			0.75	1.30	1.32	0.42	2.86	0.99	1.06	0.79	1.58
			0.95	1.43	1.43	0.41	2.89	0.99	1.06	0.80	1.52
		Heavy	0.50	1.13	1.41	0.70	4.88	1.00	1.15	0.74	2.11
			0.75	1.16	1.38	0.67	4.59	1.00	1.13	0.73	2.07
			0.95	1.24	1.37	0.65	4.72	1.00	1.11	0.75	2.06
		Overall				0.41	4.88			0.73	2.11

a.The size fractions of 1, 3, 5, and 10μm for the nominal scenario are 0.14%, 1.46%, 8.40%. and 90%, The size fractions of 1, 3, 5, and 10μm for the light scenario for the light scenario are 0.28%, 2.92%, 16.80%, and 80%. The size fractions of 1, 3, 5, and 10μm for the heavy scenario and 0.07%, 0.73%, 4.20%, and 95%.
b. If a negative release quantity is identified, it will be assumed 0.
c. Bold shows the qualified surface particle size combination.
d. Values in the 'Overall' row come from the lowest 5% and the highest 95% ratios.

Table 3-3 includes the results when a single size fraction, the 1µm size fraction, is selected for identification. When samples are taken from either the untracked floor or the HVAC filter, the ratios for the human risk and the amount of spores leaving the room are greatly overestimated, indicating these identification strategies are not accurate. However, if samples are collected from walls, the ratios for human risk are close to one, but the ratios of quantity of spores leaving the room are far below one. This phenomenon arises because 1µm deposit to the walls in greater proportion than other size fractions (Figure 3-4). Thus assuming all spores are 1µm results in an underestimation of total release quantity. Since the estimated release quantity is lower than its actual value, the approach also underestimates the number of spores leaving the room. However, the estimate of risk is close to the full model because all the spores are assumed to be from the most dangerous size fraction, 1µm [11]. Table 3-4 includes the results for approaches to identify 10µm size fraction. In contrast to the 1µm scenarios, release quantities are underestimated. When samples are taken from untracked floor and the HVAC filter, the ratios of human risk and the amount of spores exiting the room are less than one. However if samples are taken from walls, the release quantity is overestimated due to its low rate at which 10µm spores deposit to walls compared to other size fractions. This results in an overestimation of the number of spores leaving the room (see Figure 3-4).

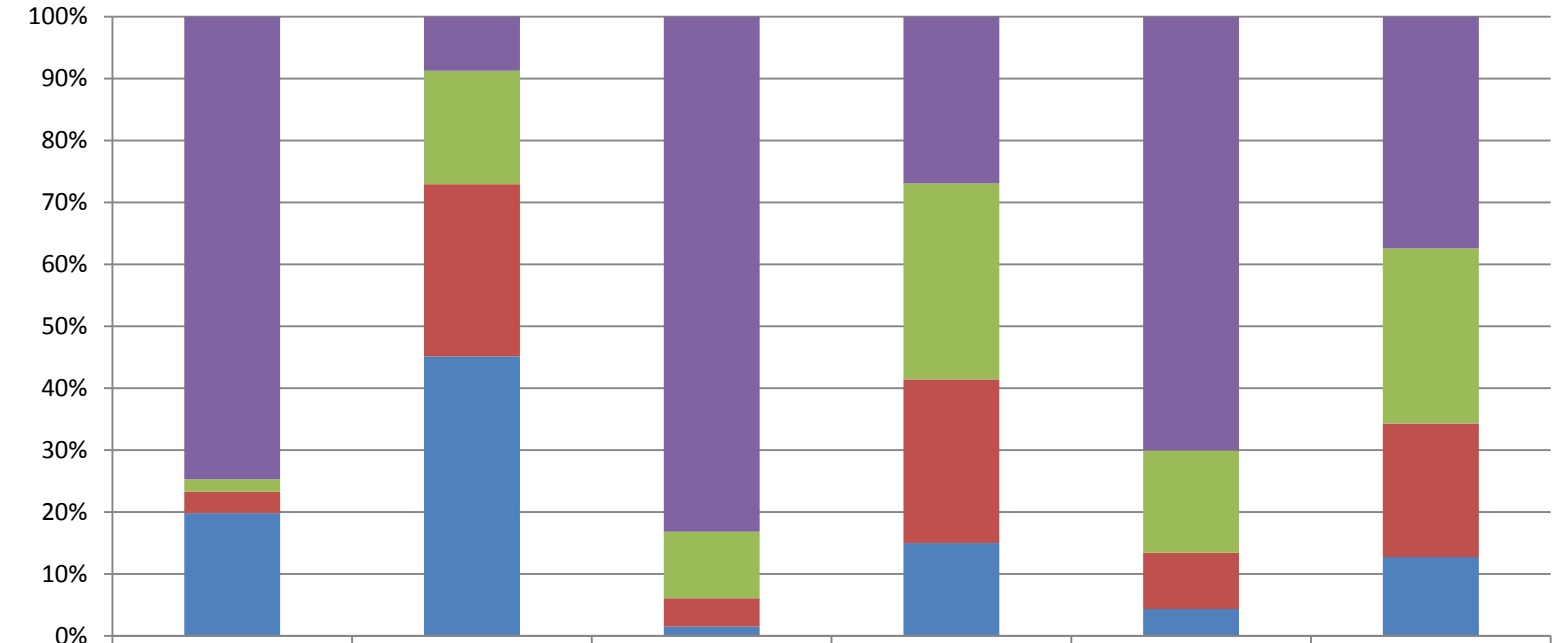

	Air compartment	Floor	Wall	HVAC filter	Outside	Nasal Passage
1 μm	0.49%	12.95%	0.62%	55.74%	29.93%	0.27%
3 μm	0.01%	27.13%	0.08%	65.53%	7.04%	0.21%
5 μm	0.02%	41.19%	0.03%	54.71%	3.89%	0.16%
10 μm	0.13%	66.89%	0.01%	31.02%	1.86%	0.09%

Figure 3-4 The distribution of *Bacillus anthracis* with different diameters after 8 hours.

The percentages in the table are distributions of *B. anthracis* spores among different compartments, while the heights of different colors in one bar denote the distribution of spore sizes in that compartment.

Table 3-3 Results for approaches to identify 1 micron size fraction

Selected compartments	Set of size distribution	HVAC operation condition	Ratio of occupants' risk				Ratio of spores exiting the room			
			No measurement error	Measurement error			No measurement error	Measurement error		
				50%	5%	95%		50%	5%	95%
Untracked floor	Nominal	0.50	183.54	184.80	119.86	230.24	84.83	85.72	47.44	123.82
		0.75	175.64	176.12	111.43	220.65	83.78	84.12	45.01	123.21
		0.95	165.41	165.92	107.83	205.04	82.25	82.64	45.59	118.42
	Light	0.50	114.72	114.18	73.57	145.08	72.48	71.97	40.02	105.94
		0.75	108.57	110.13	69.70	138.18	70.91	72.45	39.07	105.43
		0.95	100.74	99.65	64.65	124.95	68.68	67.56	37.69	97.80
	Heavy	0.50	255.79	251.93	156.45	320.39	92.01	89.89	47.17	134.83
		0.75	248.06	249.84	153.65	314.43	91.39	92.41	47.42	137.76
		0.95	237.74	236.79	148.31	298.00	90.49	89.92	47.22	133.99
	Overall				64.65	320.39			37.69	137.76
Wall	Nominal	0.50	1.02	1.02	0.64	1.38	0.33	0.33	0.20	0.44
		0.75	1.01	1.02	0.65	1.39	0.33	0.33	0.21	0.46
		0.95	1.00	1.01	0.67	1.33	0.34	0.34	0.23	0.45
	Light	0.50	0.79	0.79	0.54	1.03	0.35	0.35	0.24	0.46
		0.75	0.79	0.79	0.54	1.04	0.36	0.36	0.25	0.48
		0.95	0.79	0.79	0.56	1.02	0.37	0.37	0.27	0.48
	Heavy	0.50	1.26	1.26	0.74	1.78	0.31	0.31	0.18	0.44
		0.75	1.25	1.25	0.74	1.80	0.31	0.31	0.19	0.45
		0.95	1.24	1.24	0.72	1.75	0.32	0.32	0.18	0.45
	Overall				0.54	1.80			0.18	0.48

Table 3-3 Results for approaches to identify 1 micron size fraction (continued)

Selected compartments	Set of size distribution	HVAC operation condition	Ratio of occupants' risk				Ratio of spores exiting the room			
			No measurement error	Measurement error			No measurement error	Measurement error		
				50%	5%	95%		50%	5%	95%
HVAC filter	Nominal	0.50	25.70	25.49	14.96	35.66	8.57	8.49	4.90	12.08
		0.75	24.90	25.01	14.17	34.88	8.51	8.55	4.76	12.13
		0.95	23.72	23.37	13.97	32.68	8.41	8.28	4.87	11.78
	Light	0.50	17.67	17.53	10.97	24.00	8.23	8.16	5.03	11.36
		0.75	17.01	16.91	11.21	22.73	8.15	8.09	5.29	11.05
		0.95	16.06	16.11	10.23	21.23	7.98	8.01	5.00	10.71
	Heavy	0.50	34.15	34.31	18.87	47.85	8.76	8.80	4.76	12.48
		0.75	33.43	33.77	17.36	47.63	8.73	8.82	4.45	12.66
		0.95	32.31	32.19	17.86	46.61	8.68	8.64	4.71	12.75
	Overall				10.97	47.85			4.45	12.75

a.The size fractions of 1, 3, 5, and 10μm for the nominal scenario are 0.14%, 1.46%, 8.40%. and 90%, The size fractions of 1, 3, 5, and 10μm for the light scenario for the light scenario are 0.28%, 2.92%, 16.80%, and 80%. The size fractions of 1, 3, 5, and 10μm for the heavy scenario and 0.07%, 0.73%, 4.20%, and 95%.
b. If a negative release quantity is identified, it will be assumed 0.
c. Bold shows the qualified surface particle size combination.
d. Values in the 'Overall' row come from the lowest 5% and the highest 95% ratios.

Table 3-4 Results for approaches to identify 10 micron size fraction

Selected compartments	Set of size distribution	HVAC operation condition	Ratio of occupants' risk				Ratio of spores exiting the room			
			No measurement error	Measurement error			No measurement error	Measurement error		
				50%	5%	95%		50%	5%	95%
Untracked floor	Nominal	0.50	0.44	0.44	0.21	0.64	0.85	0.85	0.41	1.25
		0.75	0.42	0.42	0.22	0.60	0.84	0.83	0.45	1.21
		0.95	0.39	0.40	0.21	0.58	0.82	0.83	0.44	1.21
	Light	0.50	0.27	0.27	0.16	0.39	0.72	0.73	0.42	1.06
		0.75	0.25	0.26	0.15	0.37	0.71	0.73	0.42	1.04
		0.95	0.24	0.23	0.13	0.33	0.69	0.68	0.38	0.96
	Heavy	0.50	0.61	0.61	0.31	0.93	0.92	0.91	0.47	1.39
		0.75	0.60	0.60	0.31	0.88	0.91	0.92	0.47	1.35
		0.95	0.57	0.57	0.30	0.84	0.90	0.89	0.47	1.33
	Overall				0.13	0.93			0.38	1.39
Wall	Nominal	0.50	0.57	0.57	0.36	0.77	1.11	1.11	0.70	1.49
		0.75	0.56	0.56	0.36	0.76	1.12	1.12	0.72	1.53
		0.95	0.55	0.55	0.35	0.74	1.15	1.15	0.74	1.54
	Light	0.50	0.44	0.44	0.30	0.59	1.20	1.19	0.82	1.59
		0.75	0.44	0.44	0.30	0.58	1.22	1.22	0.85	1.62
		0.95	0.43	0.44	0.31	0.57	1.27	1.28	0.89	1.67
	Heavy	0.50	0.71	0.71	0.41	0.99	1.06	1.06	0.61	1.49
		0.75	0.70	0.70	0.42	1.00	1.07	1.08	0.64	1.54
		0.95	0.68	0.69	0.40	0.95	1.08	1.10	0.63	1.51
	Overall				0.30	1.00			0.61	1.67

Table 3-4 Results for approaches to identify 10 micron size fraction (continued)

Selected compartments	Set of size distribution	HVAC operation condition	Ratio of occupants' risk				Ratio of spores exiting the room			
			No measurement error	Measurement error			No measurement error	Measurement error		
				50%	5%	95%		50%	5%	95%
HVAC filter	Nominal	0.50	0.49	0.49	0.28	0.69	0.95	0.95	0.53	1.34
		0.75	0.47	0.47	0.26	0.67	0.95	0.94	0.52	1.35
		0.95	0.45	0.45	0.24	0.64	0.94	0.94	0.51	1.33
	Light	0.50	0.34	0.34	0.21	0.46	0.92	0.92	0.58	1.24
		0.75	0.32	0.32	0.21	0.44	0.91	0.90	0.58	1.23
		0.95	0.30	0.30	0.19	0.42	0.89	0.89	0.55	1.21
	Heavy	0.50	0.65	0.66	0.36	0.95	0.98	0.99	0.53	1.43
		0.75	0.63	0.63	0.33	0.92	0.97	0.96	0.50	1.41
		0.95	0.61	0.60	0.33	0.88	0.97	0.96	0.53	1.40
	Overall				0.19	0.95			0.51	1.43

a.The size fractions of 1, 3, 5, and 10μm for the nominal scenario are 0.14%, 1.46%, 8.40%. and 90%, The size fractions of 1, 3, 5, and 10μm for the light scenario for the light scenario are 0.28%, 2.92%, 16.80%, and 80%. The size fractions of 1, 3, 5, and 10μm for the heavy scenario and 0.07%, 0.73%, 4.20%, and 95%.
b. If a negative release quantity is identified, it will be assumed 0.
c. Bold shows the qualified surface particle size combination.
d. Values in the 'Overall' row come from the lowest 5% and the highest 95% ratios.

3.4 Application of the sampling scheme

Based on the above results, identifying 3, 5, and 10μm particle size fractions based on samples from the untracked floor, walls, and the HVAC filter is recommended as a modeling and sampling scheme. To examine how such an approach might be applied, and what degree of uncertainty would be present in results, concentration measurements from a large scale field test are analyzed below.

In September 2008, Battelle Energy Alliance conducted five release events of *Bacillus atrophaeus*, a surrogate for *Bacillus anthracis*, at Idaho National Laboratory (INL) in a typical two-story commercial building (Building PBF632) in order to support the Department of Homeland Security (DHS), the Environmental Protection Agency (EPA), and the Joint Program Executive Office Chemical and Biological Defense's (JPEOCBD) Sample Collection Operation Test Plan. Among the five tested release events, Events 1, 2, and 4 were performed on the first floor of the building, while Events 3 and 5 were performed on the second floor. For each release event, *Bacillus atrophaeus* spores were aerosolized through a battery powered generator, and surface concentrations were measured using collection methods: vacuum, wipe, and swab. Between release events, the building was decontaminated and the effectiveness of decontamination was verified by clearance samples. For details of this field test, please refer to the official report [4].

To create the matrix $\vec{Z}$, it is necessary to estimate sample recovery variability and uncertainty associated with different collection methods. This was done using settling plate samples as a reference by a multivariate regression model. Recovery efficiencies (γ_j) are estimated as:

$$Y_{i,j,k} = \sum_{i=1}^{n_i} \beta_i I_{i,k} + \sum_{j=1}^{n_j} \gamma_j J_{j,k} + \varepsilon_{i,j,k} \quad (13)$$

where the dependent variable is the log transformed surface concentration $Y_{i,j,k}$, i indexes the combination of room and sampling event where the sample was taken (thus rooms are indexed separately for each of the sampling events), j indexes collection method, and k indexes the measurements within each room-event and sampling method combination. The model has two classes of parameters: 1) β_i the nuisance parameters, which account for the effects of $I_{i,k}$, the indicator of location-event combination ($I_{i,k}$ is 1 when the k^{th} sample is from the i^{th} location-event combination and 0 otherwise), and 2) γ_j the collection method recovery fractions, which account for the effects of $J_{j,k}$, the collection method indicator ($J_{j,k}$ is 1 when the k^{th} sample is sampled by the j^{th} collection method and 0 otherwise). The error terms of this regression ($\varepsilon_{i,j,k}$) are collection method specific, following a normal distribution with a mean of zero and a standard deviation of σ_j ($\varepsilon_{i,j,k} \sim N(o,\sigma_j)$). Parameters are estimated by maximum likelihood estimation (MLE) using data from the 3 release events with more than 55% detectable concentrations (Events 1, 4, and 5) for a total of 550 observations, which consist of 146 swabs samples, 76 Vacuum samples, 227 wipes samples, and 101 settling plate samples. The inverse of the information matrix is used to estimate standard errors of model parameters. The standard error of γ_j, denoted by σ_j, is of particular interest since this is the uncertainty in mean recovery (relative to the settling plate data that were used as a reference). The normality

of the residual errors from the best fitted model has been verified, and values of σ_j and σ_γ, are present in Table 3-5 by sample collection method.

Table 3-5 The standard deviation and its uncertainty for the error term

Collection method	Parameter value (log scale)		Sample quantity (log scale)		
	σ_γ	σ_j	n=1	n=4	n=25
Swab	0.32	0.94	0.99	0.57	0.38
Vacuum	0.18	0.67	0.69	0.38	0.22
Wipe	0.25	0.97	1.00	0.54	0.31

For samples taken from an unknown surface, the overall uncertainty has two sources, uncertainty in mean recovery (σ_γ) and variability in the recovery from sample to sample (σ_j). The sampling variability can be reduced by increasing sample size. However, unless a reference method is available, increasing the sample size will not reduce uncertainty in the recovery fraction. While a reference method (i.e., settling plate data) was available for this field study, it would not be available in the aftermath of an actual biological attack. Thus for a given collection method j, its residual error, (i.e., the elements of matrix $\vec{Z}$), is generated by the following distribution:

$$\ln \varepsilon_j \sim N\ (0, \sqrt{\sigma_\gamma^2 + \frac{\sigma_j^2}{n}}) \tag{14}$$

where n is the sample size.

Based on errors calculated in this manner and shown in Table 3-5, nine different $\vec{Z}$ matrices are developed, one for each of three sample collection methods (swabs, vacuum, and wipes) and three sample sizes (1, 9, and 25). These Z matrices estimated from the field data are tested on the previously recommended sampling and modeling scheme, taking samples from untracked floor, wall, and the HVAC filter to identify 3, 5 and 10μm. A Monte Carlo simulation of 1000 iterations is used for each sampling scheme, and the ratios of human risk and amount of spores exiting the room are computed. The impacts of imperfect sample recovery and sample size are investigated by checking the quotients between the 95^{th} percentile and 5^{th} percentile of these two ratios, which represents the uncertainty of the results. The closer this quotient is to 1, the less uncertainty in the sampling scheme. Figure 3-5 illustrates this quotient as a function of sample size for nine

sampling schemes. Uncertainties in number of spores exiting the room are smaller than those in health risks to occupants of the release room. Thus health risk to occupants of the room drives the sample size requirement. Based on these inputs, it is suggested to take at least 25 samples, which results in roughly one order of magnitude difference between the 95^{th} percentile and 5^{th} percentile estimations for risk estimates in the release room. Sample sizes larger than 25 provide little benefit as the remaining uncertainty is due to uncertainty in mean recovery (σ_γ) rather than sampling variability (σ_j). Given that a reference method (i.e., settling plates) would not be available in a real release, additional samples will not reduce uncertainty in recovery rates. Accordingly once the sample size is sufficient to reduce the effect of σ_j on overall uncertainty then there is little benefit to further sampling. One potential option to reduce σ_γ would be to conduct positive control studies. While this option is not explored further here, the expected reduction in σ_γ could be used with the approach described here to estimate the benefit of such positive control studies. Among the three sample collection methods, samples taken by wipes have the most sampling variability and hence are the most sensitive to sample size, followed by swab and vacuum. One should beware that conclusions might change under different settings, such as the type of released agents, release location (indoor vs. outdoor), the sample extraction method used, the material used for sampling, etc.

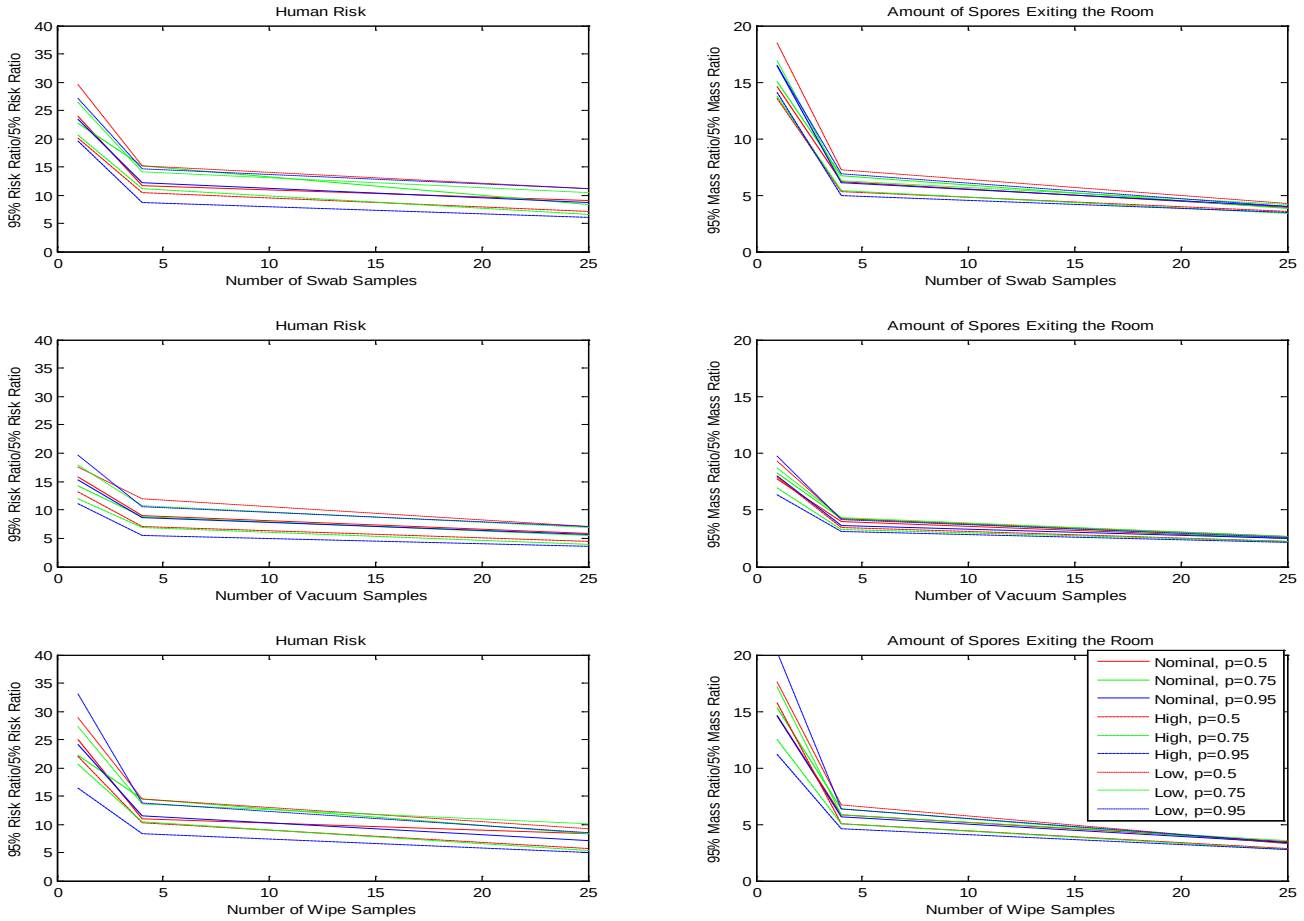

Figure 3-5 The relationship between a sample scheme's reliability and its sample size

(Identification targets are 3, 5 and 10μm, and samples are taken from untracked floor, wall and the HVAC filter)

3.5 Discussion

This analysis provides a framework for determining how much detail can feasibly be included in models and provides guidance on appropriate sampling schemes. This analysis suggests that 1) a 3 size fraction model (3, 5, and 10μm), which can be estimated based on aggregate surface sampling of the untracked floor, wall, and the HVAC filter, provides reasonable and conservative estimates of risk and number of spores leaving the release room; and 2) in an example application, a sample size of about 25 provided order of magnitude estimates of risk, but unless a reference is available to enable uncertainties in recovery to be reduced, there is little benefit to taking more than 25 samples.

Calculations involved in this paper depends on the complete mixing assumption, which is generally true for fine particles as deposition rates are slow relative to mixing rates. However, the immediate vicinity of a release may contain large amounts of coarse particles due to rapid deposition of these particles before mixing can occur. More detailed work, such as computational fluid dynamics modeling could provide guidance as to how to interpret surface concentration in the immediate vicinity of a release. The approach described here is applicable only to areas removed from the initial release. Whether this framework is applicable can be readily ascertained from sampling data. Areas of a room showing spatial variability in sampling results would be areas for which the complete mixing assumption is not valid. Results from areas with consistent and uniform concentrations would be appropriate for use with this method.

3.6 Appendix B

Table B-1. Inputs and their values used in Equation 1 and 6

Parameter Symbol	Meaning	Unit	Best Estimate	**Source**
V	Volume of model the office	m^3	78.4	Author decision
Q	Discharge from the air compartment	m^3/s	0.087	[59]
p	Fraction of air recirculated into the building by the HVAC system		0.8	[8]
ρ_p	Particle density	kg/m^3	1000	Author decision
ACH	Air change rate	times/hour	4	Author decision
Inh	Occupants' inhalation rate	m^3/hour	1.02	[101]
e	The efficiency of the filter at removing particles	1µm	0.098	[162]
		3µm	0.49	
		5µm	0.74	
		10µm	0.88	
e_n	The efficiency of the nasal passages at removing particles	1µm	0.14	[104, 161]
		3µm	0.45	
		5µm	0.62	
		10µm	0.77	

Table B-1. Inputs and their values used in Equation 1 and 6 (continued)

Parameter Symbol	Meaning	Unit	Best Estimate		Source
$\lambda_{w(ce)}$	Deposition rates onto the walls (ceilings)	$hour^{-1}$	1μm	0.1	[162]
			3μm	0.4	
			5μm	0.8	
			10μm	0.9	
$\lambda_{tf(utf)}$	Deposition rates onto the tracked (untracked) surface	$hour^{-1}$	1μm	0.1	[162]
			3μm	0.6	
			5μm	2.0	
			10μm	8.1	
μ_2	Resuspension rate from the untracked surface into the air compartment	$hour^{-1}$	1μm	1.2×10^{-4}	[162]
			3μm	1.9×10^{-3}	
			5μm	3.8×10^{-3}	
			10μm	3.4×10^{-2}	

CHAPTER 4: PRIORITIZING RISKS AND UNCERTAINTIES FROM INTENTIONAL RELEASE OF SELECTED CATEGORY A PATHOGENS

ABSTRACT

This paper synthesizes available information on five Category A pathogens (*Bacillus anthracis*, *Yersinia* pestis, *Francisella tularensis*, *Variola major* and Lassa) to develop quantitative guidelines for how environmental pathogen concentrations may be related to human health risk in an indoor environment. An integrated model of environmental transport and human health exposure to biological pathogens is constructed which 1) includes the effects of environmental attenuation, 2) considers fomite contact exposure (ingestion or dermal risk) as well as inhalational exposure, and 3) includes an uncertainty analysis to identify key input uncertainties, which may inform future research directions. A reduced form model is also derived which allows for approximate estimation of risk without the need to conduct matrix manipulations. The findings from this study provide a framework for developing the many different environmental standards that are needed for making risk-informed response decisions, such as when prophylactic antibiotics should be distributed, and whether or not a contaminated area should be cleaned up. The approach is based on the assumption of uniform mixing in environmental compartments and is thus applicable to areas sufficiently removed in time and space from the initial release that mixing has produced relatively uniform concentration. Results indicate that when pathogens are released into the air, risk from inhalation is the main component of the overall risk, while risk from ingestion (dermal contact for *B. anthracis*) is the main component of the overall risk

when pathogens are present on surfaces. Concentrations sampled from untracked floor, walls and the filter of heating ventilation and air conditioning (HVAC) system are proposed as indicators of previous exposure risk, while samples taken from touched surfaces are proposed as indicators of future risk if the building is reoccupied. A Monte Carlo uncertainty analysis is conducted and input-output correlations used to identify important parameter uncertainties. An approach is proposed for integrating these quantitative assessments of parameter uncertainty with broader, qualitative considerations to identify future research priorities.

4.1 Introduction

Biological weapons, also known as “the poor man’s atom bomb”, have been included in terrorists’ arsenal because of their capability of producing mass causalities combined with natural access to the pathogens, manageable technical challenges and relatively low costs to launch an attack [144, 190, 192]. Prior to the 2001 anthrax letter attacks, identified bioterrorism attacks included the release of *Salmonella typhimurium* to eleven restaurant salad bars in the city of Portland in 1984 to influence an election, which caused the infection of 750 people, and the release of *B. anthracis* spores in Tokyo by the religious group Aum Shinrikyo between 1990 and 1995, which failed to infect any people [13, 157]. The 2001 anthrax letter attacks infected 22 people (11 inhalational cases and 11 cutaneous cases [108]), caused the deaths of 5 people, and cost hundreds of millions of dollars in clean up costs [163]. The attacks revealed that the U.S. lacked the guidelines for a quick response to such attacks, as well as decontamination standards for bioterrorism agents [86].

As a result, research has been undertaken to better understand the risks resulting from a bioterrorist attack. Sextro et al. modeled the spread of *B. anthracis* spores in a hypothetical office suite, estimated occupants' exposure, and found that activity-related resuspension was an important source of human exposure [162]. This model did not consider environmental decay of the pathogen. While *B. anthracis* is a persistent pathogen whose environmental decay rate can be treated as zero for a short time simulation [166], Sextro et al.'s model would need to be modified to include environmental attenuation in order to be used to estimate the fate and transport of non-

persistent biological agents. Price et al. [11] created a framework to link the degree of contamination in a building to the risk to the occupants, which could also be used to establish a decontamination standard if an acceptable risk level is provided. In addition, Price et al. linked the number of negative samples to the level of statistical confidence in the determination that the building had been effectively decontaminated [146]. However, this study did not provide a mechanistic model to describe the long term fate and transport and overall mass balance of the released pathogens, instead using a proportionality relationship to link the short term surface concentration of deposited pathogens to the short term concentration of aerosolized ones. Hong et al. [12] modeled the distribution of both air and surface-released *B. anthracis* spores in an office, and used concentrations found in different environmental media (i.e., surface, wall, ventilation filter, etc.) to infer future or past aerosol exposure. At the same time, they applied probability sampling theory in determining the minimum sampling area corresponding to certain levels of confidence in meeting allowable residual risk targets. The variability during sampling recovery and the potential for clumping of *B. anthracis* were taken into account. Besides not including pathogen decay, the above-mentioned studies quantify only inhalational risk, and omit threats from ingestion and dermal contact.

While models for *B. anthracis* have focused on a single pathway, inhalation exposure, mathematical models have been developed for influenza that take multiple disease transmission routes, such as inhalation and ingestion, into account [9, 182, 195]. Nicas and Gang introduced a Markov chain model to quantify multiple-pathway exposure to influenza for a health-care worker who had close contact with a patient. Three

exposure routes were concerned, hand-mucous membranes, inhalation, and direct projection of pathogen-containing droplets onto mucous membranes. In a subsequent study, Nicas et al. applied their model to quantify the relative importance of different influenza virus exposure pathways, and pointed out that model uncertainties had significant impacts on the conclusion as to which pathway is dominant [132, 133]. Atkinson and Wein constructed a four-person household transmission model to quantify the dominant transmission route for pandemic influenza [9, 195]. Both of the studies performed analysis on the recognized major transmission pathways: droplet, airborne, and contacts [2, 193]. However, the above-mentioned studies adopted fixed parameter values in the computations instead of distributions across possible values, which does not account for variability and uncertainty. There is evidence that including uncertainty and variability is important. Smieszek compared predictions from a mechanistic exposure model and empirical data from a contact diary study to analyze the impacts of different contact intensities and durations. Results showed that treating all the contacts equally overestimated the expected number of infected individuals [170]. A study by Julian et al. used Monte Carlo simulation to analyze variability and uncertainty in the risk due to nondietary ingestion of rotavirus relying on a micro-level activity time series, which may inspire future high-resolution microbial risk assessment [63, 96].

These multiple pathway models have been applied to common transmissible pathogens but have not addressed Category A agents. They have generally sought to identify which pathways are of concern, rather than informing the development of quantitative standards for response actions. To address the need for such quantitative

standards this paper synthesizes available information on five Category A pathogens to develop a framework for relating environmental pathogen concentrations to human health risk. The five pathogens considered are: *B. anthracis*, *Y. Pestis*, *F. tularensis*, *Variola major*, and Lassa. Properties of each of these pathogens are described below.

B. anthracis is a Gram-positive, facultative anaerobic, rod-shaped bacterium of the genus *Bacillus*. It is the causative agent of anthrax, an acute disease in humans and animals, which is highly lethal in some forms. *B. anthracis* is one of only a few bacteria that can form long-lived spores. *Y. pestis*, the causative agent of plague, is a Gram-negative facultative anaerobic bipolar-staining bacillus bacterium belonging to the family *Enterobacteriaceae*. Plague may be manifested in one of three forms: bubonic, pneumonic, and septicemic plague [106]. *Francisella tularensis* is a pathogenic species of Gram-negative bacteria that causes the zoonotic disease tularemia. *F. tularensis* is reported to be one of most infectious organisms known. It is an intracellular pathogen, replicating mainly in macrophages, and has also been reported in amoebae [186]. *Variola major* is the causative agent of smallpox. There has been no effective treatment developed for this disease, which has an average 30% mortality rate. Lassa virus, the causative agent of one type of hemorrhagic fever, infects more than 200,000 people per year causing more than 3,000 deaths with a mortality rate of about 15% among the hospitalized cases [51]. The selected Category A pathogens represent a range of environmental persistencies from a pathogen with a very low decay rate (*B.anthracis*), to several with high decay rates (*Y.Pestis, F. tularensis*, and Lassa), as well as one with a moderate decay rate (*Variola major*).

The objective of this study is to expand the framework that Hong et al. [85] developed for linking environmental concentrations of *B. anthracis* with human health risk by 1) including the effects of environmental attenuation, 2) considering a variety of different pathogens instead of a single one (*B. anthracis*), 3) taking account of contact exposure (ingestion or dermal risk) as well as inhalational exposure, and 4) conducting an uncertainty analysis and identifying key input uncertainties. Both detailed and reduced form solutions to the equations linking risk to environmental concentrations are developed, which could benefit in making risk-informed response decisions, such as determining when prophylactic antibiotics should be distributed, and whether or not a contaminated area should be cleaned up. Monte Carlo methods are used to assess uncertainty in the results and identify important uncertainties in input parameters so that future research may be directed towards reducing them.

4.2 Methods

4.2.1 Fate and transport model

In this study, an occupant is modeled as continuously present in a one-room office with a heating, ventilation, and air conditioning (HVAC) system (Figure 4-1). This person has the chance of inhaling aerosolized pathogens and ingesting pathogens deposited on the touched surfaces through the surface-hand-mouth transmission route. For *B. anthracis*, the ingestion risk is replaced by cutaneous risk since this was a more important exposure route than ingestion in the 2001 anthrax letter attacks [108]. A system of first-order differential equations is established to describe the fate and transport of

released pathogens (Equation 1). Pathogens are modeled as transitioning among 10 states: air, touched surfaces (horizontal surfaces from which spores may be re-suspended by human activities), tracked floor (horizontal surfaces from which spores may be re-suspended by walking or other activities), untracked floor (horizontal surfaces from which there is no re-suspension), walls, HVAC filter, the nasal passages, hands of an occupant of the office, all areas external to the room, and inactivated pathogens. Mathematically this is represented by:

$$\begin{pmatrix} \dot{M}_{air} \\ \dot{M}_{ts} \\ \dot{M}_{tf} \\ \dot{M}_{utf} \\ \dot{M}_{w} \\ \dot{M}_{f} \\ \dot{M}_{ec} \\ \dot{M}_{n} \\ \dot{M}_{h} \\ \dot{M}_{d} \end{pmatrix} = \begin{pmatrix} [(1-e)p-1]\frac{Q}{Vol} - (\lambda_{ts} + \lambda_{tf} + \lambda_{utf} + \lambda_{w} + \frac{Inh\ e_n}{Vol} + \gamma_{air}) & \mu_2 & \mu_2 & 0 & 0 & 0 & 0 & 0 & 0 & 0 \\ \lambda_{ts} & -(\mu_2 + \gamma_{ts} + r_{sh} f_{sh}) & 0 & 0 & 0 & 0 & 0 & r_{hs} f_{hs} & 0 \\ \lambda_{tf} & 0 & -(\mu_2 + \gamma_{tf}) & 0 & 0 & 0 & 0 & 0 & 0 \\ \lambda_{utf} & 0 & 0 & -\gamma_{utf} & 0 & 0 & 0 & 0 & 0 \\ \lambda_{w} & 0 & 0 & 0 & -\gamma_{w} & 0 & 0 & 0 & 0 \\ ep\frac{Q}{Vol} & 0 & 0 & 0 & 0 & -\gamma_{f} & 0 & 0 & 0 \\ (1-p)\frac{Q}{Vol} & 0 & 0 & 0 & 0 & 0 & -\gamma_{ec} & 0 & 0 \\ \frac{Inh\ e_n}{Vol} & 0 & 0 & 0 & 0 & 0 & 0 & -\gamma_{n} & 0 \\ 0 & r_{sh} f_{sh} & 0 & 0 & 0 & 0 & 0 & -(\gamma_{h} + r_{hs} f_{hs}) & 0 \\ \gamma_{air} & \gamma_{ts} & \gamma_{tf} & \gamma_{utf} & \gamma_{w} & \gamma_{f} & \gamma_{ec} & \gamma_{n} & \gamma_{h} & 0 \end{pmatrix} \begin{pmatrix} M_{air} \\ M_{ts} \\ M_{tf} \\ M_{utf} \\ M_{w} \\ M_{f} \\ M_{ec} \\ M_{n} \\ M_{h} \\ M_{d} \end{pmatrix} \quad \text{(Eq. 1)}$$

The numbers of spores in the compartments are denoted by M_{air} (air), M_{ts}, (touched surfaces), M_{tf}, (tracked floor), M_{utf}, (untracked floor), M_w (walls), M_f (filter), M_{ec} (external compartment), M_{ce} (ceiling), M_n (nasal passages), M_h (hands), and M_d (decay). Deposition from the air compartment is modeled as a first-order process with rate constants of λ_{ts} (deposition to touched surfaces), λ_{tf} (deposition to tracked floor), λ_{utf} (untracked floor), λ_w (walls), and λ_{ce} (ceiling). A second source of removal is by the HVAC system. The total air flow rate through the HVAC system is denoted by Q (units

of m^3/s), p (dimensionless) is the fraction of total air flow that is recirculated into the building by the HVAC system, e (dimensionless) is the efficiency of the filter at removing particles, and Vol is the volume of the room (m^3). Removal to the occupants' nasal passages is also modeled with Inh (m^3/s), denoting the breathing flow rate, and e_n (dimensionless), the efficiency of the nasal passages at removing particles. Removal by losing viability is modeled as a first order rate with separate decay rates for air and other surfaces, denoted by the subscripts γ_{air}, and γ_f. Resuspension from the tracked floor due to occupants walking and other activities is also modeled as a first order process with rate constant μ_2 (units of s^{-1}). The interactions between human and fomites are represented by hand-surface (r_{hs}) and surface- hand (r_{sh}) contact rates, as well as mass transfer fractions between hand to surface (f_{hs}), surface to hand (f_{sh}), and hand to mouth (f_{hm}).

The deposition rates can be expressed in terms of parameters representing the indoor air flow conditions [103, 131, 207]:

$$\lambda_{tf\,(utf)} = \frac{A_{tf\,(utf)}}{Vol} \times \frac{V_t}{1 - e^{-\frac{\pi V_t}{2\sqrt{Dk_e}}}} \qquad \text{(Eq. 2)}$$

$$\lambda_w = \frac{A_w}{Vol} \times \frac{2}{\pi} \sqrt{Dk_e} \qquad \text{(Eq. 3)}$$

$$\lambda_c = \frac{A_c}{Vol} \times \frac{V_t}{e^{\frac{\pi V_t}{2\sqrt{Dk_e}}} - 1} \qquad \text{(Eq. 4)}$$

$$V_t = \frac{gD^2(\rho_p - \rho_{air})}{18\mu_{air}} \qquad \text{(Eq. 5)}$$

where D is the particle's diffusivity, K_e is turbulence intensity, and V_t is particle settling velocity, which is given in Equation 5 as a function of the particle's diameter (D), the viscosity of air (μ_{air}), the density of the particle (ρ_p), and the density of air (ρ_{air}).

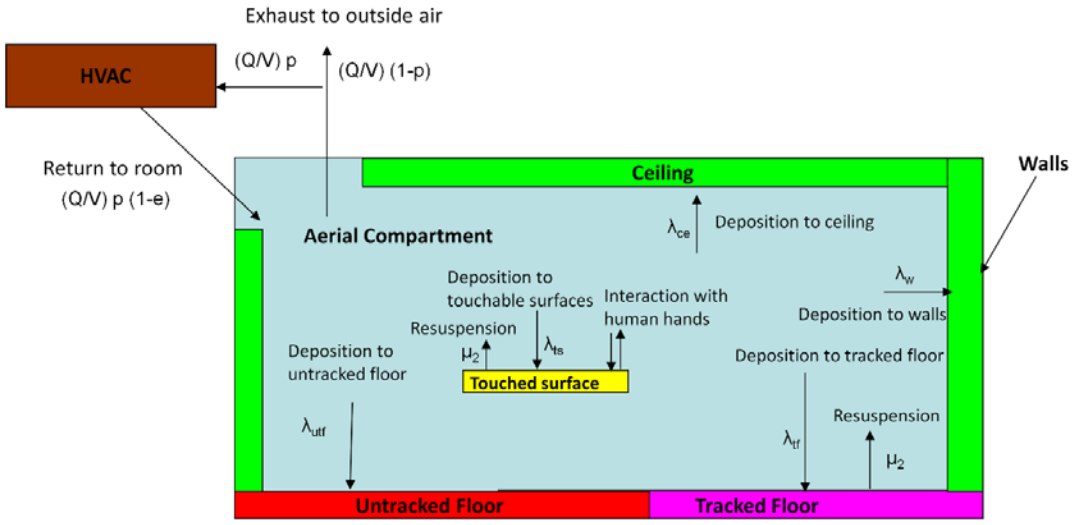

Figure 4-1 Schematic of model

4.2.2 Release scenarios

Two pathogen release scenarios are considered. In the first scenario, pathogens are released to the air compartment. The occupant directly inhales aerosolized pathogens and ingests the deposited ones via surface-hand-mouth contacts. Environmental concentrations measured at the end of the exposure period are used to characterize the risk from the past aerosol release, and as such it is termed the retrospective scenario. In the second scenario, pathogens are initially present on the touched surfaces, where they may be ingested by surface-hand-mouth contacts. In addition, human-caused resuspension introduces the pathogens into the air where they can be inhaled by the occupant. Environmental concentrations at the beginning of the exposure period are used to predict the future risk and as such the scenario is termed the prospective scenario. This scenario addresses the residual risk present after aerosolized particles have had the opportunity to deposit onto surfaces, a key issue in establishing a decontamination standard.

Solving Equation 1 yields the concentration of released pathogens in each compartment over time. The total exposure dose ($dose_t$) is composed of two sources: inhalation and ingestion. Based on Equation 6, the inhalation dose is obtained by integrating the inhalation rate (Inh) and the pathogen's air concentration (C_{air}) over the total exposure duration (t_2-t_1), while the ingestion dose equals the integral of the hand-mouth contact rate (r_{hm}), mass transfer fraction from hand to month during each contact (f_{hm}), the involved area of a human hand (A_h), and the pathogen's concentration on the hand (C_h) over the same exposure period:

$$dose_t = Inh\int_{t_1}^{t_2} C_{air}(t)dt + A_h r_{hm} f_{hm}\int_{t_1}^{t_2} C_h(t)dt \quad \text{(Eq. 6)}$$

For dermal contact, ingestion dose is replaced by the total amount of pathogen transferred to the hand from touched surfaces:

$$dose_t = Inh\int_{t_1}^{t_2} C_{air}(t)dt + r_{sh} f_{sh}\int_{t_1}^{t_2} C_{ts}(t)dt \quad \text{(Eq. 7)}$$

This equation is applied for *B. anthracis* instead of Equation 6, where C_{ts} is pathogen's concentration on the touched surface. However, separate dose-response coefficients are used for the different exposure pathways for anthrax. The dermal dose-response parameter is tuned so as to produce equal numbers of dermal and inhalation cases for the aerosol release scenario, as was observed in the 2001 attacks.

4.2.3 Dose-response functions

The exponential (Equation 7) and beta-Poisson (Equation 8) dose-response models, which have been widely used in microbial risk assessment [71], are used in this study:

$$P(dose_t) = 1 - e^{-Rdose_t} \quad \text{(Eq. 7)}$$

$$P(dose_t) = 1 - \left[1 + \frac{dose_t}{N_{50}} \times \left(2^{\frac{1}{\alpha}} - 1\right)\right]^{-\alpha} \quad \text{(Eq. 8)}$$

In Equations 7 and 8, P ($dose_t$) is the probability of positive response (infection,

illness, or death) for a population average dose, which allows for Poisson variability in individual exposure [71]. R is the parameter of the exponential dose-response model, N_{50} and α are the parameters of the beta-Poisson model. When the risk is relatively small, a first-order Taylor series can be used to approximate Equations 7 and 8 as [85]:

$$P(dose_t) \approx R dose_t \quad \text{(Eq. 7a)}$$

$$P(dose_t) \approx \frac{\alpha}{\beta} dose_t = \frac{\alpha}{(\frac{N_{50}}{2^{\frac{1}{\alpha}} - 1})} dose_t \quad \text{(Eq. 8a)}$$

This transformation can simplify the low dose risk estimation, which is where this approach is intended for use (i.e., for areas removed from the initial release where concentrations will be relatively uniform over spatial scales of interest. When the exposure dose is high, the full model (Equations 7 and 8) should be used.

4.2.4 Linking pathogen concentrations to risk

4.2.4.1 Retrospective scenario

Given that it is rarely possible to have real-time pathogen air concentrations during a biological attack, the objective in the retrospective scenario is to use surface samples to infer what exposure and risk resulted from the release. Thus, the following discussion develops relationships between pathogen concentrations on surfaces and average dose.

After an aerosol release, the amount of pathogens in the air (M_{air}), on the touched surfaces (M_{ts}), and on occupants' hands (M_h) can be acquired by solving Equation 9, which is obtained by separating out the compartments which exchange microbes from Equation 1, with the resuspension process omitted because of its minimal impact over the short time period required for the aerosol release to disperse (hours) [85]:

$$\begin{pmatrix} \dot{M}_{air} \\ \dot{M}_{ts} \\ \dot{M}_{h} \end{pmatrix} = \begin{pmatrix} [(1-e)p-1]\frac{Q}{Vol} - (\lambda_{ts} + \lambda_{tf} + \lambda_{utf} + \lambda_{w} + \frac{Inh\ \ e_n}{Vol} + \gamma_{air}) & 0 & 0 \\ \lambda_{ts} & -(\gamma_{ts} + r_{sh} f_{sh}) & r_{hs} f_{hs} \\ 0 & r_{sh} f_{sh} & -(\gamma_h + r_{hs} f_{hs}) \end{pmatrix} \begin{pmatrix} M_{air} \\ M_{ts} \\ M_h \end{pmatrix} \quad \text{(Eq. 9)}$$

The number of pathogens in the air, on the touched surface, and on hands are provided by Equation 10 to 12 as solutions to Equation 9.

$$M_{air} = M_{air0} \mathrm{e}^{-\mathrm{At}} \quad \text{(Eq. 10)}$$

$$M_{ts} = M_{air0} \left\{ \frac{AB-BF}{e^{At}\Omega} - \frac{(AB-BF)cosh(\frac{\Theta}{2}t)}{e^{\frac{C+F}{2}t}\Omega} + \frac{(C-F)(AB-BF)\sinh(\frac{\Theta}{2}t) + 2BE\sinh(\frac{\Theta}{2}t)e}{e^{\frac{C+F}{2}t}\Omega\Theta} \right\} \quad \text{(Eq. 11)}$$

$$M_h = \frac{BEM_{air0}}{\Omega} \left\{ \frac{2A-C-F+\Theta}{2e^{(\frac{C+F+\Theta}{2})t}\Theta} - \frac{C-2A+F+\Theta}{2e^{(\frac{C+F-\Theta}{2})t}\Theta} - e^{-At} \right\} \quad \text{(Eq. 12)}$$

where sinh and cosh are hyperbolic trigonometric functions. Symbols Θ and Ω stand for the common terms $\sqrt{(C-F)^2 + 4Ee}$ and $Ee - A^2 + AC + AF - CF$ in Equations 11 and 12, respectively. The coefficients represented by A to F are listed below:

$$A = -[(1-e)p-1]\frac{Q}{Vol} + (\lambda_{ts} + \lambda_{tf} + \lambda_{utf} + \lambda_{w} + \frac{Inh\ \ e_n}{Vol} + \gamma_{air})$$

$$B = \lambda_{ts}$$

$$C = \gamma_{ts} + r_{sh} f_{sh}$$

$$D = r_{hs} f_{hs}$$

$$E = r_{sh} f_{sh}$$

$$F = \gamma_h + r_{hs} f_{hs}$$

Combining Equations 10, 12 with Equation 6, the total exposure dose from time t_1 to t_2 can be written in terms of the amount of pathogens released (Equation 13).

$$\begin{aligned} dose_t &= dose_{inh} + dose_{ing} \\ &= \int_{t_1}^{t_2} \left(\frac{Inh}{Vol} M_{air} + r_{hm} f_{hm} M_h\right) dt \\ &= M_{air0} \left\{ \frac{2BEH}{C+F} \left(\frac{(C-2A+F) - \frac{2(C-A+F)\Theta^2}{(4Ee+\Theta(C+F)+(C-F)^2)}}{2e^{\frac{C+F+\Theta}{2}t}\Theta\Omega} - \frac{(C-2A+F) - \frac{2(C-A+F)\Theta^2}{(4Ee-\Theta(C+F)+(C-F)^2)}}{2e^{\frac{C+F-\Theta}{2}t}\Theta\Omega} \right) - \left(\frac{G}{A} - \frac{BEH}{A\Omega}\right) e^{-At} \right\} \Bigg|_{t_1}^{t_2} \end{aligned}$$

(Eq. 13)

where the coefficients represented by G and H are listed below:

$$G = \frac{Inh}{Vol}$$

$$H = r_{hm} f_{hm}$$

The overall risk is composed of inhalation risk and ingestion risk. In this study, it is assumed that these two types of risk are independent of each other; in this case the overall risk is expressed in Equation 14:

$$Risk_{overall} = 1 - (1 - Risk_{inh})(1 - Risk_{ing}) \qquad \text{(Eq. 14)}$$

In reality there is little evidence to assess the joint effects of inhalation and ingestion exposures, but this assumption is probably most defensible at low risk levels when the probability of successful colonization by both routes is low.

Equations 13 and 14 solve the forward problem of estimating risk from a known release amount. The inverse problem is to estimate the release amount from measured environmental concentrations. The amount of released pathogens (M_{air0}), can be estimated by Equation 11, if the number of pathogens deposited on the touched surfaces (M_{ts}) can be acquired from surface sampling and the time after release (t) is known. However, the mass on touched surface is influenced by many parameters such as touch rate and transfer rate, which are generally highly uncertain. The mass on the untracked floor is most suitable for estimating the release quantity as it provides an integration of air concentration values over time without human interference. This can be obtained by taking the expression from the fourth row of Equation 1:

$$\frac{dM_{utf}}{dt} = \lambda_{utf} e^{-At} M_{airo} - \gamma_{utf} M_{utf} \qquad \text{(Eq. 15)}$$

and integrating it to give the release quantity, where t stands for the elapsed time when measurements are taken:

$$M_{airo} = \frac{M_{utf}(A - \gamma_{utf})}{\lambda_{utf}\left(e^{-\gamma_{utf} t} - e^{-At}\right)} \qquad \text{(Eq. 16)}$$

Once the release quantity (M_{air0}) is known, Equation 13 can be used to estimate risk. Concentrations in the compartments omitted from Equation 9 (i.e., the compartments that do not transfer microbes to other compartments, namely HVAC filters,

walls, nasal passages, and the external compartments) can be obtained by integrating the produce of the air concentration and the transfer rates from the air over time.

4.2.4.2 Prospective scenario

The prospective scenario considers a case where the initial aerosol release has dissipated. However, the time scale for attenuation of microbes can be much longer on surfaces than in the air (i.e., pathogens on surfaces are not subject to attenuation by deposition or by air exchange with the exterior of the building). Thus, much of the longer-term risk to occupants will come from microbes on surfaces as surface can serve as a reservoir both for re-suspension into the air compartment and for exposure via fomite contact. In such cases surfaces could be sampled to assess whether a building is suitable for re-occupancy. Thus, the prospective scenario can be thought of as a re-occupancy assessment. The initial conditions are that Category A pathogens are present on the touched surfaces in a quantity equal to the area of the touched surfaces (A_{surf}) multiplied by the corresponding concentration (C_{surf}), which would be estimated from surface sampling (Equation 17). Thus the initial conditions can be expressed as:

$$Init = \begin{bmatrix} M_{air} \\ M_{ts} \\ M_{tf} \\ M_{h} \end{bmatrix} = \begin{bmatrix} 0 \\ C_{ts}A_{ts} \\ 0 \\ 0 \end{bmatrix} \quad \text{(Eq. 17)}$$

Due to the longer time scale associated with the prospective scenario, human-caused resuspension cannot be omitted. Thus, the tracked floor compartment is included in the system of equations to be solved:

$$\begin{pmatrix} \dot{M}_{air} \\ \dot{M}_{ts} \\ \dot{M}_{tf} \\ \dot{M}_{h} \end{pmatrix} = \begin{pmatrix} [(1-e)p-1]\frac{Q}{V} - (\lambda_{ts} + \lambda_{tf} + \lambda_{utf} + \lambda_{w} + \frac{Inh\, e_n}{V} + \gamma_{air}) & \mu_2 & \mu_2 & 0 \\ \lambda_{ts} & -(\mu_2 + \gamma_{htf} + r_{sh} \times f_{sh}) & 0 & r_{hs} \times f_{hs} \\ \lambda_{tf} & 0 & -\mu_2 & 0 \\ 0 & r_{sh} \times f_{sh} & 0 & -\gamma_h - r_{hs} \times f_{hs} \end{pmatrix} \begin{pmatrix} M_{air} \\ M_{ts} \\ M_{tf} \\ M_{h} \end{pmatrix} \quad \text{(Eq. 18)}$$

Since taking the resuspension into account increases the solutions' complexity, it is less cumbersome to express the solution (Equations 20 to 21) in terms of the eigenvalues ($\vec{D}$) and eigenvectors ($\vec{\nu}$) of the following matrix [153]:

$$\begin{pmatrix} [(1-e)p-1]\frac{Q}{V} - (\lambda_{ts} + \lambda_{tf} + \lambda_{utf} + \lambda_{w} + \frac{Inh\, e_n}{V} + \gamma_{air}) & \mu_2 & \mu_2 & 0 \\ \lambda_{ts} & -(\mu_2 + \gamma_{htf} + r_{sh} \times f_{sh}) & 0 & r_{hs} \times f_{hs} \\ \lambda_{tf} & 0 & -\mu_2 & 0 \\ 0 & r_{sh} \times f_{sh} & 0 & -\gamma_h - r_{hs} \times f_{hs} \end{pmatrix} \quad \text{(Eq. 19)}$$

$$M_{air} = C_1 \nu_{1,1} e^{-D_{1,1}t} + C_2 \nu_{1,2} e^{-D_{2,2}t} + C_3 \nu_{1,3} e^{-D_{3,3}t} + C_4 \nu_{1,4} e^{-D_{4,4}t} \quad \text{(Eq. 20)}$$

$$M_{ts} = C_1 \nu_{2,1} e^{-D_{1,1}t} + C_2 \nu_{2,2} e^{-D_{2,2}t} + C_3 \nu_{2,3} e^{-D_{3,3}t} + C_4 \nu_{2,4} e^{-D_{4,4}t} \quad \text{(Eq. 21)}$$

$$M_{tf} = C_1 \nu_{3,1} e^{-D_{1,1}t} + C_2 \nu_{3,2} e^{-D_{2,2}t} + C_3 \nu_{3,3} e^{-D_{3,3}t} + C_4 \nu_{3,4} e^{-D_{4,4}t} \quad \text{(Eq. 22)}$$

$$M_{h} = C_1 \nu_{4,1} e^{-D_{1,1}t} + C_2 \nu_{4,2} e^{-D_{2,2}t} + C_3 \nu_{4,3} e^{-D_{3,3}t} + C_4 \nu_{4,4} e^{-D_{4,4}t} \quad \text{(Eq. 23)}$$

where $\vec{C}$ is a vector of the coefficients determined by the ratio of the vector of initial conditions ($\overrightarrow{Init}$) and eigenvectors ($\vec{\nu}$) of Equation 19a (Equation 24):

$$\vec{C} = \vec{\nu}^{-1} \overrightarrow{Init} \quad \text{(Eq. 24)}$$

Equations 20 to 23 provide the concentrations of the pathogen on different surfaces over time. The total exposure dose can be calculated via integration. To conservatively estimate exposure dosage, one may use the maximum exposure duration which is achieved if $t_1=0$ and $t_2=\infty$.

$$
\begin{aligned}
dose_{t\_\max} &= dose_{inh} + dose_{ing} \\
&= \int_0^{\infty} \left(\frac{Inh}{Vol} M_{air} + r_{hm} f_{hm} M_h\right) dt \\
&= \int_0^{\infty} \left(\frac{Inh}{Vol} \sum_{i=1}^{4} C_i \nu_{1,i} e^{-D_{i,i}t} + r_{hm} f_{hm} \sum_{i=1}^{4} C_i \nu_{4,i} e^{-D_{i,i}t}\right) dt \\
&= \frac{Inh}{Vol} \sum_{i=1}^{4} \frac{C_i \nu_{1,i}}{D_{i,i}} + (r_{hm} f_{hm}) \sum_{i=1}^{4} \frac{C_i \nu_{4,i}}{D_{i,i}}
\end{aligned}
\qquad \text{(Eq. 25)}
$$

The equations derived in this section provide the exposure input for dose-response models (Equations 7 and 8) and thereby link the surface concentration of a pathogen with an occupant's future risk. Solving for prospective risk requires working out the eigenvectors for Equation 19 and then inverting the resulting matrix to obtain the solution (Equation 24). Solving for retrospective risk involves essentially the same procedure, although in our presentation these operations have been shown without matrix notation. In order to simplify the solution procedure, one may seek to further decouple portions of the system of equations to develop approximate solutions that do not require matrix operations. This procedure is shown in Appendix I, and Equations 26 and 27 (a is for ingestion risk, b is for dermal contact risk) are the resulting approximate solutions.

$$
\begin{aligned}
risk_{retro} &= 1 - (1 - risk_{inh\_retro})(1 - risk_{ing\_retro}) \\
&\approx 1 - (1 - k \times dose_{inh\_retro})(1 - k \times dose_{ing\_retro}) \\
&\approx 1 - \left[1 - k \times M_{airo} \frac{Inh}{Vol} \times \frac{1}{\phi_{retro}} \left(1 - e^{-\phi_{retro} \times 480}\right)\right] \left[1 - k \times M_{airo} r_{hm} f_{hm} \left[r_{sh} f_{sh} \left(\lambda_{ts} \frac{1}{\phi_{retro}} (1 - e^{-\phi_{retro} \times 480})\right) \frac{1}{\phi_{pros}} (1 - e^{-\phi_{pros} \times 480})\right] \frac{1}{\phi_{hand}} (1 - e^{-\phi_{hand} \times 480})\right]
\end{aligned}
$$

(Eq. 26)

$$
\begin{aligned}
risk_{pros\_ing} &= 1-(1-risk_{inh\_pros})(1-risk_{ing\_pros}) \\
&\approx 1-(1-k\times dose_{inh\_pros})(1-k\times dose_{ing\_pros}) \\
&\approx 1-(1-k\times M_{tso}\frac{\frac{\mu_2}{\phi_{pros}}\frac{Inh}{Vol}\frac{1}{\phi_{retro}}}{(1-\frac{r_{sh}f_{sh}}{\phi_{pros}}\frac{r_{hs}f_{hs}}{\phi_{hand\_ing}})})(1-k\times M_{tso}\frac{\frac{r_{sh}f_{sh}}{\phi_{pros}}\frac{r_{hm}f_{hm}}{\phi_{hand\_ing}}}{(1-\frac{r_{sh}f_{sh}}{\phi_{pros}}\frac{r_{hs}f_{hs}}{\phi_{hand\_ing}})})
\end{aligned}
\quad \text{(Eq. 27a)}
$$

$$
\begin{aligned}
risk_{pros\_dermal} &= 1-(1-risk_{inh\_pros})(1-risk_{\mathrm{dermal}\_pros}) \\
&\approx 1-(1-k\times dose_{inh\_pros})(1-k\times dose_{\mathrm{dermal}\_pros}) \\
&\approx 1-(1-k\times M_{tso}\frac{\frac{\mu_2}{\phi_{pros}}\frac{Inh}{Vol}\frac{1}{\phi_{retro}}}{(1-\frac{r_{sh}f_{sh}}{\phi_{pros}}\frac{r_{hs}f_{hs}}{\phi_{hand\_dermal}})})(1-k\times M_{tso}\frac{\frac{r_{sh}f_{sh}}{\phi_{pros}}\frac{1}{\phi_{hand\_dermal}}}{(1-\frac{r_{sh}f_{sh}}{\phi_{pros}}\frac{r_{hs}f_{hs}}{\phi_{hand\_dermal}})})
\end{aligned}
\quad \text{(Eq. 27b)}
$$

where $r_{hm}f_{hm}$ is set to 1 for dermal contact, and ϕ_{retro}, ϕ_{pros}, and ϕ_{hand} are given by:

$$\phi_{retro} = \lambda_{ts} + \lambda_{tf} + \lambda_{utf} + \lambda_w + \frac{Inhe_n}{Vol} + \gamma_{air} + [1-(1-e)p]\frac{Q}{Vol} \quad \text{(Eq. 28)}$$

$$\phi_{pros} = \mu_2 + \gamma_{fomite} + r_{sh}f_{sh} \quad \text{(Eq. 29)}$$

$$\phi_{hand\_ing} = r_{hm}f_{hm} + \gamma_{fomite} + r_{hs}f_{hs} \quad \text{(Eq. 30a)}$$

$$\phi_{hand\_dermal} = \gamma_{fomite} + r_{hs}f_{hs} \quad \text{(Eq. 30b)}$$

For the beta-Poisson model these equations would hold at low dose, except that R would be replaced by α/β. At higher doses (where the Taylor series linearization does not hold) one would compute the exposure dose using Equations K and N from the Appendix C, and then input this dose into the appropriate dose response model.

4.2.5 Model Inputs

Environmental decay rates, best fit dose-response models, and dose response parameters for different pathogens are listed in Tables 4-1 and 4-2, while other parameters such as the dimensions of the room, the operational parameters of the HVAC system, the deposition velocities of released pathogens, etc. are included in Table 4-3. Since the particle size of a pathogen affects its deposition velocity, resuspension rate, filter removal, and even dose-response coefficient [11], this study considers four different aerodynamic diameters: 1 μM, 3 μM, 5 μM, and 10 μM.

Table 4-1 Category A Pathogen's Environmental Persistency

Pathogen	Averaged decay rate in the air (γ_{air}) (hr^{-1})	Range of decay rate in the air (γ_{air}) (hr^{-1})[a]	Condition	Source	Averaged decay rate on fomite (γ_f) (hr^{-1})	Range of decay rate on the fomite (γ_f) (hr^{-1})[a]	Condition	Source
B. anthracis	8.16×10^{-5}	(1.11×10^{-5}, 1.97×10^{-4})	NA	[26, 124]	3.36×10^{-5}	(1.92×10^{-5}, 4.64×10^{-5})	NA	[26, 68, 134, 179]
Y. pestis	2.75	(2.10, 3.49)	T=26°C, rH=20-87%	[205]	4.55×10^{-1}	(0.04, 1.24)	T=11-22°C, rH=30-55% metal, steel, glass, paper, and Polyethylene	[154, 204]
F. tularensis	3.27	(0.55, 9.20)	T=20-40°C, rH=85%	[38, 39, 58]	2.39×10^{-1}	(0.01, 0.46)	T=25-37°C, rH=10-100% on metal	[204]
Variola major	4.55×10^{-2}	(1.00×10^{-2}, 1.30×10^{-1})	T=10-34°C, rH=20-80%	[73, 74]	6.89×10^{-3}	(5.45×10^{-3}, 9.95×10^{-3})	T=25-37°C, rH=3-96% on glass	[112]
Lassa	2.6	(0.78, 4.14)	T=24-28°C, rH=30-80%	[177]	7.67×10^{-1}[b]	(0.68, 0.92)	T=20°C, rH=NA on aluminum	[72]

a. Uniform distribution is assumed between the maximum and minimum values.
b. Due to the lack of information on Lassa, the average of the decay rates of *Bunyaviridae hantavirus*, Sicilian virus Sabin, and Crimean-Congp on fomites are used for Lassa.

Table 4-2 Best Fit Dose-Response Model

Pathogen	Strain information	Exposed animal and route	Dose-response function type	Best-fit Virulence coefficient[a]	Ranges of virulence coefficients (95% Confidence Interval)	Distributions of virulence coefficients	Source
B. anthracis[b]	ATCC 6605	Female Hartley guinea pigs (250 to 300 g), intranasal	Exponential	7.15×10^{-6}	$(6.26\times10^{-6}, 7.43\times10^{-6})$	Normal distribution $(6.93\times10^{-6}, 3.98\times10^{-7})$	[3]
Y. pestis	CO92	C57BL/6 mice, intranasal	Exponential	1.02×10^{-3}	$(9.87\times10^{-4}, 1.05\times10^{-3})$	Normal distribution $(1.02\times10^{-3}, 1.91\times10^{-5})$	[106]
F. tularensis	SCHU S-4	Monkey (4000-5000g), aerosol	Exponential	5.32×10^{-2}	$(5.28\times10^{-2}, 5.36\times10^{-2})$	Normal distribution $(5.32\times10^{-2}, 2.22\times10^{-4})$	[43][c]
Variola major	Yamada	Swiss Webster albino mice (age from 2 hr to 6 days), intraperitoneal	Beta-Poisson	2.31×10^{-6}	$(8.19\times10^{-7}, 4.80\times10^{-6})$	Normal distribution $(2.65\times10^{-6}, 1.21\times10^{-6})$	[113][d]
Lassa	NA	Out-bred Hartley guinea pigs (180 to 300g), aerosol	Beta-Poisson	3.58×10^{-2}	$(4.16\times10^{-4}, 5.59\times10^{-1})$	Log-Normal distribution (-1.69, 0.80)	[177][e]

a. In exponential dose-response model, k is used as virulence coefficient, while in beta-Poisson dose-response model, the ratio of α/β is used as virulence coefficient.
b. The intestinal risk is replaced by cutaneous risk since the fractions of inhalational anthrax and cutaneous anthrax were the same in the 2001 anthrax letters attacks [108]
c. The data for 2.1 μm particles are used.
d. The data for 4.5 μm or less in diameter are used.
e. The data for the age group of 5 days and above are used.

Table 4-3 Model Inputs

Symbol	Meaning	Units	Value		Source
V	Room dimensions	m^3	5.6×5.6×2.5		Assumed a typical office [59, 162]
A_{ts}	Area-touchable surfaces	m^2	5.6×5.6×0.75×0.25		
A_{tf}	Area-tracked floor	m^2	5.6×5.6×0.75×0.75		
A_{utf}	Area-untracked floor	m^2	5.6×5.6×0.25		
A_{ce}	Area- ceiling	m^2	5.6×5.6		
A_w	Area- wall	m^2	5.6×2.5×4		
A_f	Filter area	m^2	3.8×10^{-2} (2.8×10^{-2}-5.6×10^{-2})		*Q*/A = 137m/min (91-183 m/min)
A_n	Area of nasal passages	m^2	0.8		[104]
A_h	Area of hand touched surface	m^2	2.0×10^{-3}		Authors' assumption
ACH	Air changes per hour	hr^{-1}	4		[8]
Q	Discharge	m^3/s	0.087		Q = V×ACH/3600 (in seconds)
f	Proportion tracked		0.75		[8]
Init	Amount of released pathogens	Count	1.0×10^4		Authors' assumption
D	Particle diffusivity	m^2/s	D=1μM	2.8×10^{-11}	Estimated from [130]
			D=3μM	8.5×10^{-12}	
			D=5μM	5.0×10^{-12}	
			D=10μM	2.5×10^{-12}	
e	Filter efficiency		D=1μM	0.098	[162]
			D=3μM	0.49	
			D=5μM	0.74	
			D=10μM	0.88	

Table 4-3 Model Inputs (Continued)

Symbol	Meaning	Diameter	Unit	Value scale					
				Lower bound	Source	Upper bound	Source	Input value	Source
e_n	Nasal passages particle remove efficiency	1μM		0.02	[104]	0.25	[161]	0.14	Midpoint of range
		3μM		0.22		0.68		0.45	
		5μM		0.42		0.81		0.62	
		10μM		0.62		0.91		0.77	
μ_2	Resuspension rate	1μM	s^{-1}	1.2×10^{-10}	[162, 185]	3.3×10^{-8}	[162, 185]	3.3×10^{-8}	[162, 185]
		3μM		1.7×10^{-7}		1.7×10^{-6}		5.3×10^{-7}	
		5μM		1.1×10^{-6}		3.3×10^{-6}		2.2×10^{-7}	
		10μM		8.8×10^{-7}		9.4×10^{-6}		1.1×10^{-6}	
Inh	Breathing rate		m^3/hr	0.8	[101]	2.0	[101]	1.02	[101]
p	Recirculation fraction			0	[8]	1	[8]	0.75	[162]
ρ	Density of particle		g/cm^3	1.0	Authors' assumption	3.0	Authors' assumption	1.0	Authors' assumption
K_e	Turbulence intensity		s^{-1}	2.60×10^{-2}	[207]	4.50×10^{-1}	[207]	2.40×10^{-1}	Midpoint of range

Table 4-3 Model Inputs (Continued)

Symbol	Meaning (Unit)	Upper bound	Source	Lower bound	Source	Best estimate	Source
f_{h-s}	Mass transfer fraction from hand to surface during each contact	0.338	[5]	0.010	[6]	0.174	Middle point
f_{s-h}	Mass transfer fraction from surface to hand during each contact	0.658	[141]	0.008	[6]	0.333	Middle point
f_{h-m}	Mass transfer fraction from hand to mouth during each contact	0.410	[141]	0.330	[141]	0.350	[132]
r_{h-m}	Hand-mouth contacting rate (hr^{-1})	8	Authors' assumption	5	Authors' assumption	8	[132]
r_{h-s}	Hand-surface contacting rate (hr^{-1})	6	Authors' assumption	3	Authors' assumption	6	Authors' assumption

4.3 Results

Figure 4-2 presents the inhalation, ingestion and overall risks associated with the aerosol release (i.e., the retrospective scenario) of 1 micron Category A pathogens. The overall risk matches the inhalation risk, indicating that risk from inhalation is the main component of overall risk. Particle deposition drives the time required for this risk to reach steady state. Hence, the time to reach this asymptote is the same for different pathogens of the same size.

Figure 4-3 presents different types of risks associated with the presence of 1 micron Category A pathogens on surfaces (i.e., the prospective scenario), which indicates that risk from ingestion (dermal contact for *B. anthracis*) is the main component of overall risk. In Figure 4-3, the time scale over which each pathogen's overall risk reaches its asymptote varies over 4 orders of magnitude, which can be explained by the huge variability among pathogen attenuation rates.

To summarize which exposure routes dominate under which conditions, Figure 4-4 presents the ratio of accumulated inhalation and ingestion exposure. If pathogens are aerosolized (retrospective scenario), the dominant exposure route is inhalation (see also Figure 4-2), because inhalation is more significant for small particle sizes, which remain in the air longer before settling. If pathogens are initially present on a surface (prospective scenario), the dominant exposure route is ingestion (see also Figure 4-3), and this trend is most significant for small particle sizes as they are least prone to resuspension.

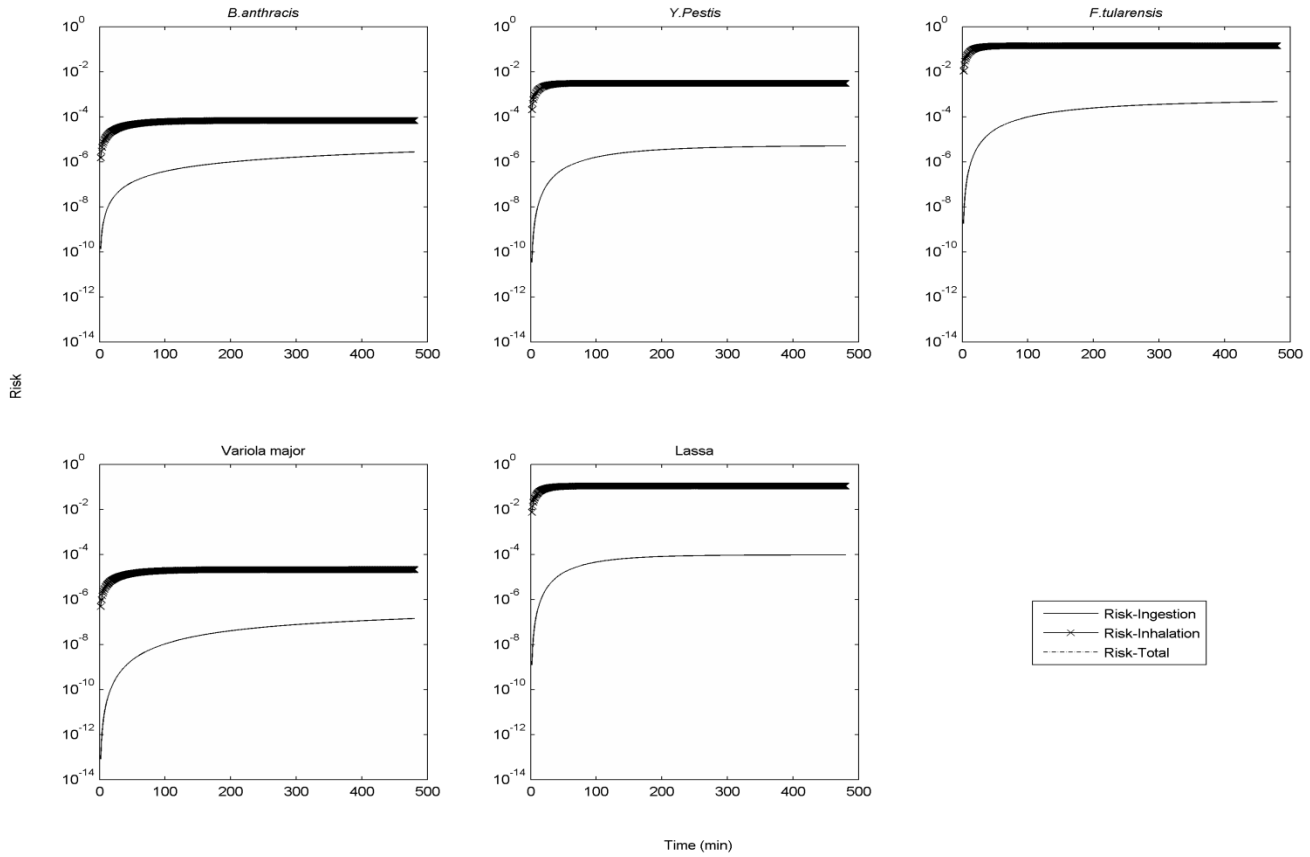

Figure 4-2 Different types of risks associated with aerosol release of 1 micron Category A pathogens.

(Release quantity is 1000 unclumped pathogens. For *B. anthracis*, the ingestion risk is replaced by cutaneous risk since the fractions of inhalational anthrax and cutaneous anthrax were the same in the 2001 anthrax letters attacks[108])

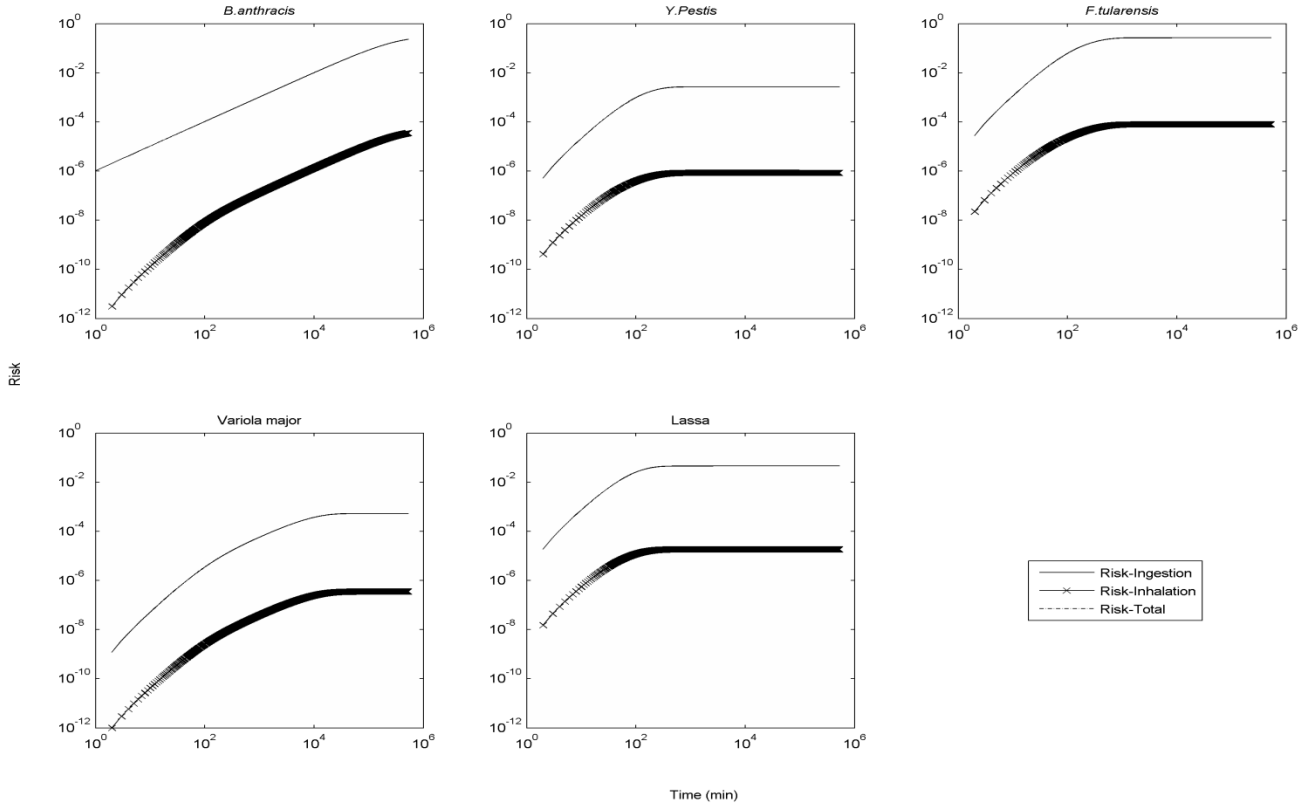

Figure 4-3 Different types of risks associated with surface release of 1 micron Category A pathogens.

(Release quantity is 1000 unclumped pathogens. For *B. anthracis*, the ingestion risk is replaced by cutaneous risk since the fractions of inhalational anthrax and cutaneous anthrax were the same in the 2001 anthrax letters attacks [108])

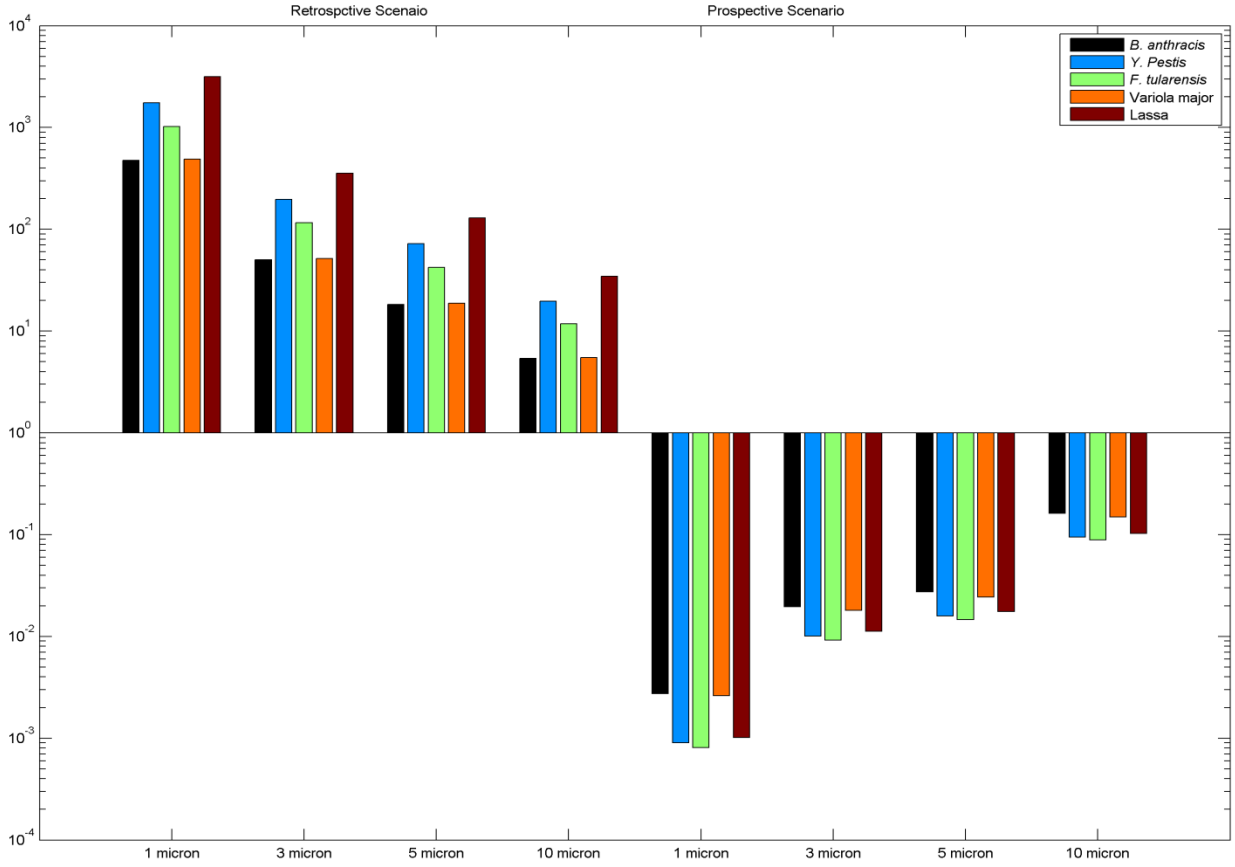

Figure 4-4 The ratio of accumulative inhalation and ingestion exposure.

4.3.1 Linking pathogen concentrations to risk

Another application of the model is to link measured pathogen concentrations on the surfaces with health risk. In the case of a persistent pathogen, a surface concentration reflects a fraction of the integral of the air concentration (provided there has been no resuspension from the surface). In contrast, for a pathogen subject to environmental decay, surface concentrations reflect both the integrated air concentrations and surface decay over time. The relationship between surface concentration and accumulated (retrospective) dose changes as pathogen concentrations attenuate on the surface over time. As deposited microbes decay, each surviving microbe becomes indicative of a larger number having been present previously. Figure 4-5, which depicts the retrospective risk for a concentration of 10 pathogens per m^2 on an HVAC filter, illustrates this. If one finds the concentration of Lassa virus particles is 10 pathogens per m^2 with a diameter of 1 μm on an HVAC system filter 1 hour after a release, this implies that occupants were subject to a risk of 1.0×10^{-3} due to the past 1 hour of exposure. The same concentration found 4 hours after the release would imply a risk close to 1.0×10^{-2}, as fewer of the deposited virus remain viable after 4 hours. In reality it may not be realistic to detect pathogens in the environment on anything approaching the time scale of several hours, but this serves as an example of how great a challenge it is to use environmental samples to characterize risks associated with a pathogen that attenuates in the environment. In contrast risks associated a given concentration of *B. anthracis* (a persistent microbe) are relatively constant over time.

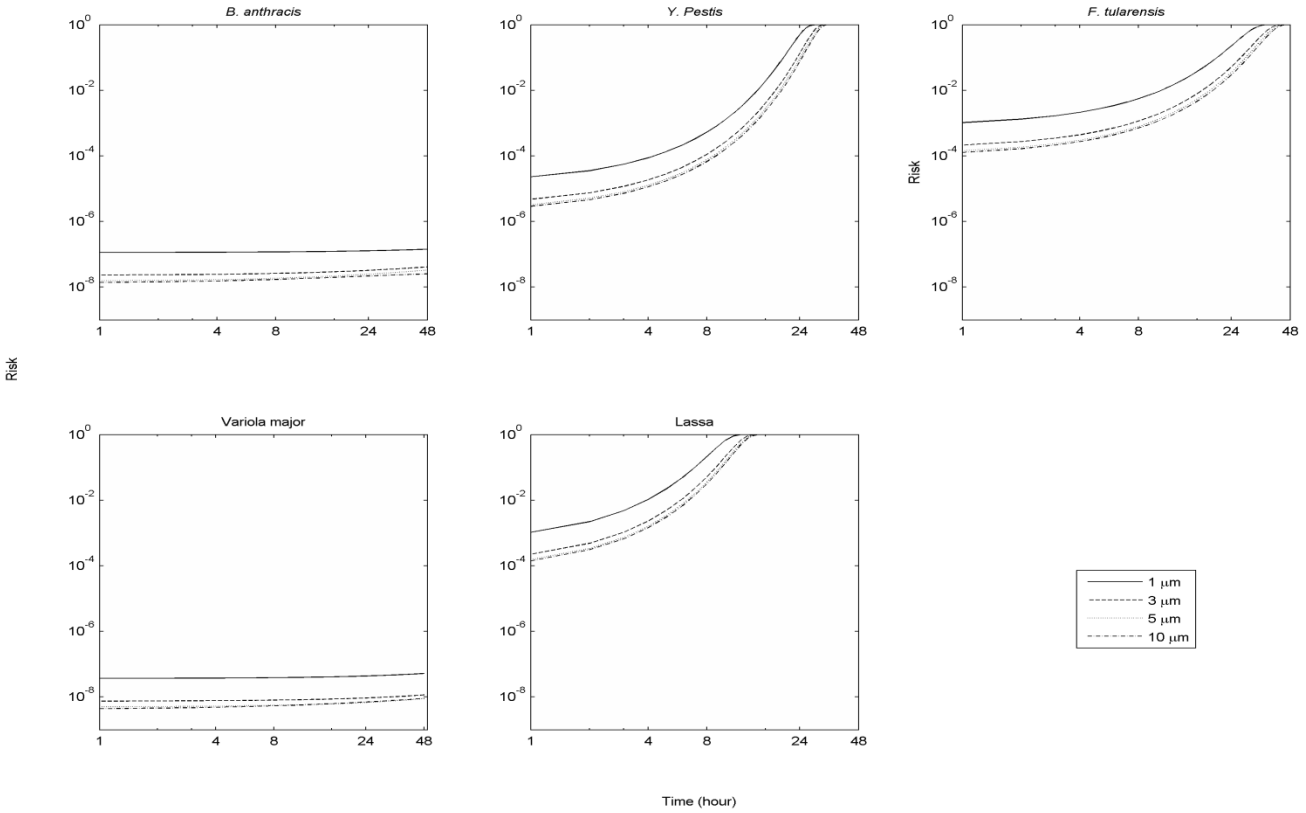

Figure 4-5 Relationship between risks to the exposed people and pathogen concentration identified from the HVAC filter.

(A concentration of 10 organisms/m^2 was found at HVAC filter at different time after an aerosol release.)

The results of this modeling can be summarized in a series of charts that link surface concentration to previous exposure risk for different time periods (Figures 4-6 to 4-10). The slope of each figure is proportional to the pathogen's dose-response coefficient. The difference between curves for the same pathogen for different time periods reflects the environmental persistence of the pathogen. A rapidly decaying pathogen will have widely separated curves to reflect that the same concentration of pathogens remaining after a longer time period implies a higher exposure risk (i.e., each pathogen remaining indicates that a greater number were present during the earlier part of the exposure period), while a persistent pathogen will have closely spaced curves as the risk to concentration relationship is relatively constant over time.

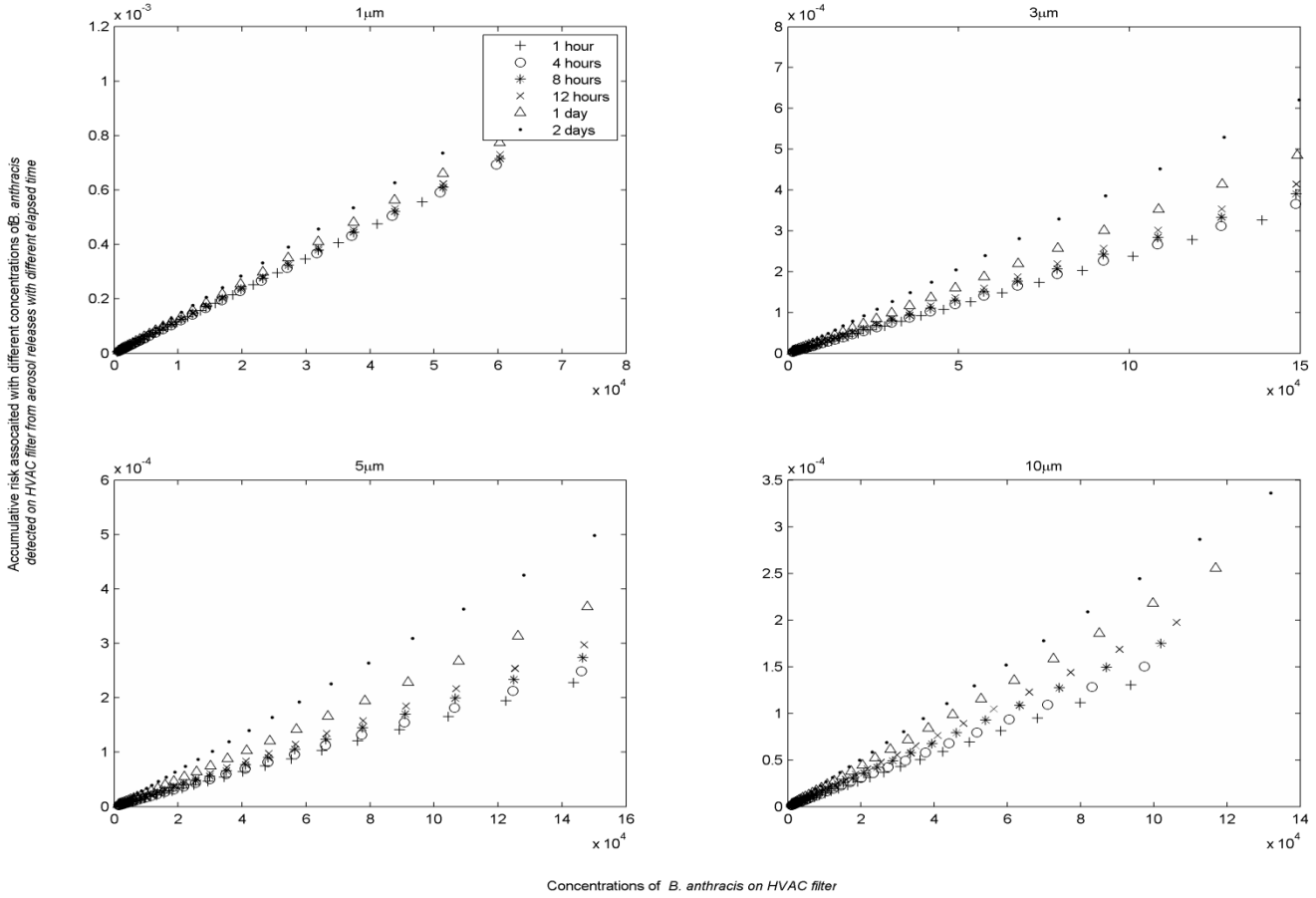

Figure 4-6. Retrospective risks associated with *B. anthracis* HVAC concentrations after an aerosol release.

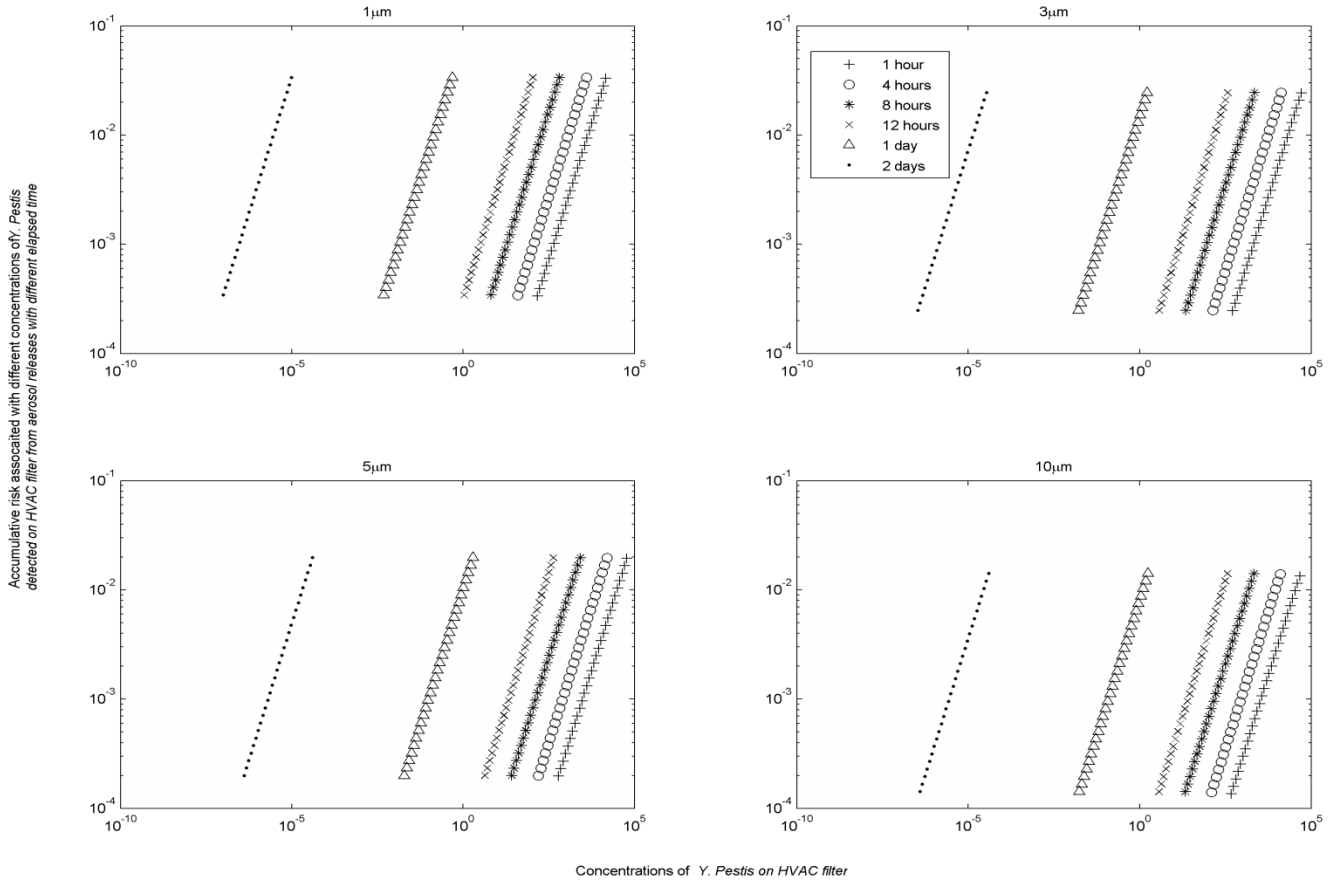

Figure 4-7. Cumulative retrospective risks associated with *Y. pestis* HVAC concentrations after an aerosol release.

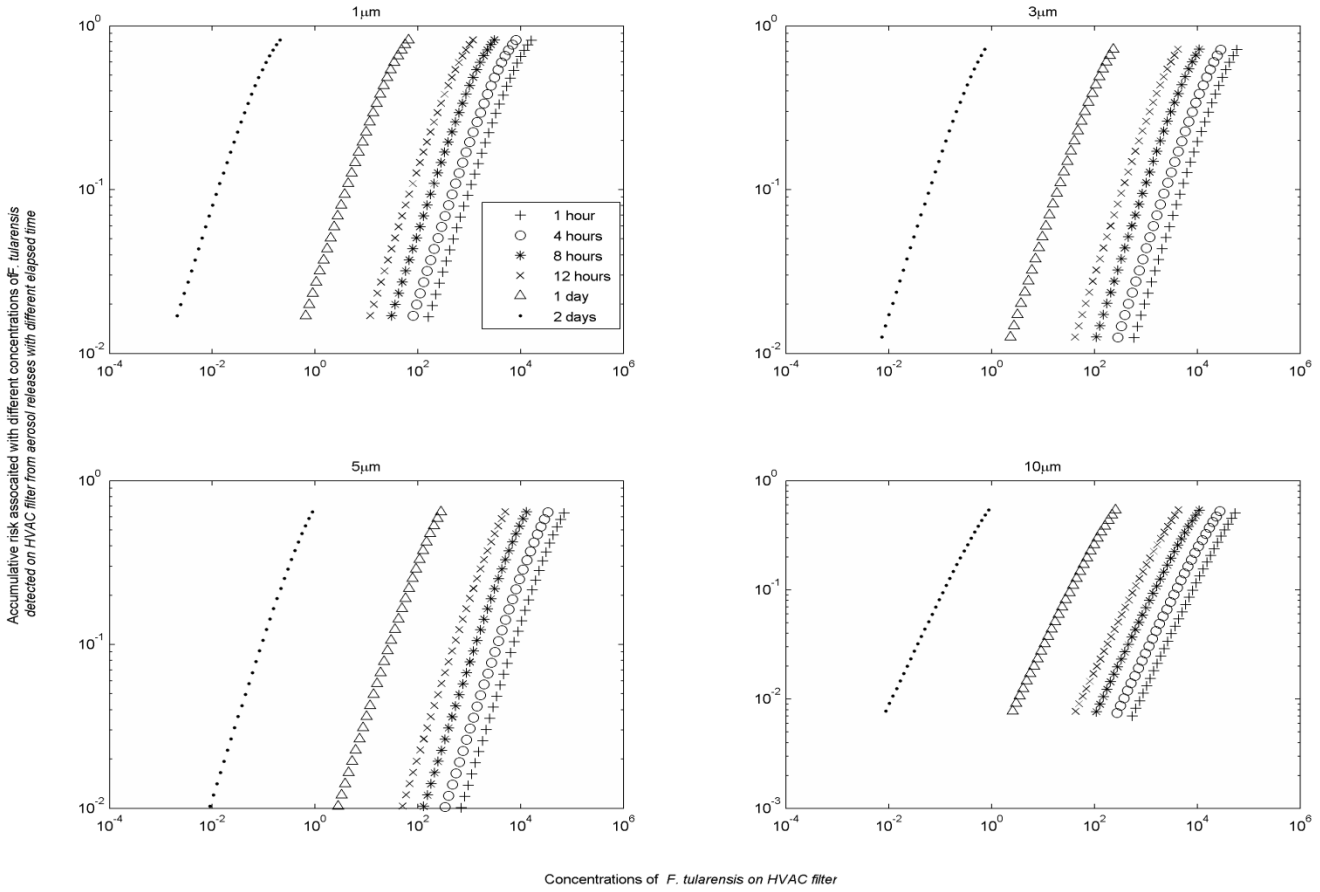

Figure 4-8 Cumulative retrospective risks associated with *F. tularensis* HVAC concentrations after an aerosol release.

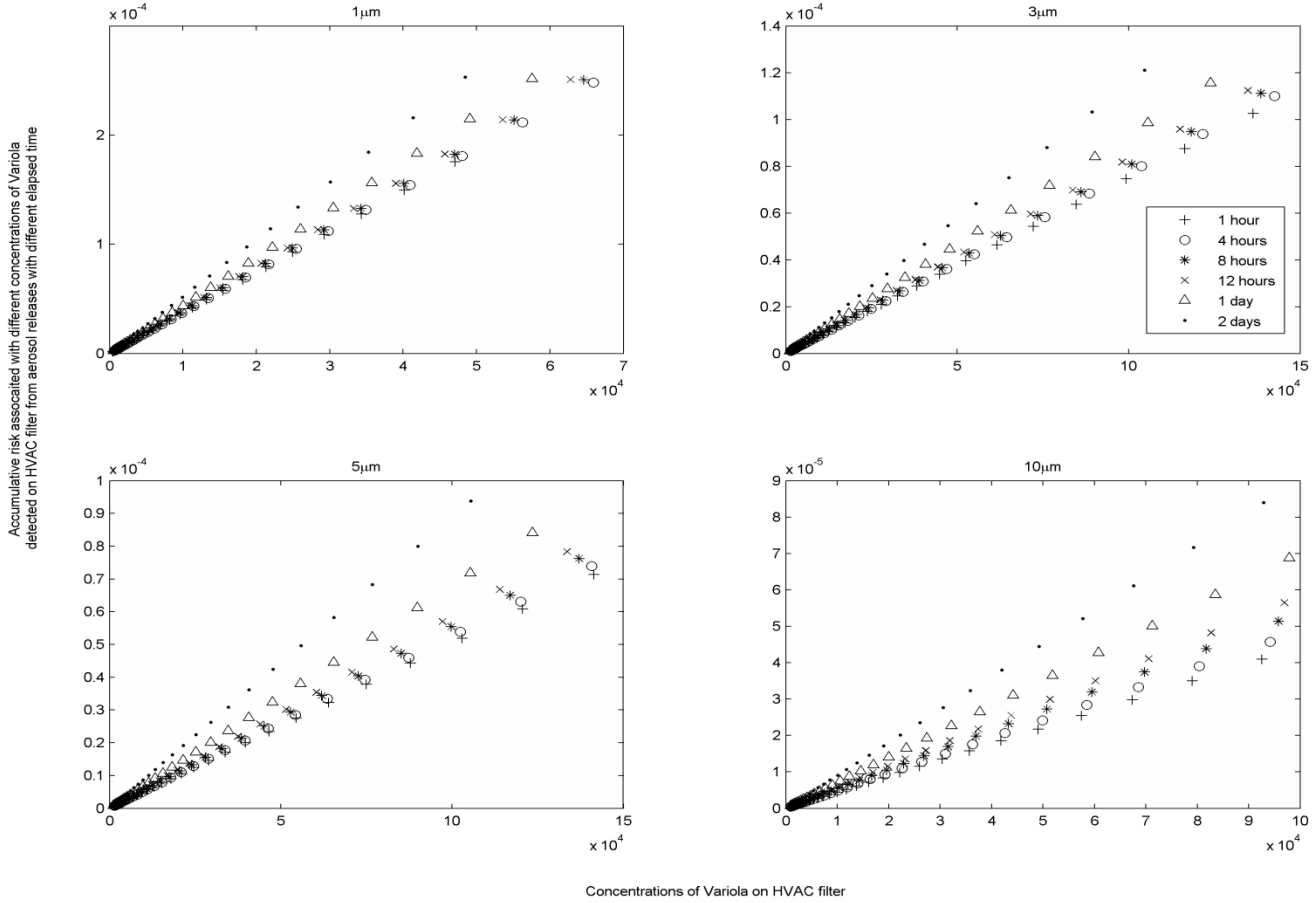

Figure 4-9 Cumulative retrospective risks associated with *Variola major* HVAC concentrations after an aerosol release.

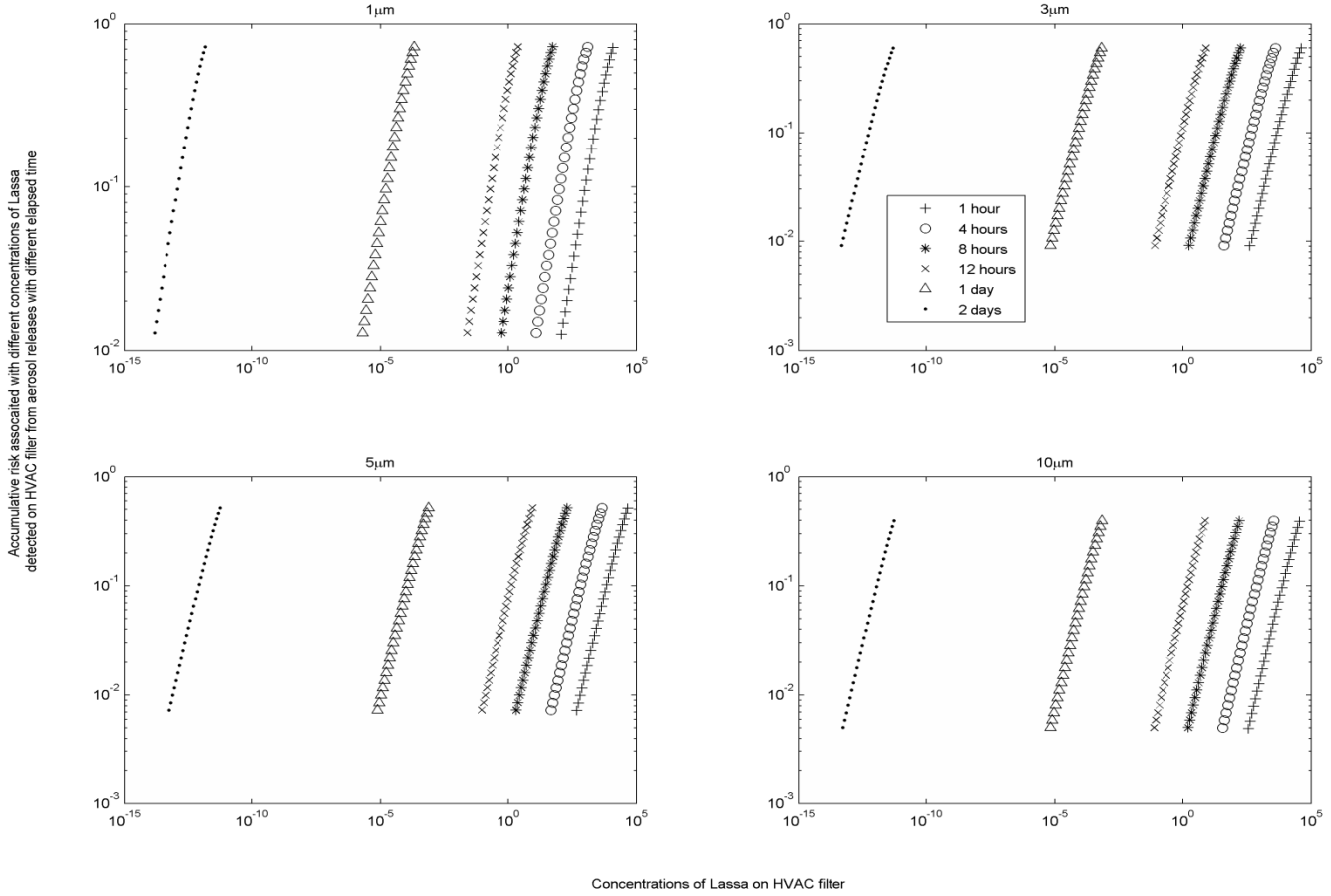

Figure 4-10 Cumulative retrospective risks associated with Lassa HVAC concentrations after an aerosol release.

There are essentially two options for addressing prospective (re-occupancy) risk, restrict access to the contaminated site until pathogen concentrations decline to acceptable levels through natural attenuation or actively decontaminate the site. The selection of a strategy depends on the survival capability of the pathogens. If the passive decontamination approach is chosen, the time required depends on the initial concentration to reach a given residual risk target, but one can get a rough idea of the relative feasibility of this approach by comparing the time to achieve a significant concentration reduction across different pathogens. The time scale for a 6-log risk reduction due to natural attenuation for different pathogens is shown in Table 4-4. Values in Table 4-4 vary by more than 4 orders of magnitude. *B. anthracis* has a best estimate of 17,100 days or over 46 years. It is probably more appropriate to compare the upper bound as pathogens will reside in a wide variety of different microenvironments and decay rates would be expected to vary among microenvironments. Decontamination would only be achieved once even the pathogens in the more protected microenvironments have decayed. For *B. anthracis* this upper bound would be over 82 years. In contrast, a greater than 6 order of magnitude decay of Lassa would occur in less than a day. These estimates are very sensitive to the assumption of log linear decay. Deviations from log linear decay are widely reported. However in many cases a biphasic approach could be adopted in which a rapid log-linear decay rate is used for the first several days and a second, lower log-linear decay rate is used subsequently. While parameters for such biphasic attenuation models are not yet available for these pathogens, the approach presented here can be readily adapted to biphasic decay. The relevant equations would be unchanged,

but the mass distribution in each compartment at the end of the first phase would constitute the initial conditions for the second phase.

Table 4-4 Time scale for a 6-log risk reduction due to natural attenuation

Pathogen	Time (days)		
	Min	Max	Best estimate
B. anthracis	1.24×10^{4}	3.00×10^{4}	1.71×10^{4}
Y. pestis	4.63×10^{-1}	1.44×10^{1}	1.27
F. tularensis	1.25	5.75×10^{1}	2.41
Variola major	5.79×10^{1}	1.05×10^{2}	8.38×10^{1}
Lassa	6.25×10^{-1}	8.46×10^{-1}	7.50×10^{-1}

Table 4-5 presents the concentrations of pathogens associated with a 1 in 1000 risk. Concentrations corresponding to different risk levels can be found by multiplying these values by the desired risk level/10^{-3}, provided that the risk is low enough to be approximately a linear function of exposure (which is roughly accurate for risks $<10^{-2}$). In the retrospective scenarios (the first two columns), the concentrations become lower (standards would become more stringent) as the time after the release increases. Values for *B. anthracis* presented here are substantially lower than reported previously [85], as the previous study considered only inhalation risk, while this study considers dermal risk as well as inhalation risk for *B. anthracis*. Even if sampling could be conducted within 24 hours (which is an extremely optimistic assumption), it would be difficult to characterize risk at the 1 in 1,000 level for any of the pathogens, as this would require quantifying pathogens at levels ranging from 5-7 pathogens/m^2 for *Variola major* to 10-11/m^2 for Lassa.

Table 4-5 Concentrations of pathogens on horizontal surfaces associated with risk of 10^{-3}

(Prospective exposure duration =1 year)

Pathogen	Diameter	Concentrations (organisms/m^2)				
		Retrospective sampling 8 hours after release	Retrospective sampling 24 hours after release	Prospective for immediate occupancy	Prospective after 24 hours access restriction	Prospective after 48 hours access restriction
B. anthracis	1μM	1.6	2×10^{-1}	3.0×10^{1}	3.0×10^{1}	2.9×10^{1}
	3μM	4.2	4×10^{-1}	6.4×10^{2}	6.7×10^{2}	7.0×10^{2}
	5μM	7.0	7×10^{-1}	1.9×10^{3}	2.0×10^{3}	2.2×10^{3}
	10μM	1.6×10^{1}	1.0	7.6×10^{3}	1.2×10^{4}	2.1×10^{4}
Y. pestis	1μM	2×10^{-3}	1×10^{-6}	1.8×10^{2}	9.0×10^{6}	4.9×10^{11}
	3μM	9×10^{-3}	2×10^{-6}	1.8×10^{2}	9.3×10^{6}	5.3×10^{11}
	5μM	1×10^{-2}	2×10^{-6}	1.8×10^{2}	9.5×10^{6}	5.8×10^{11}
	10μM	1×10^{-2}	1×10^{-6}	1.8×10^{2}	1.8×10^{7}	2.0×10^{12}
F. tularensis	1μM	2×10^{-4}	2×10^{-6}	1.7	5.1×10^{2}	1.6×10^{5}
	3μM	7×10^{-4}	4×10^{-6}	1.0	5.3×10^{2}	1.7×10^{5}
	5μM	9×10^{-4}	4×10^{-6}	1.0	5.3×10^{2}	1.8×10^{5}
	10μM	8×10^{-4}	2×10^{-6}	1.0	1.1×10^{3}	7.0×10^{5}
Variola major	1μM	3.1×10^{1}	7.0	1.1×10^{3}	1.4×10^{3}	1.6×10^{3}
	3μM	7.3×10^{1}	7.0	1.3×10^{3}	1.8×10^{3}	2.1×10^{3}
	5μM	8.0×10^{1}	7.0	1.6×10^{3}	2.2×10^{3}	2.7×10^{3}
	10μM	7.4×10^{1}	5.0	4.7×10^{3}	1.2×10^{4}	2.5×10^{3}
Lassa	1μM	6×10^{-6}	1×10^{-11}	8.0	7.4×10^{8}	7.3×10^{16}
	3μM	2×10^{-5}	4×10^{-11}	8.0	7.9×10^{8}	8.0×10^{16}
	5μM	3×10^{-5}	4×10^{-11}	9.0	8.3×10^{8}	8.8×10^{16}
	10μM	4×10^{-5}	3×10^{-11}	8.0	1.5×10^{9}	3.0×10^{17}

For the prospective case (columns 3-5), if a pathogen decays rapidly, most of the risk will attenuate relatively rapidly. In such cases a much less stringent concentration standard can be set if access to the building is restricted for a period after the sampling is conducted. The differences in values for different Category A pathogens are driven by virulence and environmental persistency, which are both pathogen dependent. *B. anthracis* has relatively high concentrations despite being very persistent, because it has a relatively low infectivity (proportional to parameter k from dose-response functions). The strictest concentration values are for *F. tularensis* despite its low persistence because of its high infectivity.

The concentrations associated with immediate re-occupancy are in many cases well below applicable limits of detection. For example a negative sampling result for Lassa, used to estimate the prospective risk for immediate occupancy, would not provide much confidence because the applicable standard of 9 organisms per m^2 is well below feasible detection levels. However, a negative result coupled with a 24-hour restriction on access would provide some level of confidence as the standard for this case of 7.36×10^8 organisms per m^2 is readily detectable. In this latter case, demonstrating achievement of a risk target of 1 in a million (a concentration of 7.36×10^5 organisms per m^2 or 73.6 organisms per cm^2) would likely be feasible as well. If one assumes that a 0.09 m^2 surface is sampled with a recovery of 0.38 [85, 110], and a detection limit of 10 organisms, then the resulting minimum detectable pathogen concentration is 292 organisms per m^2. Table 4-6 compares risks associated with this concentration across different organisms.

Table 4-6 Equipment detection limit associated risk

Pathogen	Diameter	Risk (95% confidence interval)
B. anthracis	1μM	2.30×10^{-2} (5.81×10^{-4}, 4.33×10^{-1})
	3μM	6.80×10^{-4} (2.25×10^{-5}, 6.54×10^{-3})
	5μM	1.92×10^{-4} (1.00×10^{-5}, 1.16×10^{-3})
	10μM	1.17×10^{-5} (3.18×10^{-6}, 2.84×10^{-4})
Y. pestis	1μM	2.86×10^{-3} (9.63×10^{-5}, 1.63×10^{-2})
	3μM	2.85×10^{-3} (1.01×10^{-4}, 1.58×10^{-2})
	5μM	2.84×10^{-3} (1.04×10^{-4}, 1.51×10^{-2})
	10μM	2.69×10^{-3} (1.04×10^{-4}, 1.37×10^{-2})
F. tularensis	1μM	2.57×10^{-1} (1.54×10^{-2}, 9.17×10^{-1})
	3μM	2.55×10^{-1} (1.58×10^{-2}, 8.96×10^{-1})
	5μM	2.54×10^{-1} (1.60×10^{-2}, 8.65×10^{-1})
	10μM	2.31×10^{-1} (1.56×10^{-2}, 8.06×10^{-1})
Variola major	1μM	2.79×10^{-4} (9.72×10^{-6}, 6.10×10^{-4})
	3μM	2.43×10^{-4} (7.84×10^{-6}, 5.06×10^{-4})
	5μM	2.14×10^{-4} (5.93×10^{-6}, 4.06×10^{-4})
	10μM	7.35×10^{-5} (3.42×10^{-6}, 3.32×10^{-4})
Lassa	1μM	5.43×10^{-2} (1.04×10^{-2}, 7.00×10^{-1})
	3μM	5.43×10^{-2} (1.09×10^{-2}, 7.00×10^{-1})
	5μM	5.42×10^{-2} (1.12×10^{-2}, 6.99×10^{-1})
	10μM	5.26×10^{-2} (1.12×10^{-2}, 6.95×10^{-1})

It is assumed that the detection limit is 10 organisms which comes from sampling a 0.09 m^2 surface with the pathogen concentration 292 organisms per m^2 and the recovery rate is 0.38 [85].

4.3.2 Parameter uncertainties

Another objective of this study is to compare risk and uncertainties across different pathogens. Using the input distributions listed in Table 4-1 and Table 4-2, Equations 26 and 27 are evaluated in a Monte Carlo analysis to estimate risks for different pathogens, and results from retrospective and prospective scenarios are presented in the form of box plots (Figure 4-11). The relative risk presented by different pathogens in an air release are largely determined by their dose-response parameters, because the exposure duration in air is limited by the particle deposition rate (which is the same across different pathogens) rather than the decay rate. However, air decay rate does have an impact, when decay is rapid enough to occur over the time scale during which particulates are typically suspended (minutes to hours depending on the diameter of the particles) which is the case for *Y. pestis*, *F. tularensis*, and Lassa. The relative risks for different pathogens in a surface release are affected by both fomite decay rates and dose-response parameters. In general the risk from releasing the same amount of pathogens can be ranked as Lassa, *F. tularensis, Y. Pestis, B. anthracis*, and *Variola major* (in decreasing order). This analysis does not include secondary transmission risks (which may be particularly important for all but *B. anthracis* and *F. tularensis* [30]*)* and as such does not capture a critical component of risk for pathogens, such as *Variola major*, which are subject to secondary transmission. Instead it addresses the question as to which pathogens are subject to the greatest uncertainty in setting surface concentration standards for primary exposure. Uncertainties presented by Lassa are highest across most of the cases, indicating that this organism may be a priority for further study (pending consideration of factors such as its likely use in an attack).

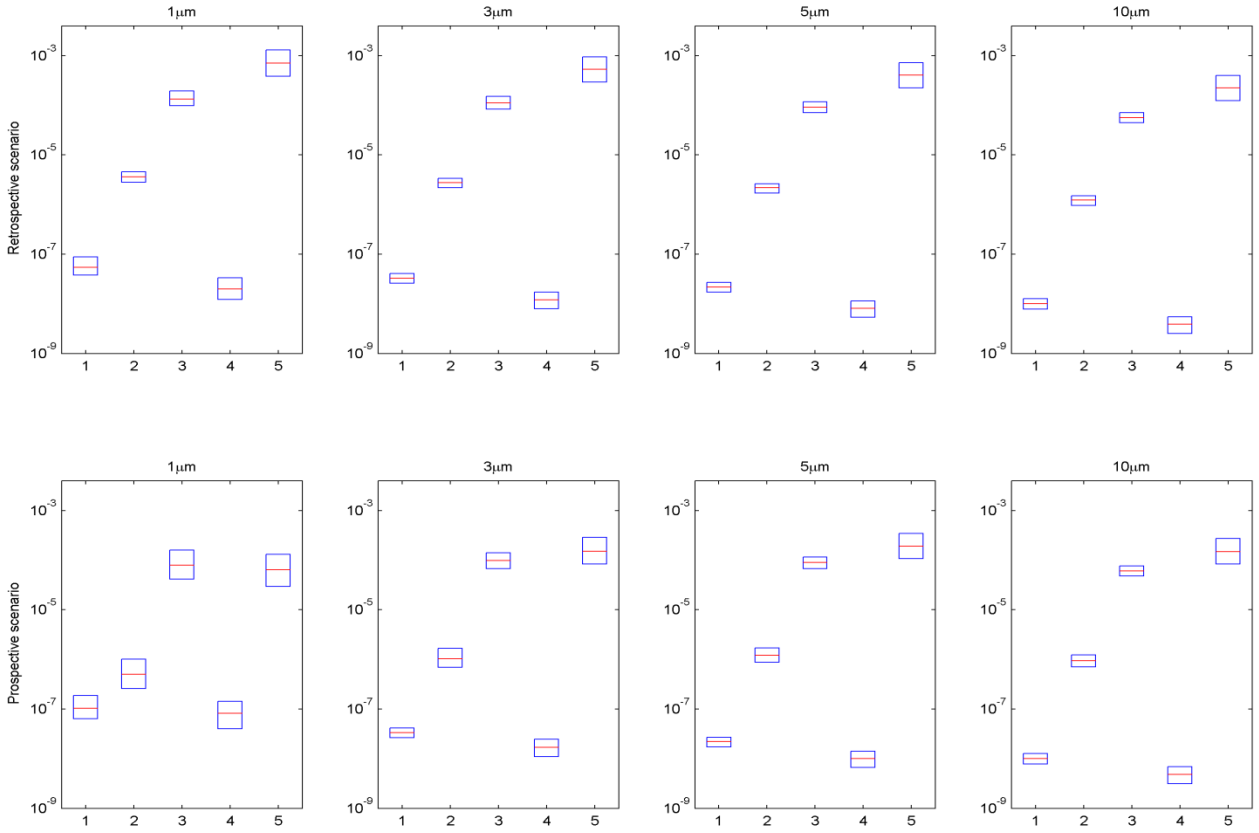

Figure 4-11 Risk and uncertainty for different pathogens

Medians shown in red, 1st and 3rd quartiles in blue. (1. *B. anthracis*, 2. *Y. pestis*, 3. *F. tularensis*, 4. *Variola major*, and 5. Lassa)

Correlations between the input parameter values and the model output (risk) are used to assess the importance of uncertainties in different parameters. These correlations were computed separately for each pathogen, for ingestion and inhalation risk for both the retrospective and prospective scenarios for all four particle sizes considered. Table 4-7 summarizes the 3 most important uncertain inputs by exposure pathway and scenario for each pathogen (with the range of values across the four particle sizes shown in brackets). Detailed results are included in Appendix II (Tables S2-S6). Uncertainties in mass transfer fraction from surface to hand (f_{sh}) have major impacts on ingestion dose, and uncertainty in the breathing rate (Inh) plays an important role in determining the inhalation dose in the retrospective scenario. In the prospective scenario, the ingestion dose is most closely related to the mass transfer fraction from surface to hand (f_{sh}), while the inhalation dose is most closely related to the pathogen resuspension rate (μ_2).

Table 4-7 Parameter uncertainties with most influence on risk

Pathogen	Retrospective scenario		Prospective scenario	
	Ingestion risk	Inhalation risk	Ingestion risk	Inhalation risk
B. anthracis	Dose-response coefficient (r) (0.66-0.76)	Air change rate (ACH) (0.31-0.72)	Dose-response coefficient (r) (0.63-0.87)	Air change rate (ACH) (0.44-0.75)
	Mass transfer fraction from surface to hand (f_{sh}) (0.21-0.36)	Breathing rate (Inh) (0.27-0.65)	Mass transfer fraction from surface to hand (f_{sh}) (0.16-0.32)	Breathing rate (Inh) (0.14-0.53)
	Air change rate (ACH) (0.081-0.21)	Density of the particle (ρ_p) (0.052-0.61)	Resuspension rate (μ_2) (0.047, 0.29)	Resuspension rate (μ_2) (0.022-0.32)
Y. pestis	Decay rate on fomite (γ_f) (0.56-0.61)	Breathing rate (Inh) (0.73-0.78)	Decay rate on fomite (γ_f) (0.53-0.56)	Decay rate on fomite (γ_f) (0.51-0.63)
	Mass transfer fraction from surface to hand (f_{sh}) (0.47-0.51)	Air change rate (ACH) (0.28-0.52)	Mass transfer fraction from surface to hand (f_{sh}) (0.34-0.38)	Resuspension rate (μ_2) (0.21-0.35)
	Density of the particle (ρ_p) (0.12-0.24)	Density of the particle (ρ_p) (0.026-0.54)	Hand-surface contacting rate (r_{hs}) (0.071-0.079)	Breathing rate (Inh) (0.15-0.18)
F. tularensis	Mass transfer fraction from surface to hand (f_{sh}) (0.44-0.67)	Decay rate in the air (γ_{air}) (0.46-0.75)	Decay rate on fomite (γ_f) (0.64-0.65)	Decay rate on fomite (γ_f) (0.42-0.59)
	Decay rate in the air (γ_{air}) (0.23-0.43)	Breathing rate (Inh) (0.35-0.69)	Mass transfer fraction from surface to hand (f_{sh}) (0.41-0.47)	Resuspension rate (μ_2) (0.18-0.33)
	Decay rate on fomite (γ_f) (0.33-0.49)	Decay rate on fomite (γ_f) (0.18-0.42)	Hand-surface contacting rate (r_{hs}) (0.12-0.13)	Decay rate in the air (γ_{air}) (0.14-0.26)
Variola major	Mass transfer fraction from surface to hand (f_{sh}) (0.45-0.67)	Dose-response coefficient (r) (0.44-0.73)	Mass transfer fraction from surface to hand (f_{sh}) (0.60-0.67)	Dose-response coefficient (r) (0.30-0.61)
	Dose-response coefficient (r) (0.38-0.54)	Air change rate (ACH) (0.19-0.54)	Dose-response coefficient (r) (0.51-0.57)	Air change rate (ACH) (0.25-0.45)
	Air change rate (ACH) (0.11-0.37)	Breathing rate (Inh) (0.25-0.40)	Resuspension rate (μ_2) (0.15-0.46)	Resuspension rate (μ_2) (0.25-0.39)
Lassa	Dose-response coefficient (r) (0.60-0.70)	Dose-response coefficient (r) (0.69-0.87)	Dose-response coefficient (r) (0.72)	Dose-response coefficient (r) (0.61-0.80)
	Mass transfer fraction from surface to hand (f_{sh}) (0.40-0.47)	Breathing rate (Inh) (0.26-0.28)	Mass transfer fraction from surface to hand (f_{sh}) (0.51)	Breathing rate (Inh) (0.17-0.23)
	Decay rate in the air (γ_{air}) (0.057-0.21)	Decay rate in the air (γ_{air}) (0.082-0.31)	Resuspension rate (μ_2) (0.26-0.40)	Decay rate in the air (γ_{air}) (0.089-0.24)

Values of coefficients between selected parameters and risks to the exposed people are listed in parenthesis.

As noted above this analysis captures only one aspect of uncertainty, that of uncertainty in primary exposure. This may be the appropriate framework for pathogens that are not subject to secondary transmission as well as for decisions where one seeks to cut off environmental transmission of a pathogen after a widespread environmental contamination event. Additional risk and uncertainty would be applicable for decisions where secondary transmission is a concern.

4.4. Discussion

This study presents an integrated fate and transport, dose-response model to estimate the inhalation and ingestion risks associated with environmental pathogens. Scenarios to estimate the past risk and to predict future risk are introduced. A reduced form model is developed and used to compare risks and uncertainties for different pathogens.

In addition, this study also identified important parameter uncertainties in risk assessment models. Specifically, the input-output correlations presented in Table 4-7 indicate which parameter uncertainties have the greatest effect on risk estimates. However, several other factors must be considered in settling research priorities. Whether the high correlation is due to variability or epistemic uncertainty is one such factor. Parameters such as inhalation rate and air exchange rate will vary considerably from person to person and from building to building, respectively. However, they are not subject to great epistemic uncertainty. The ranges within these parameters vary have

already been well characterized. Additional research would not reduce the inherent variability in such parameters but only serve to further characterize an already well-characterized variability distribution.

Another factor to consider is whether a particular parameter is common across pathogens such that a study of a single surrogate organism might be helpful in improving risk assessments for multiple pathogens. Strictly speaking, any parameter can be considered pathogen specific. However, some distinctions can perhaps be made between dose-response parameters and environmental decay rates, both of which are observed to vary over orders of magnitude and depend on very complex pathogen-host and pathogen-environment interactions, and general physical transfer rates, such as surface-hand and hand-surface transfer fractions and re-aerosolization rates, which might vary less from pathogen to pathogen.

A third consideration is the extent to which an uncertainty is reducible by further research. Dose-response is an example of an uncertainty that is difficult to reduce through research. In part this is due to cost, as such research generally requires vertebrate animals and extensive biosafety precautions. There are other more fundamental challenges as well. Laboratory experiments 1) must be conducted at high doses with limited numbers of animals, leaving great uncertainty as to the effects of lower doses; 2) generally do not consider the effects of previous exposures, which might greatly affect the dose response coefficients; and 3) must be conducted with animal models that may not accurately represent human dose response. Despite these limitations, further animal studies would at

least reduce the confidence intervals for the dose-response parameters used here. These dose-response model parameter uncertainties are the uncertainties reflected in the correlations summarized in Table 4-7 (i.e., applicability of the animal model to humans and validity of extrapolation from high to low dose were not addressed by this analysis), which means that further animal dosing studies would effectively reduce the uncertainty considered here. Thus, dose-response uncertainty is considered by the authors to be researchable, although the difficulties and expense of working with vertebrate animals with extensive biosafety precautious are significant.

As an example of how one might integrate these different factors, Table 4-8 summarizes the authors' view of future research priorities based on these different factors. In Table 4-8, The percentages in the right hand columns indicate the frequency with which the parameter was one of the top three sources of risk for different pathogens (the retrospective scenario percentages are based on inhalation risk, and the prospective scenario percentages are based on ingestion risk). A low research priority for research is assigned to all three parameters subject to variability rather than epistemic uncertainty: breathing rate, density, and air exchange rate. The remaining 6 parameters all were judged to be subject to epistemic uncertainty. The degree of "Generality" (divided into 3 categories in order of priority: common across pathogens, similarities expected, pathogen specific) was an important factor in distinguishing among high and medium priority parameters, with both of the medium priority parameters (decay on fomites and decay in the air) considered to be pathogen specific. Three of the high priority parameters (resuspension rate, hand surface contact rate, and mass transfer fraction for surface to

hand) were ranked highly partly because similarities across organisms would be expected making surrogate research more generally relevant and partly because the input-output correlations indicated they were important parameters. Dose-response parameters were given high priority for research despite being judged both pathogen-specific and difficult to research, because these parameters were relatively frequently among the parameters responsible for the greatest uncertainty in risk (13% of retrospective cases and 20% of prospective cases).

Table 4-8 Properties of parameters uncertainty

Authors' priority	Parameter	Symbol	Uncertainty vs. Variability	Generality	Researchable	Percentage in the top 3 uncertainty parameters among retrospective scenario (%)	Percentage in the top 3 uncertainty parameters among prospective scenario (%)
High	Mass transfer fraction from surface to hand	f_{sh}	Both	Similarities expected	Yes	0	33
High	Dose-response coefficients	k	Both	Pathogen specific	Difficult	13	20
High	Resuspension rate	μ_2	Both	Similarities expected	Yes	0	20
High	Hand-surface contacting rate	r_{hs}	Both	Similarities expected	Yes	0	13
Moderate	Decay rate on fomite	γ_f	Both	Pathogen specific	Yes	7	13
Moderate	Decay rate in the air	γ_{air}	Both	Pathogen specific	Yes	13	0
Low	Breathing rate	Inh	Variability	Common across pathogen	Yes	33	0
Low	Air change rate	ACH	Variability	Common across pathogen	Yes	20	0
Low	Density of the particle	ρ_p	Variability	Common across pathogen	Yes*	13	0

* Density can readily be measured but it is not clear that laboratory values could reflect density in an actual release

+ The percentages in the retrospective scenario is based on inhalation risk in the retrospective scenario, while the percentages in the prospective scenario is based on ingestion risk in the prospective scenario of Table 4-7.

Judgments listed in Table 4-8 are all based on the authors' understanding and previous experience. The intent is to provide an example framework for integrating the computational results provided by the model with broader considerations that influence the costs and benefits expected from future research. The sources of input into this ranking process should be broadened by scientifically collecting opinions from experts in the future [127].

The fate and transport model is based on the assumption that pathogens are instantly uniformly mixed in a compartment. This fails to capture the short-term dynamics associated with the immediate vicinity of a release. For example, surface samples might not be reflective of the localized high concentrations associated with opening a letter containing pathogens and might underestimate risk in this case. A more detailed approach, such as computational fluid dynamics, would be a useful extension to this study. The study also considers risk from a release of only one pathogen. Little information is available on the effects of mixtures of pathogens. This approach would be most valid at low risk levels when interactions among pathogens, such as successful colonization by more than one pathogen would be unlikely.

Another assumption is that pathogen attenuation rate outside the host is log linear over time. In reality microorganisms often exhibit “tailing” in which a small, highly resistant subpopulation attenuates at a very low rate. Thus the assumption of log-linear decay may not be health protective. Accordingly the values calculated here are not intended as suggested environmental standards. These calculations are provided to

illustrate the suggested approach and to allow a comparison of uncertainties so that future research can be prioritized.

This study modeled environmental fate and transport using a small number of homogeneous compartments when in reality surfaces may vary in characteristics, such as the frequency with which they are touched, the rate at which pathogens attenuate (influenced in turn by relative humidity, intensity of ultraviolet light, etc. [166]), and the ease with which pathogens are re-aerosolized or transferred to hands from them. Modeling these heterogeneities may improve our understanding of pathogen fate and transport in the environment but would require detailed parameter inputs beyond what are currently available in the literature. Such heterogeneities might provide protected microenvironments that could allow pathogens to persist longer and present greater health risks than estimated here, which makes this a priority for future research.

The framework developed here may help inform whether active decontamination is required after a release. If a pathogen with a slow environmental attenuation rate is released (i.e., *B. anthracis*), then environmental decontamination may be required. In contrast, if a pathogen with fast environmental attenuation rate is released (eg., Lassa), the decision maker may opt to restrict access to the contaminated site until the residual risk declines to a level judged acceptable for re-occupancy. The choice between active decontamination and passive attenuation involves comparing the costs of remediation and opportunity costs of restricting access to the building. While previous research has addressed policy options for bioterrorism, this research has not considered the

opportunity costs of removing buildings from service [91, 123]. Thus, further study is needed to inform the choice between active remediation and passive attenuation.

This analysis considered viable organisms. However, the environmental concentrations which would be used as inputs to the risk models developed here would likely be measured by quantitative PCR (qPCR), which has been proven effective in quantifying biological warfare agents (i.e., *B. antracis*, and *Y. pestis*) due to its rapid, early, and accurate results [200]. Despite the advantages of qPCR analysis, several knowledge gaps need to be addressed The first is that the qPCR does not distinguish between living or dead pathogens. While researchers have identified assays to discriminate between viable and dead fecal *bacteroidales* bacteria, similar methods have not been applied to Category A pathogens [10, 53]. Second there is little information on the decay of the qPCR signal over time, which would be an essential parameter for the retrospective assessment of risk after a release. Thus, studies are needed to quantify parameters such as, the efficiency of DNA extraction, the degradation of nucleic acids overtime, and the reactivity of primer and probe [24, 110, 156].

4.5 Appendix C

This appendix describes how the system of equations given by Equation 1 in the main body of the paper can be simplified to allow reduced form solutions to be developed.

Retrospective scenario

In the retrospective scenario, resuspension makes a negligible contribution to dose, due to the relatively short exposure period compared the rates of resuspension (in this case the exposure period is assumed to be is 8 hours, the duration of a working day). Neglecting re-suspension separates the air compartment from the effects of other compartments so that air concentration follows a simple first order decay model. The inhaled dose can be calculated as:

$$\begin{aligned} dose_{inh\_\text{retro}} &\approx \frac{Inh}{Vol}\int_0^{\text{a}} M_{airo} e^{-\phi_{retro} t_1} dt_1 \\ &= \frac{Inh}{Vol} \times M_{airo} \times \frac{1}{\phi_{retro}} e^{-\phi_{retro} t}\Big|_0^{t_1} \\ &= \frac{Inh}{Vol} \times M_{airo} \times \frac{1}{\phi_{retro}} \left(1 - e^{-\phi_{retro} \times 480}\right) \end{aligned} \qquad \text{(Eq. A)}$$

where

$$\phi_{retro} = \lambda_{ts} + \lambda_{tf} + \lambda_{utf} + \lambda_w + \frac{Inhe_n}{Vol} + \gamma_{air} + [1-(1-e)p]\frac{Q}{Vol} \qquad \text{(Eq. 31)}$$

The ingested pathogens ($dose_{ing\_retro}$) are the organisms which deposit on the touched surface (M_{ts}) from the initial release in the air (M_{air0}) (Equation B):

$$M_{ts} = \int_0^a \lambda_{ts} M_{airo} e^{-\phi_{retro} t_1} dt_1 \quad \text{(Eq. B)}$$

remain alive until being transferred to the hand (M_{hand}) (Equation C):

$$M_{hand} = \int_0^a r_{sh} f_{sh} M_{ts} e^{-\phi_{pros} t_2} dt_2 \quad \text{(Eq. C)}$$

and are ingested ($dose_{ing\_retro}$) during surface-hand-mouth contact in the exposure period (Equation D):

$$\begin{aligned} dose_{ing\_retro} &= \int_0^a r_{hm} f_{hm} M_{hand} e^{-\phi_{hand} t_3} dt_3 \\ &= \int_0^a r_{hm} f_{hm} \left[\int_0^a r_{sh} f_{sh} M_{ts} e^{-\phi_{pros} t_2} dt_2 \right] e^{-\phi_{hand} t_3} dt_3 \\ &= \int_0^a r_{hm} f_{hm} \left[\int_0^a r_{sh} f_{sh} \left(\int_0^a \lambda_{ts} M_{airo} e^{-\phi_{retro} t_1} dt_1 \right) e^{-\phi_{pros} t_2} dt_2 \right] e^{-\phi_{hand} t_3} dt_3 \\ &= r_{hm} f_{hm} \left[r_{sh} f_{sh} \left(M_{airo} \lambda_{ts} \frac{1}{\phi_{retro}} (1 - e^{-\phi_{retro} a}) \right) \frac{1}{\phi_{pros}} (1 - e^{-\phi_{pros} a}) \right] \frac{1}{\phi_{hand}} (1 - e^{-\phi_{hand} a}) \end{aligned} \quad \text{(Eq. D)}$$

where

$$\phi_{pros} = \mu_2 + \gamma_{fomite} + r_{sh} f_{sh} \quad \text{(Eq. 32)}$$

$$\phi_{hand} = r_{hm} f_{hm} + \gamma_{fomite} + r_{hs} f_{hs} \quad \text{(Eq. 33)}$$

To simplify the calculation, three assumptions are made during the derivation of Equation D: 1) pathogen resuspension and back transfer from hands to the surface are omitted due to their relatively low rates resulting in small fractions being back transferred, which is also health conservative; 2) all integration steps are from t=0 to t=a which provides an upper bound on the amount of pathogen transferred to the next step; 3) the

pathogens will not be transferred to hands until depositing on the touched surface, and the pathogens will not be ingested until they are transferred to hands.

Prospective scenario

In the prospective scenario, the majority of the inhaled dose ($dose_{inh\_pros}$) comes from two sources (Figure C-1). The first source consists of organisms that are inhaled right after being resuspended ($dose_{inh1\_pros}$) (Equation E).

$$dose_{inh1\_pros} = \int_0^a \frac{Inh}{Vol}\left(\int_0^a \mu_2 M_{tso} e^{-\phi_{pros} t_1} dt_1\right) e^{-\phi_{retro} t_2} dt_2 \qquad \text{(Eq. E)}$$

The second are those organisms which experienced a certain number of "surface-hand-surface" travels before being resuspended and inhaled $dose_{inh2\_pros}$ (Equation F).

$$dose_{inh2\_pros} = \int_0^a \frac{Inh}{Vol}\left(\int_0^a \mu_2 \Theta M_{tso} e^{-\phi_{pros} t_1} dt_1\right) e^{-\phi_{retro} t_2} dt_2 \qquad \text{(Eq. F)}$$

where Θ is the total fraction of resuspended pathogens surviving a number of n "surface-hand-surface" cycles:

$$\Theta = \sum_{n=1}^{\infty}\left[\int_0^a r_{hs} f_{hs}\left(\int_0^a r_{sh} f_{sh} M_{tso} e^{-\phi_{pros} t_{a1}} dt_{a1}\right) e^{-\phi_{hand} t_{b1}} dt_{b1}\right]^n \qquad \text{(G)}$$

Θ is composed as a summation of a geometric series with element of Θ_n, where n indexes the number of "surface-hand-surface" cycle. In the n^{th} cycle, pathogens survived from the $n\text{-}1^{th}$ cycle ($\Theta_{n-1} M_{tso}$) are first transferred to hands (Equation H), and then back transferred to the surface (Equation I).

$$\Theta_{n\_sh} = \int_0^a r_{sh} f_{sh} \Theta_{n-1} M_{tso} e^{-\phi_{pros} t_{an}} dt_{an} \quad \text{(H)}$$

$$\Theta_n = \Theta_{n\_sh} \Theta_{n\_hs} = \int_0^a r_{hs} f_{hs} \Theta_{n\_sh} e^{-\phi_{hand} t_{bn}} dt_{bn} \quad \text{(I)}$$

Combine Equation H and I:

$$\Theta_n = \int_0^a r_{hs} f_{hs} \left(\int_0^a r_{sh} f_{sh} \Theta_{n-1} e^{-\phi_{pros} t_{an}} dt_{an} \right) e^{-\phi_{hand} t_{bn}} dt_{bn} = \left(\Theta_1\right)^n \quad \text{(J)}$$

For both sources, pathogen resuspension happens before inhalation. The maximum inhalation dose is reached when the exposure duration goes to infinity (Equation K):

$$\begin{aligned} dose_{inh\_pros} &= dose_{inh1\_pros} + dose_{inh2\_pros} \\ &= \int_0^a \frac{Inh}{Vol} \left(\int_0^a \mu_2 (1+\Theta) M_{tso} e^{-\phi_{pros} t_1} dt_1 \right) e^{-\phi_{retro} t_2} dt_2 \\ &= \int_0^a \frac{Inh}{Vol} \left\{ \int_0^a \mu_2 \left\{ 1 + \sum_{n=1}^{\infty} \left[\int_0^a r_{hs} f_{hs} \left(\int_0^a r_{sh} f_{sh} M_{tso} e^{-\phi_{pros} t_{a1}} dt_{a1} \right) e^{-\phi_{hand} t_{b1}} dt_{b1} \right]^n \right\} M_{tso} e^{-\phi_{pros} t_1} dt_1 \right\} e^{-\phi_{retro} t_2} dt_2 \\ &\overset{a \to \infty}{\approx} M_{tso} \frac{\mu_2}{\phi_{pros}} \frac{Inh}{Vol} \frac{1}{\phi_{retro}} \sum_{n=0}^{\infty} \frac{r_{sh} f_{sh}}{\phi_{pros}} \frac{r_{hs} f_{hs}}{\phi_{hand}} \\ &= M_{tso} \frac{\frac{\mu_2}{\phi_{pros}} \frac{Inh}{Vol} \frac{1}{\phi_{retro}}}{\left(1 - \frac{r_{sh} f_{sh}}{\phi_{pros}} \frac{r_{hs} f_{hs}}{\phi_{hand}}\right)} \end{aligned} \quad \text{(Eq. K)}$$

Similarly, the prospective ingestion dose ($dose_{ing\_pros}$) comes from two sources (Figure C-2). The first source is direct ingestion of the pathogens released on the touched surface ($dose_{ing1\_pros}$) (Equation L):

$$dose_{ing1\_pros} = \int_0^a r_{hm} f_{hm} \left[\int_0^a r_{sh} f_{sh} M_{ts0} e^{-\phi_{pros} t_1} dt_1 \right] e^{-\phi_{hand} t_2} dt_2 \quad \text{(Eq. L)}$$

where $\int_0^a r_{sh} f_{sh} M_{ts0} e^{-\phi_{pros} t_1} dt_1$ is the mass transferred to victims hand.

The second source is those organisms which experience a certain number of "surface-hand-surface" travels before being ingested ($dose_{ing2\_pros}$) (Equation M), which contains the common factor Θ as described above. The maximum ingestion dose is reached when exposure goes to infinity (Equation N).

$$dose_{ing\,2\_\mathrm{pros}} = \int_0^a r_{hm} f_{hm} \left[\int_0^a r_{sh} f_{sh} \Theta M_{ts0} e^{-\phi_{pros} t_1} dt_1 \right] e^{-\phi_{hand} t_2} dt_2 \qquad \text{(Eq. M)}$$

$$\begin{aligned}
dose_{ing_\mathrm{pros}} &= dose_{ing1_pros} + dose_{ing2_pros} \\
&= \int_0^a r_{hm} f_{hm} \left[\int_0^a r_{sh} f_{sh} (1+\Theta) M_{ts0} e^{-\phi_{pros} t_1} dt_1 \right] e^{-\phi_{hand} t_2} dt_2 \\
&= \int_0^a r_{hm} f_{hm} \left\{ \int_0^a r_{sh} f_{sh} \left\{ 1 + \sum_{n=1}^{\infty} \left[\int_0^a r_{hs} f_{hs} \left(\int_0^a r_{sh} f_{sh} M_{tso} e^{-\phi_{pros} t_{a1}} dt_{a1} \right) e^{-\phi_{hand} t_{b1}} dt_{b1} \right]^n \right\} M_{ts0} e^{-\phi_{pros} t_1} dt_1 \right\} e^{-\phi_{hand} t_2} dt_2 \\
&\overset{a\to\infty}{\approx} M_{tso} \frac{r_{sh} f_{sh}}{\phi_{pros}} \frac{r_{hm} f_{hm}}{\phi_{hand}} \sum_{n=0}^{\infty} \frac{r_{sh} f_{sh}}{\phi_{pros}} \frac{r_{hs} f_{hs}}{\phi_{hand}} \\
&= M_{tso} \frac{\frac{r_{sh} f_{sh}}{\phi_{pros}} \frac{r_{hm} f_{hm}}{\phi_{hand}}}{\left(1 - \frac{r_{sh} f_{sh}}{\phi_{pros}} \frac{r_{hs} f_{hs}}{\phi_{hand}}\right)}
\end{aligned} \qquad \text{(Eq. N)}$$

Table C-1 compares the exposure dose approximated by the above-mentioned equations with the exact results from solving Equation 18. The overall risk is acquired by inputting inhalation and ingestion doses into Equation 14 separately for the retrospective (Equation 26) and the prospective scenario (Equation 27).

$$\begin{aligned}
risk_{retro} &= 1 - (1 - risk_{inh_\mathrm{retro}})(1 - risk_{inh_\mathrm{retro}}) \\
&\approx 1 - (1 - k \times dose_{inh_\mathrm{retro}})(1 - k \times dose_{ing_\mathrm{retro}}) \\
&\approx 1 - \left[1 - k \times M_{airo} \frac{Inh}{Vol} \times \frac{1}{\phi_{retro}} \left(1 - e^{-\phi_{retro} \times 480} \right) \right] \left[1 - k \times M_{airo} r_{hm} f_{hm} \left[r_{sh} f_{sh} \left(\lambda_{ts} \frac{1}{\phi_{retro}} (1 - e^{-\phi_{retro} \times 480}) \right) \frac{1}{\phi_{pros}} (1 - e^{-\phi_{pros} \times 480}) \right] \frac{1}{\phi_{hand}} (1 - e^{-\phi_{hand} \times 480}) \right]
\end{aligned} \qquad \text{(Eq. 26)}$$

$$
\begin{aligned}
risk_{pros} &= 1-(1-risk_{inh\_pros})(1-risk_{inh\_pros}) \\
&\approx 1-(1-k\times dose_{inh\_pros})(1-k\times dose_{ing\_pros}) \\
&\approx 1-(1-k\times M_{tso}\frac{\frac{\mu_2}{\phi_{pros}}\frac{Inh}{Vol}\frac{1}{\phi_{retro}}}{(1-\frac{r_{sh}f_{sh}}{\phi_{pros}}\frac{r_{hs}f_{hs}}{\phi_{hand}})})(1-k\times M_{tso}\frac{\frac{r_{sh}f_{sh}}{\phi_{pros}}\frac{r_{hm}f_{hm}}{\phi_{hand}}}{(1-\frac{r_{sh}f_{sh}}{\phi_{pros}}\frac{r_{hs}f_{hs}}{\phi_{hand}})})
\end{aligned}
\qquad \text{(Eq. 27)}
$$

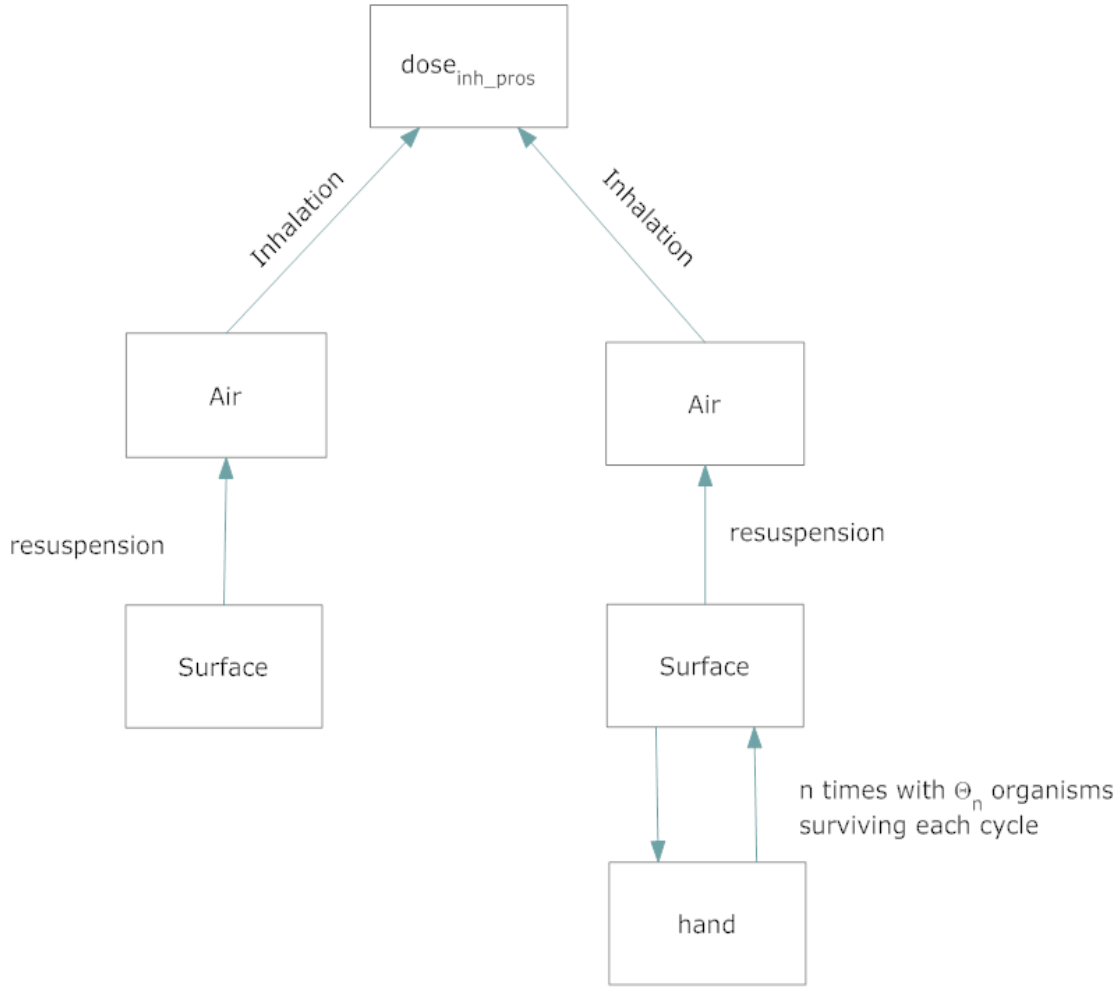

Figure C-1. Pathogen flow for estimating the inhalation dose in the prospective scenario.

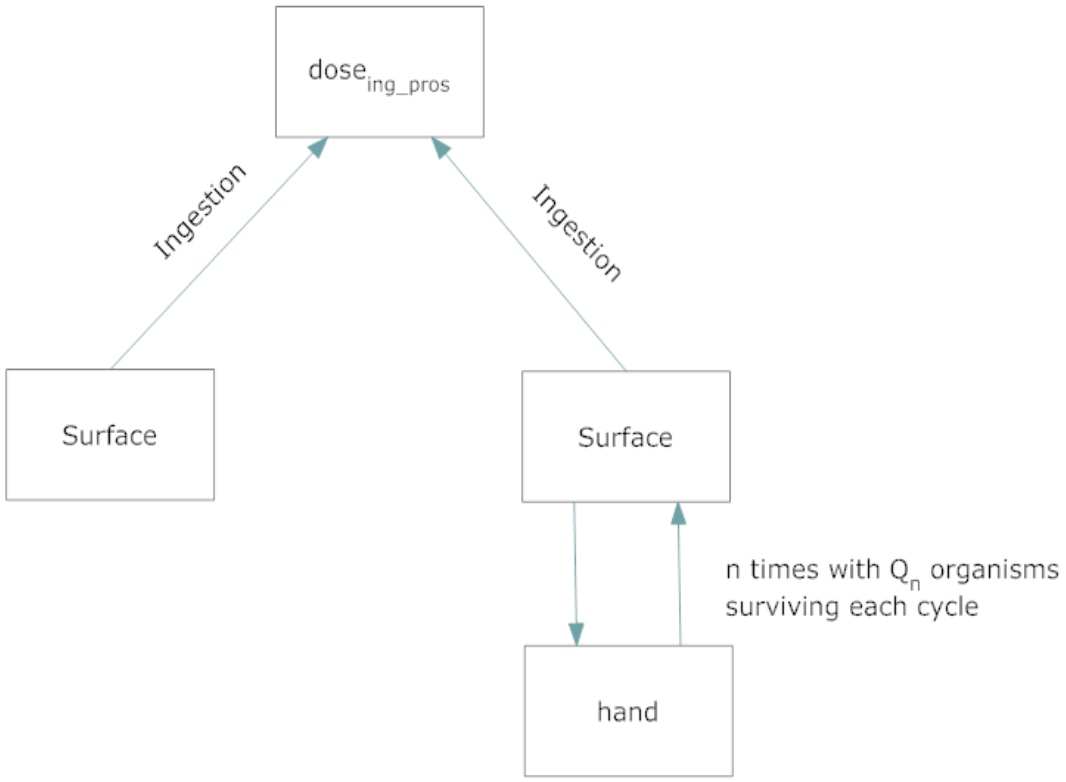

Figure C-2. Pathogen flow for estimating the ingestion dose in the prospective scenario.

Table C-1. Comparison Exposure Dose between Approximated Analytical Equation and Simulated Results (1 μm)

Pathogen	Release scenario	Inhalation dose		Ingestion dose	
		Approximated analytical equation	Full numerical simulation	Approximated analytical equation	Full numerical simulation
B. anthracis	Retrospective*	1.12×10^{4}	1.12×10^{4}	2.75×10^{1}	2.37×10^{1}
	Prospective*	2.07×10^{3}	2.10×10^{3}	7.62×10^{5}	7.64×10^{5}
Y. pestis	Retrospective*	3.32×10^{3}	3.42×10^{3}	1.98	1.96
	Prospective*	8.83×10^{-1}	8.83×10^{-1}	9.84×10^{2}	9.83×10^{2}
F. tularensis	Retrospective*	3.13×10^{3}	3.23×10^{3}	3.22	3.15
	Prospective*	1.56	1.56	1.94×10^{3}	1.94×10^{3}
Variola major	Retrospective*	1.08×10^{4}	1.08×10^{4}	2.57×10^{1}	2.23×10^{1}
	Prospective*	1.65×10^{2}	1.65×10^{2}	6.33×10^{4}	6.32×10^{4}
Lassa	Retrospective*	3.48×10^{3}	3.58×10^{3}	1.14	1.14
	Prospective*	5.34×10^{-1}	5.30×10^{-1}	5.28×10^{2}	5.27×10^{2}

*Total release quantity is 1 million spores for both retrospective and prospective scenario. The simulation period in retrospective scenario is 8 hours, while it is one year in prospective scenario.

Table C-2. Correlation coefficients for *B. anthracis*

		Retrospective scenario		Prospective scenario	
		Ingestion risk	Inhalation dose	Ingestion dose	Inhalation dose
Hand-mouth contacting rate (r_{h-m})	1 µm	0.0034	-0.013	-0.019	-0.0093
	3 µm	0.0055	-0.018	0.0027	-0.0012
	5 µm	-0.0064	-0.019	0.0011	0.0037
	10 µm	0.011	-0.021	0.0011	0.0062
Hand-surface contacting rate (r_{h-s})	1 µm	0.071	0.0018	0.066	-0.054
	3 µm	0.094	-0.0010	0.086	-0.020
	5 µm	0.12	-0.0038	0.011	-0.013
	10 µm	0.12	-0.0096	0.092	-0.011
Mass transfer fraction from hand to mouth during each contact (f_{h-m})	1 µm	-0.0084	-0.018	0.00050	-0.0093
	3 µm	-0.00055	-0.016	-0.013	-0.0012
	5 µm	-0.0037	-0.012	-0.0058	0.0037
	10 µm	-0.0075	-0.0063	0.010	0.0062
Mass transfer fraction from hand to surface during each contact (f_{h-s})	1 µm	-0.0042	0.00070	0.055	0.047
	3 µm	0.0048	0.0050	0.021	0.020
	5 µm	-0.0050	0.0075	0.0003	0.015
	10 µm	0.0060	0.0096	0.0085	0.012
Mass transfer fraction from surface to hand during each contact (f_{s-h})	1 µm	**0.21**	0.0077	**0.16**	-0.25
	3 µm	**0.30**	0.010	**0.26**	-0.082
	5 µm	**0.34**	0.012	**0.32**	-0.046
	10 µm	**0.36**	0.015	**0.28**	-0.043
Decay rate in this air (γ_{air})	1 µm	0.00030	0.0055	0.0013	-0.0020
	3 µm	0.00080	0.0089	0.0013	-0.0053
	5 µm	0.0075	0.0078	0.0049	-0.0009
	10 µm	0.0023	0.0026	-0.0021	0.0053
Decay rate on fomite (γ_f)	1 µm	-0.012	-0.017	-0.0097	-0.013
	3 µm	0.011	-0.018	-0.0005	-0.00080
	5 µm	0.0022	-0.018	0.0002	0.0022
	10 µm	-0.00090	-0.018	-0.0070	0.0031
Dose-response coefficient	1 µm	**0.66**	0.058	**0.87**	0.027
	3 µm	**0.72**	0.088	**0.73**	0.053
	5 µm	**0.76**	0.11	**0.77**	0.075
	10 µm	**0.76**	0.14	**0.63**	0.012

Table C-2. Correlation coefficients for *B. anthracis* (continued)

		Retrospective scenario		Prospective scenario	
		Ingestion dose	Inhalation dose	Ingestion dose	Inhalation dose
Breathing rate (Inh)	1 µm	0.0065	**0.27**	0.021	**0.14**
	3 µm	-0.0065	**0.40**	0.017	**0.25**
	5 µm	-0.00040	**0.53**	0.0067	**0.34**
	10 µm	0.0021	**0.65**	-0.0026	**0.53**
Nasal passages particle remove efficiency (e_n)	1 µm	-0.0030	-0.0093	-0.0064	-0.0038
	3 µm	0.0028	0.0020	0.0099	-0.012
	5 µm	0.0036	-0.017	0.00070	-0.0010
	10 µm	0.0029	0.0083	-0.00090	0.0078
Air change rate (ACH)	1 µm	**-0.18**	**-0.68**	-0.0038	**-0.44**
	3 µm	**-0.21**	**-0.72**	-0.029	**-0.70**
	5 µm	**-0.16**	**-0.62**	-0.052	**-0.75**
	10 µm	**-0.081**	**-0.31**	-0.052	**-0.63**
Resuspension rate (μ_2)	1 µm	-0.0040	0.00060	**-0.047**	**0.32**
	3 µm	0.0070	-0.0012	**-0.26**	**0.088**
	5 µm	-0.012	0.0052	**-0.18**	**0.022**
	10 µm	-0.0068	0.089	**-0.29**	**0.058**
Turbulence intensity (k_e)	1 µm	0.013	0.0084	-0.0024	-0.0040
	3 µm	0.0023	0.012	-0.013	0.00050
	5 µm	0.011	0.012	-0.0059	0.0031
	10 µm	0.0077	0.0067	-0.0067	0.0043
Density of the particle (ρ_p)	1 µm	0.10	**-0.052**	-0.0049	-0.035
	3 µm	0.080	**-0.24**	0.018	-0.096
	5 µm	0.075	**-0.40**	0.014	-0.17
	10 µm	0.030	**-0.61**	0.011	-0.40

Table C-3. Correlation coefficients for *Y. pestis*

		Retrospective scenario		Prospective scenario	
		Ingestion dose	Inhalation dose	Ingestion dose	Inhalation dose
Hand-mouth contacting rate (r_{h-m})	1 μm	0.032	0.0033	0.0071	-0.011
	3 μm	0.035	0.0087	0.0079	-0.015
	5 μm	0.038	0.012	0.0085	-0.0069
	10 μm	0.042	0.015	0.010	-0.013
Hand-surface contacting rate (r_{h-s})	1 μm	0.13	-0.012	**0.071**	-0.014
	3 μm	0.14	-0.014	**0.074**	-0.017
	5 μm	0.14	-0.017	**0.076**	-0.011
	10 μm	0.14	-0.022	**0.079**	-0.0067
Mass transfer fraction from hand to mouth during each contact (f_{h-m})	1 μm	0.029	-0.034	0.037	0.026
	3 μm	0.028	-0.035	0.036	0.036
	5 μm	0.029	-0.034	0.038	0.025
	10 μm	0.030	-0.029	0.036	0.026
Mass transfer fraction from hand to surface during each contact (f_{h-s})	1 μm	-0.11	-0.0019	-0.059	0.027
	3 μm	-0.12	-0.0024	-0.060	0.0053
	5 μm	-0.12	-0.0028	-0.062	0.023
	10 μm	-0.12	-0.0022	-0.065	0.013
Mass transfer fraction from surface to hand during each contact (f_{s-h})	1 μm	**0.47**	0.014	**0.34**	-0.0088
	3 μm	**0.48**	0.020	**0.35**	0.0026
	5 μm	**0.49**	0.021	**0.36**	-0.015
	10 μm	**0.51**	0.018	**0.38**	-0.0023
Decay rate in this air (γ_{air})	1 μm	-0.10	-0.30	-0.0057	-0.079
	3 μm	-0.082	-0.24	-0.0066	-0.058
	5 μm	-0.066	-0.18	-0.0059	-0.066
	10 μm	-0.042	-0.083	-0.0051	-0.042
Decay rate on fomite (γ_f)	1 μm	**-0.56**	-0.0029	**-0.53**	**-0.51**
	3 μm	**-0.57**	0.0037	**-0.54**	**-0.56**
	5 μm	**-0.59**	0.0048	**-0.55**	**-0.63**
	10 μm	**-0.61**	-0.0072	**-0.56**	**-0.57**
Dose-response coefficient	1 μm	0.0058	0.053	0.032	0.032
	3 μm	0.0039	0.056	0.032	0.035
	5 μm	0.0039	0.058	0.032	0.028
	10 μm	0.0055	0.059	0.030	0.038

Table C-3. Correlation coefficients for *Y. pestis* (continued)

		Retrospective scenario		Prospective scenario	
		Ingestion dose	Inhalation dose	Ingestion dose	Inhalation dose
Breathing rate (Inh)	1 µm	0.0072	**0.73**	-0.014	**0.15**
	3 µm	0.0048	**0.76**	-0.014	**0.16**
	5 µm	0.0028	**0.78**	-0.014	**0.18**
	10 µm	-0.00091	**0.76**	-0.015	**0.16**
Nasal passages particle remove efficiency (e_n)	1 µm	-0.015	0.011	-0.022	-0.012
	3 µm	0.0029	-0.014	-0.011	-0.0053
	5 µm	0.0019	0.0060	0.0088	-0.0048
	10 µm	0.0087	-0.0079	-0.00028	-0.0015
Air change rate (ACH)	1 µm	-0.11	**-0.44**	0.0036	-0.080
	3 µm	-0.13	**-0.52**	0.0034	-0.11
	5 µm	-0.12	**-0.48**	0.0035	-0.11
	10 µm	-0.070	**-0.28**	0.0023	-0.057
Resuspension rate (μ_2)	1 µm	-0.0018	0.026	-0.0048	**0.35**
	3 µm	-0.028	0.018	-0.0013	**0.31**
	5 µm	-0.00099	0.023	-0.016	**0.21**
	10 µm	-0.00023	0.019	-0.019	**0.33**
Turbulence intensity (k_e)	1 µm	0.0040	-0.010	0.0018	0.015
	3 µm	0.0037	-0.0064	0.0020	0.0074
	5 µm	0.0037	-0.0039	0.0023	0.013
	10 µm	0.0037	-0.0015	0.0019	0.010
Density of the particle (ρ_p)	1 µm	**0.24**	**-0.026**	-0.0083	-0.0058
	3 µm	**0.22**	**-0.15**	-0.0076	-0.033
	5 µm	**0.19**	**-0.30**	-0.0071	-0.070
	10 µm	**0.12**	**-0.54**	-0.0085	-0.12

Table C-4. Correlation coefficients for *F. tularensis*

		Retrospective scenario		Prospective scenario	
		Ingestion dose	Inhalation dose	Ingestion dose	Inhalation dose
Hand-mouth contacting rate (r_{h-m})	1 µm	0.033	0.016	0.011	0.0079
	3 µm	0.033	0.017	0.011	0.0071
	5 µm	0.032	0.017	0.013	-0.0044
	10 µm	0.033	0.019	0.017	-0.0082
Hand-surface contacting rate (r_{h-s})	1 µm	0.14	0.0020	0.12	0.020
	3 µm	0.17	0.0024	0.12	0.017
	5 µm	0.18	0.00099	0.13	0.021
	10 µm	0.20	-0.0019	0.13	0.023
Mass transfer fraction from hand to mouth during each contact (f_{h-m})	1 µm	0.0069	0.0043	0.033	0.0091
	3 µm	0.011	0.0094	0.034	0.0080
	5 µm	0.015	0.013	0.035	0.0067
	10 µm	0.020	0.017	0.038	0.010
Mass transfer fraction from hand to surface during each contact (f_{h-s})	1 µm	-0.12	-0.0077	-0.085	0.0063
	3 µm	-0.14	-0.0037	-0.090	0.00034
	5 µm	-0.15	0.0023	-0.096	0.014
	10 µm	-0.17	0.017	-0.10	0.0060
Mass transfer fraction from surface to hand during each contact (f_{s-h})	1 µm	**0.44**	-0.012	**0.41**	0.0031
	3 µm	**0.52**	-0.016	**0.42**	-0.0039
	5 µm	**0.58**	-0.018	**0.44**	-0.0030
	10 µm	**0.67**	-0.023	**0.47**	-0.00091
Decay rate in this air (γ_{air})	1 µm	**-0.43**	**-0.75**	0.0055	**-0.26**
	3 µm	**-0.40**	**-0.73**	0.0050	**-0.24**
	5 µm	**-0.35**	**-0.67**	0.0035	**-0.22**
	10 µm	**-0.23**	**-0.46**	-0.0036	**-0.14**
Decay rate on fomite (γ_f)	1 µm	**-0.33**	**-0.18**	**-0.65**	**-0.42**
	3 µm	**-0.39**	**-0.21**	**-0.65**	**-0.50**
	5 µm	**-0.43**	**-0.26**	**-0.64**	**-0.56**
	10 µm	**-0.49**	**-0.42**	**-0.64**	**-0.59**
Dose-response coefficient	1 µm	0.015	0.0049	0.021	0.0015
	3 µm	0.017	0.0091	0.022	-0.00098
	5 µm	0.017	0.0097	0.022	-0.000097
	10 µm	0.016	0.0061	0.020	0.013

Table C-4. Correlation coefficients for *F.tularensis* (continued)

		Retrospective scenario		Prospective scenario	
		Ingestion dose	Inhalation dose	Ingestion dose	Inhalation dose
Breathing rate (Inh)	1 µm	-0.023	**0.35**	-0.011	0.12
	3 µm	-0.029	**0.45**	-0.013	0.14
	5 µm	-0.033	**0.54**	-0.015	0.17
	10 µm	-0.038	**0.69**	-0.018	0.20
Nasal passages particle remove efficiency (e_n)	1 µm	-0.024	-0.0042	0.011	0.00061
	3 µm	0.015	0.00042	0.0077	-0.018
	5 µm	0.00056	0.0051	0.010	-0.013
	10 µm	0.0072	-0.00095	0.0066	0.012
Air change rate (ACH)	1 µm	-0.13	-0.23	0.0025	-0.087
	3 µm	-0.16	-0.30	0.0026	-0.10
	5 µm	-0.15	-0.31	0.0036	-0.11
	10 µm	-0.089	-0.22	0.0048	-0.073
Resuspension rate (μ_2)	1 µm	0.0029	-0.0027	0.0053	**0.26**
	3 µm	-0.0079	0.015	-0.0075	**0.26**
	5 µm	-0.016	-0.011	-0.020	**0.18**
	10 µm	-0.0076	0.038	-0.060	**0.33**
Turbulence intensity (k_e)	1 µm	0.0032	0.018	**0.020**	0.018
	3 µm	-0.0020	0.013	**0.020**	0.0078
	5 µm	-0.0056	0.010	**0.020**	0.00072
	10 µm	-0.011	0.0089	**0.021**	-0.011
Density of the particle (ρ_p)	1 µm	0.22	-0.0066	-0.019	-0.014
	3 µm	0.23	-0.077	-0.019	-0.040
	5 µm	0.21	-0.18	-0.018	-0.067
	10 µm	0.15	-0.44	-0.015	-0.13

Table C-5. Correlation coefficients for *Variola major*

		Retrospective scenario		Prospective scenario	
		Ingestion dose	Inhalation dose	Ingestion dose	Inhalation dose
Hand-mouth contacting rate (r_{h-m})	1 µm	0.070	0.040	0.057	-0.018
	3 µm	0.080	0.048	0.062	-0.013
	5 µm	0.081	0.044	0.056	-0.0078
	10 µm	0.075	0.033	0.061	-0.0065
Hand-surface contacting rate (r_{h-s})	1 µm	0.10	-0.0070	0.19	0.0013
	3 µm	0.12	-0.0092	0.19	0.00018
	5 µm	0.14	-0.0060	0.19	-0.0045
	10 µm	0.16	0.0036	0.17	-0.0011
Mass transfer fraction from hand to mouth during each contact (f_{h-m})	1 µm	0.021	0.013	0.016	0.0092
	3 µm	0.016	0.0036	0.019	0.0047
	5 µm	0.013	-0.0039	0.021	0.0088
	10 µm	0.011	-0.013	0.025	0.0016
Mass transfer fraction from hand to surface during each contact (f_{h-s})	1 µm	-0.11	0.0027	-0.16	0.022
	3 µm	-0.13	0.0025	-0.17	0.030
	5 µm	-0.15	0.0039	-0.17	0.029
	10 µm	-0.16	0.0044	-0.15	0.027
Mass transfer fraction from surface to hand during each contact (f_{s-h})	1 µm	**0.45**	-0.013	**0.67**	-0.033
	3 µm	**0.54**	-0.012	**0.67**	-0.017
	5 µm	**0.61**	-0.011	**0.67**	-0.011
	10 µm	**0.67**	-0.0064	**0.60**	0.00058
Decay rate in this air (γ_{air})	1 µm	-0.023	-0.055	-0.010	-0.19
	3 µm	-0.014	-0.032	-0.015	-0.14
	5 µm	-0.0090	-0.024	-0.0066	-0.11
	10 µm	-0.0043	-0.017	-0.013	-0.081
Decay rate on fomite (γ_f)	1 µm	0.0045	0.0030	-0.059	-0.11
	3 µm	-0.0021	-0.0025	-0.017	-0.15
	5 µm	-0.0072	-0.0047	-0.014	-0.15
	10 µm	-0.012	-0.0060	-0.00080	-0.12
Dose-response coefficient	1 µm	**0.38**	**0.44**	**0.57**	**0.30**
	3 µm	**0.45**	**0.57**	**0.56**	**0.45**
	5 µm	**0.50**	**0.67**	**0.56**	**0.57**
	10 µm	**0.54**	**0.73**	**0.51**	**0.61**

Table C-5 Correlation coefficients for *Variola major* (continued)

		Retrospective scenario		Prospective scenario	
		Ingestion dose	Inhalation dose	Ingestion dose	Inhalation dose
Breathing rate (Inh)	1 µm	-0.0043	**0.25**	0.010	0.18
	3 µm	-0.00019	**0.32**	0.0038	0.27
	5 µm	0.00032	**0.37**	0.0099	0.34
	10 µm	-0.00060	**0.40**	0.015	0.36
Nasal passages particle remove efficiency (e_n)	1 µm	-0.015	-0.077	-0.0043	-0.025
	3 µm	-0.048	-0.024	0.0057	0.018
	5 µm	-0.015	0.0052	0.013	-0.00094
	10 µm	-0.0092	-0.0059	-0.011	-0.0064
Air change rate (ACH)	1 µm	**-0.37**	**-0.54**	0.018	**-0.41**
	3 µm	**-0.36**	**-0.53**	0.0042	**-0.45**
	5 µm	**-0.27**	**-0.42**	-0.0092	**-0.45**
	10 µm	**-0.11**	**-0.19**	-0.028	**-0.25**
Resuspension rate (μ_2)	1 µm	0.0031	-0.0038	**-0.46**	**0.36**
	3 µm	0.0045	0.0069	**-0.15**	**0.39**
	5 µm	-0.0041	0.011	**-0.16**	**0.25**
	10 µm	-0.013	0.039	**-0.35**	**0.39**
Turbulence intensity (k_e)	1 µm	0.0043	0.010	-0.022	-0.015
	3 µm	0.0096	0.016	-0.018	-0.017
	5 µm	0.0077	0.013	-0.020	-0.012
	10 µm	0.0028	0.055	-0.024	-0.0089
Density of the particle (ρ_p)	1 µm	0.19	-0.069	-0.0065	-0.039
	3 µm	0.14	-0.20	-0.0022	-0.14
	5 µm	0.099	-0.29	0.0025	-0.21
	10 µm	0.031	-0.40	0.018	-0.31

Table C-6 Correlation coefficients for Lassa

		Retrospective scenario		Prospective scenario	
		Ingestion dose	Inhalation dose	Ingestion dose	Inhalation dose
Hand-mouth contacting rate (r_{h-m})	1 μm	0.014	0.0017	0.033	0.0088
	3 μm	0.017	0.0035	0.033	0.022
	5 μm	0.020	0.0059	0.033	0.021
	10 μm	0.024	0.0095	0.033	0.019
Hand-surface contacting rate (r_{h-s})	1 μm	0.098	-0.022	-0.055	-0.0023
	3 μm	0.10	-0.024	-0.055	-0.0031
	5 μm	0.11	-0.027	-0.055	-0.0081
	10 μm	0.11	-0.031	-0.055	-0.0083
Mass transfer fraction from hand to mouth during each contact (f_{h-m})	1 μm	0.019	-0.0038	0.033	0.0088
	3 μm	0.023	-0.0042	0.033	0.022
	5 μm	0.024	-0.0050	0.033	0.021
	10 μm	0.025	-0.0079	0.033	0.019
Mass transfer fraction from hand to surface during each contact (f_{h-s})	1 μm	-0.074	0.011	-0.055	-0.0023
	3 μm	-0.083	0.0077	-0.055	-0.0031
	5 μm	-0.090	0.0045	-0.055	-0.0081
	10 μm	-0.098	0.0018	-0.055	-0.0083
Mass transfer fraction from surface to hand during each contact (f_{s-h})	1 μm	**0.40**	-0.018	**0.51**	0.0027
	3 μm	**0.42**	-0.016	**0.51**	-0.0058
	5 μm	**0.44**	-0.013	**0.51**	-0.0015
	10 μm	**0.47**	-0.0086	**0.51**	-0.012
Decay rate in this air (γ_{air})	1 μm	**-0.21**	**-0.31**	-0.025	**-0.24**
	3 μm	**-0.16**	**-0.24**	-0.025	**-0.18**
	5 μm	**-0.12**	**-0.18**	-0.025	**-0.17**
	10 μm	**-0.057**	**-0.082**	-0.025	**-0.089**
Decay rate on fomite (γ_f)	1 μm	-0.092	-0.017	-0.093	-0.057
	3 μm	-0.099	-0.018	-0.093	-0.057
	5 μm	-0.11	-0.020	-0.092	-0.079
	10 μm	-0.11	-0.025	-0.091	-0.078
Dose-response coefficient	1 μm	**0.60**	**0.69**	**0.72**	**0.61**
	3 μm	**0.64**	**0.75**	**0.72**	**0.73**
	5 μm	**0.67**	**0.80**	**0.72**	**0.80**
	10 μm	**0.70**	**0.87**	**0.72**	**0.73**

Table C-6 Correlation coefficients for Lassa (continued)

		Retrospective scenario		Prospective scenario	
		Ingestion dose	Inhalation dose	Ingestion dose	Inhalation dose
Breathing rate (Inh)	1 μm	0.0066	**0.26**	0.011	**0.17**
	3 μm	0.0093	**0.27**	0.011	**0.19**
	5 μm	0.011	**0.28**	0.011	**0.23**
	10 μm	0.012	**0.28**	0.011	**0.20**
Nasal passages particle remove efficiency (e_n)	1 μm	0.016	0.030	0.0022	0.011
	3 μm	0.0040	-0.012	-0.0033	0.0050
	5 μm	-0.0049	0.0014	0.016	0.011
	10 μm	0.0029	0.018	0.010	0.0022
Air change rate (ACH)	1 μm	-0.13	-0.20	-0.0030	-0.15
	3 μm	-0.14	-0.22	-0.0031	-0.16
	5 μm	-0.13	-0.19	-0.0031	-0.17
	10 μm	-0.070	-0.098	-0.0031	-0.085
Resuspension rate (μ_2)	1 μm	0.0065	0.0084	**0.40**	0.021
	3 μm	0.022	0.016	**0.38**	0.026
	5 μm	0.0090	0.0030	**0.26**	0.0042
	10 μm	0.011	0.00046	**0.37**	-0.021
Turbulence intensity (k_e)	1 μm	0.0054	-0.0056	-0.0013	0.0067
	3 μm	0.0069	-0.0041	-0.0013	-0.0021
	5 μm	0.0080	-0.0023	-0.0014	0.0063
	10 μm	0.0098	0.00054	-0.0013	-0.0033
Density of the particle (ρ_p)	1 μm	0.19	-0.0056	0.0085	0.011
	3 μm	0.17	-0.050	0.0085	-0.033
	5 μm	0.15	-0.11	0.0086	-0.090
	10 μm	0.087	-0.19	0.0088	-0.16

CHAPTER 5: CONCLUSION AND FUTURE RESEARCH

5.1 General conclusion

This dissertation developed methods for characterizing risks from a release of biological agents. The contributions of this dissertation include: 1) a BMC approach to calibrate inputs for an integrated fate, transport, and risk assessment model; 2) an approach for determining the location and quantity of samples for characterizing a release of pathogenic microbes; 3) a framework employing surface contaminations of pathogenic microbes to infer human health risk; 4) applying this framework to 5 Category A pathogens, and systematically analyzed sources of uncertainty in modeled parameters.

Chapter 2 adopted the BMC method, a robust tool for high dimensional model calibration, to update parameter values for an integrated fate, transport, and risk assessment model. As a Bayesian approach, this method compared model predictions, based on people's prior belief, with surface measurements for concentrations of released *B. anthracis* on various locations, and reweighted the distributions for model inputs. The benefits of applying the BMC process include: 1) updated parameter ranges (or validation of prior knowledge) for a model predicting the spatial distribution of released biological agents; 2) significantly reduced uncertainties in the estimated human health risk, which provide more accurate information for the decision makers seeking to identify the proper response (i.e., when to distribute prophylactic antibiotic). In addition, Chapter 2

conducted a multivariate regression analysis, which aimed to select the best human health risk indicators.

Chapter 3 focused on characterizing important information of a biological release, such as the quantity and particulate size, based on surface sampling results. It developed a 7-step evaluation framework for choosing the sampling and modeling approach which most accurately recovers details of a release from surface samples. Then the performance of the recommended sampling scheme was tested by feeding with data from a large scale field test. The findings from this chapter not only answered the question "what is the best place to sample?", but also provided insights for the question "how many samples should be taken?". However, the answers to those two questions depend on the precision of sampling results, which is usually impacted by the sample recovery efficiency. Ideally, the required number of surface samples should equal the number of particle sizes to be identified. When one considers that the sampling results could be biased, more samples are necessary. Thus, the methodology developed in this chapter shows its value, since it systemically enumerates and evaluates all the possible approaches and chooses the one most resistant to bias. This sampling plan evaluation process should be considered as part of preparations towards a biological agent attack. Field tests should be executed before a 'real' bioterrorism attack, since the characterized release amount and its consequences identified from different sampling plans can be compared with the 'correct information', which would be unavailable during a biological agent attack.

Chapter 4 extended the fate, transport, and risk assessment model by synthesizing available information on five Category A pathogens (*Bacillus anthracis*, *Yersinia pestis, Francisella tularensis, Variola major* and Lassa) to develop quantitative guidelines for how environmental pathogen concentrations may be related to human health risk. These findings provide critical information for developing a risk-informed biological attack response system. Questions such as " how to estimate if risks warrant the distribution of prophylactic antibiotics?", and " how to choose between active or passive decontamination approaches?" were addressed. In addition, this chapter differentiated the sources of uncertainties (epistemic uncertainty vs. variability) for modeled parameters. An approach was proposed for how to integrate these quantitative assessments of parameter uncertainty with broader, qualitative considerations to identify future research priorities.

5.2 Future research

5.2.1 Assumptions and limitations

In all risk assessments, the estimated risk is based on a number of assumptions, which were summarized in Table 5-1. Thus, future researches should be mainly focused on those assumptions. The fate and transport model, predicting the spatial distribution of released biological agents, was a critical element for the risk assessment framework, since many conclusions were drawn based on its predictions. However, this model was established based on the assumption that pathogens were instantly uniformly mixed in a compartment. This assumption failed to capture localized areas of high risks, such as a

high concentrated puff of pathogens right after initial release. Thus the approach developed in the dissertation was more appropriate for the situation somewhat removed in time and space from the initial release. In the future, I recommend a more detailed approach, such as computational fluid dynamics, to extend the fate and transport model, although this would be quite computationally intensive.

Table 5-1 Table of major assumptions

Where	Assumption	Why	Drawback	Future suggestion
Fate and transport model	Instantly uniformly mixed	Simplify the model	Fail to capture localized areas of high risks	Build a zonal model or CFD model
Dose-response model	Same dose-response coefficient for different exposure routes	Knowledge gap	Fail to represent low dose and repeated doses over time	Computer simulation (computational biology)
	Model is based on high dose lab tests with limited animals	Knowledge gap		
Analytical method	Viable pathogens are measured	Knowledge gap	Actual response characterization may include measurements of non-viable organisms such as qPCR	Develop quantitative knowledge of qPCR signal decay over time
Pathogen attenuation rate	Log linear over time	Simplify the model	Could underestimate pathogens' survival rate	Consider other types of model such as biphasic exponential model

As another important component for the risk assessment framework, many assumptions were employed in deriving the dose-response model. In order to improve its predictive power, the following related questions are worth further investigation: 1) How to extrapolate the results from high dose laboratory tests with limited numbers of animals to the effects of lower doses, which is more common during a biological attack?; 2) How will the dose response model be changed if the effects of previous exposure on the same population is included?; and 3) How to model interactions from exposure to multiple pathogens?

The surface sampling results used in Chapter 2 were based on measured viable pathogen concentrations. It was quantified by PCR (qPCR), which has been proven to be effective in quantifying biological warfare agents (i.e., *B. antracis*, and *Y. pestis*) due to its rapid, early, and accurate results [200]. Despite the advantages of qPCR analysis, several knowledge gaps need to be addressed in the future. The first is that qPCR does not distinguish between living or dead pathogens. While researchers have identified assays to discriminate between viable and dead fecal *bacteroidales* bacteria, similar methods have not been applied to Category A pathogens [10, 53]. Second there is little information on the decay of the qPCR signal over time, which would be an essential parameter for the retrospective assessment of risk after a release. Thus, studies are needed to quantify parameters such as, the efficiency of DNA extraction, the degradation of nucleic acids overtime, and the reactivity of primer and probe [24, 110, 156].

Pathogen attenuation rate outside the host was assumed to be log linear over time in Chapter 3. However, in reality microorganisms often exhibit “tailing” in which a small, highly resistant subpopulation attenuates at a very low rate. Thus the assumption of log-linear decay may not be health protective. In the future, this attenuation rate should be considered as a function of time, which could better characterize pathogens' inactivation process. Candidate models include biphasic exponential model, exponentially damped model, Juneja & Marks type I, II models, general logistic model, and Gompertz model [97, 201].

In order to make the BMC updating model more readily applicable, the MATLAB code developed here could be programmed into a software package to perform the updating which would enable the approach to be employed after an incident by individuals without specialized computer knowledge. In addition, the speed of BMC updating could be improved by conducting most of the computations using a parallel computing approach, such as using a GPU instead of a CPU [137].

5.2.2 Response and recovery framework

Although models and methods developed in this dissertation successfully enhanced the ability of characterizing a biological attack, it only addressed a small portion of a biological attack response and recovery framework. Thus, for the purpose of reducing the consequences of a terrorist attack, and rebuilding public confidence, future research attention should be paid on the phases of initial response, decontamination, and aftermath restoration. In the phase of initial response, biological agent detection is the

trigger of the whole response system. Thus, it should be given highest research priority, recourses should be allocated to constructing an economic and robust pathogen detection network, which would be capable of detecting multiple pathogens in real time at a low false alarm rate [116]. In this phase, another critical problem should be considered is how to treat the exposed people, since without timely medical intervention, the mortality rate for inhalational anthrax is almost 100%. Currently antibiotic storage and distribution systems, which have the capability to distribute antibiotics to the exposed people before the appearance of clinical symptoms, are designed for only three cities, Seattle, Boston, and Philadelphia [47]. Thus this system should be expanded and applied for the cities with high probability of suffering a biological attack in the future.

In the phase of decontamination, cost-benefit analysis should be introduced to lower the overall cost but maintain the residual risk within an acceptable level at the same time. Lessons learnt from the 2001 anthrax attacks indicated that the economic loss due to the disruption of work could be more than the decontamination cost [147]. Thus, it is necessary to have a set of criteria to differentiate whether it is more economical to decontaminate or destroy contaminated items. In addition, the following questions are worthy of further research: 1) how to choose the proper decontamination method especially for weaponized biological agents; 2) how to treat decontamination waste, which is a challenge to the environment; and 3) how to validate environmental sampling and laboratory analytical methodologies, which verify the effectiveness of decontamination [28, 164].

In the phase of restoration, future analysis should be focused on the following aspects: 1) how to determine a decontaminated area is clean enough, and people are ready to come back? 2) should different restoration actives (i.e., residential, business) happened parallel or sequentially; 3) how long the health conditions for the reoccupants need to be monitored; 4) what is the best strategy to let the public accept the residual contamination risk after reoccupation. In reality, the last question should be answered first. Because the official confirmation that an area is safe for reoccupation is meaningless, if the public still consider their health to be at risk. Thus, it is critical to enable the public to understand risk issues they may not be familiar with, which will require the participation of a many parties, such as government, media, etc.

LIST OF REFERENCES

1. Abramova, Faina A., et al., *Pathology of inhalational anthrax in 42 cases from the sverdlovsk outbreak of 1979.* Proceedings of the National Academy of Sciences of the United States of America, 1993. **90**(6): p. 2291-2294.

2. Aledort, Julia, et al., *Non-pharmaceutical public health interventions for pandemic influenza: An evaluation of the evidence base.* Bmc Public Health, 2007. **7**(1): p. 208.

3. Altboum, Z., et al., *Postexposure prophylaxis against anthrax: Evaluation of various treatment regimens in intranasally infected guinea pigs.* Infection and Immunity, 2002. **70**(11): p. 6231-6241.

4. Amidan, Brett G., Brent A. Pulsipher, and Brett D. Matzke, *Statistical analyses of second indoor bio-release field evaluation study at idaho national laboratory*. 2009. p. Medium: ED; Size: PDFN.

5. Ansari, S A, et al., *Rotavirus survival on human hands and transfer of infectious virus to animate and nonporous inanimate surfaces.* J. Clin. Microbiol., 1988. **26**(8): p. 1513-1518.

6. Ansari, S A, et al., *Potential role of hands in the spread of respiratory viral infections: Studies with human parainfluenza virus 3 and rhinovirus 14.* J. Clin. Microbiol., 1991. **29**(10): p. 2115-2119.

7. Arquilla, John and David Ronfeldt, *The advent of netwar: Analytic background.* Studies in Conflict & Terrorism, 1999. **22**(3): p. 193-206.

8. ASHRAE, *Ashrae handbook: Fundamentals*. Fundamentals - i-p units. 2005, Atlanta: ASHRAE.

9. Atkinson, M. P. and L. M. Wein, *Quantifying the routes of transmission for pandemic influenza.* Bulletin of Mathematical Biology, 2008. **70**(3): p. 820-867.

10. Bae, Sungwoo and Stefan Wuertz, *Discrimination of viable and dead fecal bacteroidales bacteria by quantitative pcr with propidium monoazide.* Applied and Environmental Microbiology, 2009. **75**(9): p. 2940-2944.

11. Bartrand, T. A., M. H. Weir, and C. N. Haas, *Dose-response models for inhalation of bacillus anthracis spores: Interspecies comparisons.* Risk Analysis, 2008. **28**(4): p. 1115-1124.

12. Benke, K. and A. Hamilton, *Quantitative microbial risk assessment: Uncertainty and measures of central tendency for skewed distributions.* Stochastic Environmental Research and Risk Assessment, 2008. **22**(4): p. 533-539.

13. Block, S. M., *The growing threat of biological weapons.* Molecular Biology of the Cell, 2002. **13**: p. 3-11.

14. Borio, L., et al., *Hemorrhagic fever viruses as biological weapons - medical and public health management.* Jama-Journal of the American Medical Association, 2002. **287**(18): p. 2391-2405.

15. Boyce, John M., *Recent trends in the epidemiology of tularemia in the united states.* The Journal of Infectious Diseases, 1975. **131**(2): p. 197-199.

16. Brachman, P. S., *Inhalation anthrax.* Annals of the New York Academy of Sciences, 1980. **353**.

17. Bradley A. Perkins, * , * Tanja Popovic, and Kevin Yeskey*, *Public health in the time of bioterrorism.* Emerging Infectious Diseases, 2002. **8**(10).

18. Brand, Kevin P. and Mitchell J. Small, *Updating uncertainty in an integrated risk assessment: Conceptual framework and methods.* Risk Analysis, 1995. **15**(6): p. 719-729.

19. Brookmeyer, R., E. Johnson, and S. Barry, *Modelling the incubation period of anthrax.* Statistics in Medicine, 2005. **24**(4): p. 531-542.

20. Brookmeyer, R., E. Johnson, and R. Bollinger, *Public health vaccination policies for containing an anthrax outbreak.* Nature, 2004. **432**(7019): p. 901-904.

21. Brown, G. S., et al., *Evaluation of a wipe surface sample method for collection of bacillus spores from nonporous surfaces.* Applied and Environmental Microbiology, 2007. **73**(3): p. 706-10.

22. Brown, Gary S., et al., *Evaluation of vacuum filter sock surface sample collection method for bacillus spores from porous and non-porous surfaces.* Journal of Environmental Monitoring, 2007. **9**(7): p. 666-671.

23. BURTON, NANCY CLARK, SERGEY A. GRINSHPUN, and TIINA REPONEN, *Physical collection efficiency of filter materials for bacteria and viruses.* Annals of Occupational Hygiene, 2007. **51**(2): p. 143-151.

24. Bushon, R. N., et al., *Statistical assessment of DNA extraction reagent lot variability in real-time quantitative pcr.* Letters in Applied Microbiology, 2010. **50**(3): p. 276-282.

25. Busschaert, Pieter, et al., *Sensitivity analysis of a two-dimensional quantitative microbiological risk assessment: Keeping variability and uncertainty separated.* Risk Analysis, 2011. **31**(8): p. 1295-1307.

26. Busson, B., *Ein beitrag zur kenntnis der lebensdauer von bacterium coli und milzbrandsporen.* 1911. **58**(505-509).

27. Butler, T., *Plague into the 21st century.* Clinical Infectious Diseases, 2009. **49**(5): p. 736-742.

28. Canter, Dorothy A., *Remediating anthrax-contaminated sites: Learning from the past to protect the future.* Chemical Health and Safety, 2004. **12**(4): p. 13-19.

29. Carus, W. Seth, *Bioterrorism and biocrimes: The illicit use of biological agents since 1900*. 2002: Fredonia Books.

30. CDC. *Bioterrorism agents/diseases. Available: Http://www.Bt.Cdc.Gov/agent/agentlist-category.Asp*. [cited 2011 April-27th]; Available from: http://www.bt.cdc.gov/agent/agentlist-category.asp.

31. CDC. *Bioterrorism overview*. 2007 February 12, 2007; Available from: http://www.bt.cdc.gov/bioterrorism/overview.asp.

32. CDC. *Cdc plague home page*. 2009; Available from: http://www.cdc.gov/ncidod/dvbid/plague/.

33. CDC, *Human plague--four states, 2006.* Jama, 2006. **296**(14): p. 1722-1724.

34. CDC, *Summary of notifiable diseases.* Morbidity and Mortality Weekly Report, 1998. **46**.

35. CDC, *Tularemia — united states, 1990–2000.* Morbidity and Mortality Weekly Report, 2002. **51**(9).

36. CDC, *Update: Investigation of bioterrorism-related anthrax, 2001*. MMWR: Morbidity & Mortality Weekly Report, 2001. **50**(45): p. 1008-1010.

37. Coleman, M. E., et al., *Inhalation anthrax: Dose response and risk analysis.* Biosecurity and Bioterrorism-Biodefense Strategy Practice and Science, 2008. **6**(2): p. 147-159.

38. Cox, C. S., *Aerosol survival of pasteurella-tularensis disseminated from wet and dry states.* Applied Microbiology, 1971. **21**(3): p. 482-486.

39. Cox, C. S. and L. J. Goldberg, *Aerosol survival of pasteurella-tularensis and influence of relative humidity.* Applied Microbiology, 1972. **23**(1): p. 1-3.

40. Cox, L. A. and D. A. Popken, *Bayesian monte carlo uncertainty analysis of human health risks from animal antimicrobial use in a dynamic model of emerging resistance.* Risk Analysis, 2004. **24**(5): p. 1153-1164.

41. Cox, L. A. and D. A. Popken, *Overcoming confirmation bias in causal attribution: A case study of antibiotic resistance risks.* Risk Analysis, 2008. **28**(5): p. 1155-1171.

42. Da Silva, Sandra M., James J. Filliben, and Jayne B. Morrow, *Parameters affecting spore recovery from wipes used in biological surface sampling.* Applied and Environmental Microbiology, 2011. **77**(7): p. 2374-2380.

43. Day, W. C. and R. F. Berendt, *Experimental tularemia in macaca mulatta: Relationship of aerosol particle size to the infectivity of airborne pasteurella tularensis.* Infect Immun, 1972. **5**(1): p. 77-82.

44. Dennis, D. T., *Plague as a biological weapon*, in *Bioterrorism and infectious agents: A new dilemma for 21st century*. 2005, Springer: New York. p. 37-70.

45. Dennis, D. T., et al., *Tularemia as a biological weapon - medical and public health management.* Jama-Journal of the American Medical Association, 2001. **285**(21): p. 2763-2773.

46. Dewan, P. K., et al., *Inhalational anthrax outbreak among postal workers, washington, dc, 2001.* Emerging Infectious Diseases, 2002. **8**(10): p. 1066-1072.

47. DHS, *Proposed guidance for protecting responders' health during the first week following a wide-area anthrax attack (deliberative draft)*. 2009.

48. Dienst, J., F. T., *Tularemia — a perusal of three hundred thirty-nine cases.* Journal of the Louisiana State Medical Society, 1963. **115**.

49. Dilks, David W., Raymond P. Canale, and Peter G. Meier, *Development of bayesian monte carlo techniques for water quality model uncertainty.* Ecological Modelling, 1992. **62**(1-3): p. 149-162.

50. Dixon, T. C., et al., *Anthrax.* New England Journal of Medicine, 1999. **341**(11): p. 815-826.

51. Djavani, M., et al., *Murine immune responses to mucosally delivered salmonella expressing lassa fever virus nucleoprotein.* Vaccine, 2000. **18**(15): p. 1543-1554.

52. Doolan, D. L., et al., *The us capitol bioterrorism anthrax exposures: Clinical epidemiological and immunological characteristics.* J Infect Dis, 2007. **195**(2): p. 174-84.

53. Dorevitch, Samuel, et al., *Meeting report: Knowledge and gaps in developing microbial criteria for inland recreational waters.* Environ Health Perspect, 2010. **118**(6): p. 871-876.

54. Downes, Randolph C., *The effect of smallpox on the destiny of the amerindian. By e. Wagner stearn and allen e. Stearn. (boston: Bruce humphries, inc., 1945. 139 pp. Bibliography and index. $2.50.).* The Mississippi Valley Historical Review, 1946. **32**(4): p. 627-628.

55. Dull, P. M., K. E. Wilson, B. Kournikakis, E. A. S. Whitney, C. A. Boulet, J. Y. W. Ho, et al, *Bacillus anthracis aerosolization associated with a contaminated mail sorting machine.* Emerg. Infect, 2002: p. 1044-1047.

56. Edmonds, J. M., *Efficient methods for large-area surface sampling of sites contaminated with pathogenic microorganisms and other hazardous agents: Current state, needs, and perspectives.* Applied Microbiology and Biotechnology, 2009. **84**(5): p. 811-816.

57. Edwards, K. A., H. A. Clancy, and A. J. Baeumner, *Bacillus anthracis: Toxicology, epidemiology and current rapid-detection methods.* Analytical and Bioanalytical Chemistry, 2006. **384**(1): p. 73-84.

58. Ehrlich, R. and S. Miller, *Survival of airborne pasteurella-tularensis at different atmospheric temperatures.* Applied Microbiology, 1973. **25**(3): p. 369-372.

59. EPA, *Exposure factors handbook*. 1997: Washington, DC : Exposure Assessment Group, Office of Health and Environmental Assessment, U.S. Environmental Protection Agency.

60. Estill, Cheryl Fairfield, et al., *Comparison of air sampling methods for aerosolized spores of b. Anthracis sterne.* Journal of Occupational and Environmental Hygiene, 2011. **8**(3): p. 179 - 186.

61. Estill, Cheryl Fairfield, et al., *Recovery efficiency and limit of detection of aerosolized bacillus anthracis sterne from environmental surface samples.* Applied and Environmental Microbiology, 2009. **75**(13): p. 4297-4306.

62. Evans, Martin E., et al., *Tularemia: A 30-year experience with 88 cases.* Medicine, 1985. **64**(4): p. 251-269.

63. Ferguson, A. C., et al., *Video methods in the quantification of children's exposures.* Journal of Exposure Science and Environmental Epidemiology, 2006. **16**(3): p. 287-298.

64. Field, Antony, *The 'new terrorism': Revolution or evolution?* Political Studies Review, 2009. **7**(2): p. 195-207.

65. Franco, Crystal and Nidhi Bouri, *Environmental decontamination following a large-scale bioterrorism attack: Federal progress and remaining gaps.* Biosecurity and Bioterrorism, 2010. **8**(2).

66. Frawley, D. A., et al., *Recovery efficiencies of anthrax spores and ricin from nonporous or nonabsorbent and porous or absorbent surfaces by a variety of sampling methods.* Journal of Forensic Sciences, 2008. **53**(5): p. 1102-1107.

67. GAO, *Capitol hill anthrax incident: Epa's cleanup was successful; opportunities exist to enhance contract oversight*. 2003: Washington, D.C.

68. Graham-Smith, G. S., *The longevity of dry spores of b. Anthracis.* Journal of Hydrology, 1930. **30**: p. 213-215.

69. Gurian, Patrick L., Felipe Castro, and Yi-Chang Chiu. *A bayesian monte carlo approach to model calibration for queuing systems*. in *The 84th Annual Meeting of the Transportation Research Board*. 2004. Washington, DC.

70. Haas, C. N., *The role of risk analysis in understanding bioterrorism.* Risk Analysis, 2002. **22**(4): p. 671-677.

71. Haas, Charles N., Joan B. Rose, and Charles P. Gerba, *Quantitative microbial risk assessment*. 1999, New York: Wiley.

72. Hardestam, J., et al., *Ex vivo stability of the rodent-borne hantaan virus in comparison to that of arthropod-borne members of the bunyaviridae family.* Applied and Environmental Microbiology, 2007. **73**(8): p. 2547-2551.

73. Harper, G. J., *Airborne micro-organisms-survival tests with 4 viruses.* Journal of Hygiene, 1961. **59**(4): p. 479-486.

74. Harper, G. J., *The influence of environment on the survival of airborne virus particles in the laboratory.* Arch. Gesamte Virusforsch, 1963. **13**: p. 64-71.

75. Harris, Sheldon, *Factories of death: Japanese biological warfare, 1932-1945, and the american cover-up*. 1995, Kentucky: Routledge.

76. Health, San Francisco Dept Public, *Infectious disease emergencies: A preparedness and response guide for san francisco clinicians*, P.H. Home, Editor. 2008: San Franciscol.

77. Helvacı, S., et al., *Tularemia in bursa, turkey: 205 cases in ten years.* European Journal of Epidemiology, 2000. **16**(3): p. 271-276.

78. Henderson, D. A., et al., *Smallpox as a biological weapon - medical and public health management.* Jama-Journal of the American Medical Association, 1999. **281**(22): p. 2127-2137.

79. Henderson, Donald A. and Bernard Moss, *Smallpox and vaccinia*, in *Vaccinia*, S.A. Plotkin and W.A. Orenstein, Editors. 1999, Saunders: Philadelphia.

80. Herzog, Amanda B., et al., *Implications of detection limit of various methods for bacillus anthracis in computing risk to human health.* Applied and Environmental Microbiology, 2009(75): p. 6331-6339.

81. Heymann, David L., *Control of communicable diseases manual*. 18th ed. 2004, Washington, DC: American Public Health Association.

82. Hinton, M. H., *Infections and intoxications associated with animal feed and forage which may present a hazard to human health.* The Veterinary Journal, 2000. **159**(2): p. 124-138.

83. Hoffman, Bruce, *The contrasting ethical foundations of terrorism in the 1980s.* Terrorism and Political Violence, 1989. **1**(3): p. 361-377.

84. Holty, J. E. C., et al., *Systematic review: A century of inhalational anthrax cases from 1900 to 2005.* Annals of Internal Medicine, 2006. **144**(4): p. 270-280.

85. Hong, T., P. L. Gurian, and N. F. D. Ward, *Setting risk-informed environmental standards for bacillus anthracis spores.* Risk Analysis, 2010. **30**(10): p. 1602-1622.

86. Hong, Tao, *Estimating risk of exposure to bacillus anthracis based on environmental concentration*, in *Civil, Architectural and Environmental Engineering*. 2009, Drexel: Philadelphia.

87. Hong, Tao and Patrick L. Gurian, *A bayesian approach to model calibration for weaponized b. Anthracis risk assessment (under preparation).* Environmental Science & Technology, 2011.

88. Hong, Tao, et al., *Prioritizing risks and uncertainties from intentional release of selected category a pathogens (under revision).* Plos One, 2011.

89. Hopkins, Donald R., *Ramses v:Earliest known victim?* 1980, WHO.

90. Huang, Y. and C. N. Haas, *Time-dose-response models for microbial risk assessment.* Risk Analysis, 2009. **29**(5): p. 648-661.

91. Huang, Y., et al., *How sensitive is safe? Risk-based targets for ambient monitoring of pathogens.* Sensors Journal, IEEE, 2010. **10**(3): p. 668-673.

92. Hughes-Jones, M., *1996-97 global anthrax report.* Journal of Applied Microbiology, 1999. **87**(2): p. 189-191.

93. Hughes, J. M. and J. L. Gerberding, *Anthrax bioterrorism: Lessons learned and future directions.* Emerg Infect Dis, 2002. **8**(10): p. 1013-4.

94. Inglesby, T. V., *Anthrax as a biological weapon, 2002: Updated recommendations for management (vol 287, pg 2236, 2002).* Jama-Journal of the American Medical Association, 2002. **288**(15): p. 1849-1849.

95. Jernigan, D. B., et al., *Investigation of bioterrorism-related anthrax, united states, 2001: Epidemiologic findings.* Emerg Infect Dis, 2002. **8**(10): p. 1019-28.

96. Julian, Timothy R., et al., *A model of exposure to rotavirus from nondietary ingestion iterated by simulated intermittent contacts.* Risk Analysis, 2009. **29**(5): p. 617-632.

97. Juneja, Vijay K. and Harry M. Marks, *Mathematical description of non-linear survival curves of listeria monocytogenes as determined in a beef gravy model system at 57.5 to 65 °c.* Innovative Food Science & Emerging Technologies, 2003. **4**(3): p. 307-317.

98. Kaufmann, A. F., M. I. Meltzer, and G. P. Schmid, *The economic impact of a bioterrorist attack: Are prevention and postattack intervention programs justifiable?* Emerging Infectious Diseases, 1997. **3**(2): p. 83-94.

99. Ken, Alibek and Stephen Handelman, *Biohazard: The chilling true story of the largest covert biological weapons program in the world - told from inside by the man who ran it*. 1999, Buena Park: Delta.

100. Kool, J. L., *Risk of person-to-person transmission of pneumonic plague.* Clinical Infectious Diseases, 2005. **40**(8): p. 1166-1172.

101. Kowalski, Wladyslaw Jan, *Immune building system technology*. 2003, New York: McGraw-Hill.

102. Kuhlman, M.R, *Preliminary spot report on particle size analyses*. 2001, Battelle Memorial Institute.

103. Lai, A. C. K. and W. W. Nazaroff, *Modeling indoor particle deposition from turbulent flow onto smooth surfaces.* Journal of Aerosol Science, 2000. **31**(4): p. 463-476.

104. Landahl, H., *On the removal of air-borne droplets by the human respiratory tract: I. The lung.* Bulletin of Mathematical Biology, 1950. **12**(1): p. 43-56.

105. Laqueur, W., *Postmodern terrorism.* Foreign Affairs, 1996. **75**(5): p. 24-36.

106. Lathem, W. W., et al., *Progression of primary pneumonic plague: A mouse model of infection, pathology, and bacterial transcriptional activity.* Proceedings of the National Academy of Sciences of the United States of America, 2005. **102**(49): p. 17786-17791.

107. Leduc, J. W., *Epidemiology of hemorrhagic-fever viruses.* Reviews of Infectious Diseases, 1989. **11**: p. S730-S735.

108. Lesperance, AM, *Catastrophic incident recovery: Long-term recovery from an anthrax event symposium*, in *PNNL-17659*. 2008, Pacific Northwest National Laboratory: Richland, WA.

109. Levy, Barry S. and Victor W. Sidel, *Adverse health consequences of us government responses to the 2001 terrorist attacks.* The Lancet, 2011. **378**(9794): p. 944-952.

110. Lim, D. V., et al., *Current and developing technologies for monitoring agents of bioterrorism and biowarfare.* Clinical Microbiology Reviews, 2005. **18**(4): p. 583-607.

111. Linkov, Igor, et al., *Anthrax cleanup decisions: Statistical confidence or confident response.* Environmental Science & Technology, 2011. **45**(22): p. 9471-9472.

112. Mahl, M. C. and C. Sadler, *Virus survival on inanimate surfaces.* Canadian Journal of Microbiology, 1975. **21**(6): p. 819-823.

113. Marshall, R. G. and P. J. Gerone, *Susceptibility of suckling mice to variola virus.* J Bacteriol, 1961. **82**: p. 15-19.

114. MathWorks, The. *Matlab*. 2008; Available from: http://www.mathworks.com/.

115. MAUGH, THOMAS H., *An empire's epidemic*, in *Los Angeles Times*. 2002, Eddy Hartenstein: Los Angeles.

116. McBride, Mary T., et al., *Autonomous detection of aerosolized bacillus anthracis and yersinia pestis.* Analytical Chemistry, 2003. **75**(20): p. 5293-5299.

117. Medema, Gertjan and Nicholas Ashbolt, *Qmra: Its value for risk management*. 2006.

118. Meselson, M., et al., *The sverdlovsk anthrax outbreak of 1979.* Science, 1994. **266**(5188): p. 1202-1208.

119. Meyer, K. F., *Modern therapy of plague.* J Am Med Assoc, 1950. **144**(12): p. 982-985.

120. Miller, S. L. and W. W. Nazaroff, *Environmental tobacco smoke particles in multizone indoor environments.* Atmospheric Environment, 2001. **35**(12): p. 2053-2067.

121. Mitchell-Blackwood, J., P. L. Gurian, and C. O'Donnell, *Finding risk-based switchover points for response decisions for environmental exposure to bacillus anthracis.* Human and Ecological Risk Assessment, 2011. **17**(2): p. 489-509.

122. Mitchell-Blackwood, Jade, *Using analytic models for risk-based responses to pathogenic agents in the environment*, in *Civil, Architectural, and Environmental Engineering* 2010, Drexel University: Philadelphia.

123. Mitchell-Blackwood, Jade and Patrick L. Gurian, *Finding risk-based switchover points for response decisions for environmental exposure to bacillus anthracis (in press).* Human and Ecological Risk Assessment, 2010.

124. Mitscherlich, E. and E. H. Marth, *Microbial survival in the environment: Bacteria and rickettsiae important in human and animal health*. 1984, Berlin, Germany.: Springer-Verlag.

125. Moore, Z. S., J. F. Seward, and J. M. Lane, *Smallpox.* Lancet, 2006. **367**(9508): p. 425-435.

126. Moran, Gregory J., David A. Talan, and Fredrick M. Abrahamian, *Biological terrorism.* Infectious Disease Clinics of North America, 2008. **22**(1): p. 145-187.

127. Morgan, M. Granger, et al., *Uncertainty in risk assessment.* Environmental Science & Technology, 1985. **19**(8): p. 662-667.

128. Morgan, Millett Granger and Max Henrion, *Uncertainty: A guide to dealing with uncertainty in quantitative risk and policy analysis*. 1992: Cambridge University Press.

129. Nazaroff, W. W., *Indoor particle dynamics.* Indoor Air, 2004. **14**: p. 175-183.

130. Nazaroff, W. W. and G. R. Cass, *Mass-transport aspects of pollutant removal at indoor surfaces.* Environment International, 1989. **15**(1-6): p. 567-584.

131. Nazaroff, W. W. and G. R. Cass, *Mathemtical-modeling of indoor aerosol dynamics.* Environmental Science & Technology, 1989. **23**(2): p. 157-166.

132. Nicas, M. and D. Best, *A study quantifying the hand-to-face contact rate and its potential application to predicting respiratory tract infection.* Journal of Occupational and Environmental Hygiene, 2008. **5**(6): p. 347-352.

133. Nicas, M. and S. Gang, *An integrated model of infection risk in a health-care environment.* Risk Analysis, 2006. **26**(4): p. 1085-1096.

134. Novel, R. and T. Reh., *De la longevite des spores du bacillus anthracis et de la conservation des pouvoirs pathogene et antigene.* Schweiz. Z. Pathol. Bakteriol, 1947. **10**: p. 180-192.

135. NPR. *Timeline: How the anthrax terror unfolded*. 2011 11-20-2011]; Available from: http://www.npr.org/2011/02/15/93170200/timeline-how-the-anthrax-terror-unfolded.

136. NRC, *Reopening public facilities after a biological attack: A decision-making framework*. 2005, Washington, D.C.: The National Academies Press.

137. NVIDIA, *Compute unified device architecture-programming guide*. 2007: Santa Clara.

138. Ogbu, O., E. Ajuluchukwu, and C. J. Uneke, *Lassa fever in west african sub-region: An overview.* Journal of vector borne diseases, 2007. **44**(1): p. 1-11.

139. Ott, Wayne R., *Environmental statistics and data analysis*. 1995: CRC Press, Inc.

140. Oyston, Petra C. F., Anders Sjostedt, and Richard W. Titball, *Tularaemia: Bioterrorism defence renews interest in francisella tularensis.* Nat Rev Micro, 2004. **2**(12): p. 967-978.

141. P. Rusin, S. Maxwell, C. Gerba,, *Comparative surface-to-hand and fingertip-to-mouth transfer efficiency of gram-positive bacteria, gram-negative bacteria, and phage.* Journal of Applied Microbiology, 2002. **93**(4): p. 585-592.

142. Perry, R. D. and J. D. Fetherston, *Yersinia pestis - etiologic agent of plague.* Clinical Microbiology Reviews, 1997. **10**(1): p. 35-&.

143. Pile, J. C., et al., *Anthrax as a potential biological warfare agent.* Archives of Internal Medicine, 1998. **158**(5): p. 429-434.

144. Pohanka, M. and P. Skladal, *Bacillus anthracis, francisella tularensis and yersinia pestis. The most important bacterial warfare agents - review.* Folia Microbiologica, 2009. **54**(4): p. 263-272.

145. Preston, S. D., et al., *Capillary and arterial cerebral amyloid angiopathy in alzheimer's disease: Defining the perivascular route for the elimination of amyloid beta from the human brain.* Neuropathology and Applied Neurobiology, 2003. **29**(2): p. 106-117.

146. Price, P. N., et al., *Framework for evaluating anthrax risk in buildings.* Environmental Science & Technology, 2009. **43**(6): p. 1783-1787.

147. Price, Phillip N., et al., *Anthrax sampling and decontamination: Technology trade-offs*. 2009.

148. Ramaswami, Anu, Jana B. Milford, and Mitchell J. Small, *Integrated environmental modeling: Pollutant transport, fate, and risk in the environment*. 2005: John Wiley&Sons.

149. Reshetin, V. P. and J. L. Regens, *Simulation modeling of anthrax spore dispersion in a bioterrorism incident.* Risk Analysis, 2003. **23**(6): p. 1135-1145.

150. Richards, J. L. and D. E. Grimes, *Bioterrorism: Class a agents and their potential presentations in immunocompromised patients.* Clinical Journal of Oncology Nursing, 2008. **12**(2): p. 295-302.

151. Richmond, J. K. and D. J. Baglole, *Lassa fever: Epidemiology, clinical features, and social consequences.* British Medical Journal, 2003. **327**(7426): p. 1271-1275.

152. Riley, W. J., et al., *Indoor particulate matter of outdoor origin: Importance of size-dependent removal mechanisms.* Environmental Science & Technology, 2002. **36**(2): p. 200-207.

153. Roman, Steven *Advanced linear algebra*. 2008, New York: Springer.

154. Rose, L. J., et al., *Survival of yersinia pestis on environmental surfaces.* Applied and Environmental Microbiology, 2003. **69**(4): p. 2166-2171.

155. Rosengard, Ariella M., *Smallpox: The fight to eradicate a global scourge.* The Journal of Clinical Investigation, 2003. **112**(12): p. 1775-1775.

156. Ruijter, J. M., et al., *Amplification efficiency: Linking baseline and bias in the analysis of quantitative pcr data.* Nucleic Acids Research, 2009. **37**(6): p. e45.

157. Sabelnikov, A., V. Zhukov, and C. R. Kempf, *Airborne exposure limits for chemical and biological warfare agents: Is everything set and clear?* International Journal of Environmental Health Research, 2006. **16**(4): p. 241-253.

158. Sanderson, W. T., et al., *Bacillus anthracis contamination and inhalational anthrax in a mail processing and distribution center.* Journal of Applied Microbiology, 2004. **96**(5): p. 1048-1056.

159. Sanford, Jay P., *Tularemia.* Jama, 1983. **250**(23): p. 3225-3226.

160. Schenker, U., et al., *Using information on uncertainty to improve environmental fate modeling: A case study on ddt.* Environmental Science & Technology, 2009. **43**(1): p. 128-134.

161. Schlesinger, Richard B., *Deposition and clearance of inhaled particles*, in *Concepts in inhalation toxicology*, R.O. McClellan and R.F. Henderson, Editors. 1989, Taylor&Francis: Washington, D.C. p. 191-217.

162. Sextro, R. G. , et al. *Modeling the spread of anthrax in buildings*. in *Indoor air 2002*. 2002. Monterey, CA.

163. Shane, Scott and Sun Staff. *Cleanup of anthrax will cost hundreds of millions of dollars*. 2002; Available from: http://cltv.trb.com/entertainment/bal-te.anthrax18dec18,1,1593731.story.

164. Sharp, R. J. and A. G. Roberts, *Anthrax: The challenges for decontamination.* Journal of Chemical Technology and Biotechnology, 2006. **81**(10): p. 1612-1625.

165. Simon, Steven and Daniel Benjamin, *The terror.* Survival, 2001. **43**(4): p. 05-18.

166. Sinclair, R., et al., *Persistence of category a select agents in the environment.* Applied and Environmental Microbiology, 2008. **74**(3): p. 555-563.

167. Sirisanthana, T. and A. E. Brown, *Anthrax of the gastrointestinal tract.* Emerging Infectious Diseases, 2002. **8**(7): p. 649-651.

168. Sirisanthana, T., et al., *Serological studies of patients with cutaneous and oral-oropharyngeal anthrax from northern thailand.* American Journal of Tropical Medicine and Hygiene, 1988. **39**(6): p. 575-581.

169. Slack, P., *The black-death past and present .2. Some historical problems.* Transactions of the Royal Society of Tropical Medicine and Hygiene, 1989. **83**(4): p. 461-463.

170. Smieszek, Timo, *A mechanistic model of infection: Why duration and intensity of contacts should be included in models of disease spread.* Theoretical Biology and Medical Modelling, 2009. **6**(1): p. 25.

171. Sohn, M. D., et al., *Predicting size-resolved particle behavior in multizone buildings.* Atmospheric Environment, 2007. **41**(7): p. 1473-1482.

172. Sohn, M. D., et al., *Rapidly locating and characterizing pollutant releases in buildings.* J Air Waste Manag Assoc, 2002. **52**(12): p. 1422-32.

173. Sohn, M. D., et al., *Responding to sudden pollutant releases in office buildings: 1. Framework and analysis tools.* Indoor Air, 2003. **13**(3): p. 267-276.

174. Sreedharan, P., et al., *Systems approach to evaluating sensor characteristics for real-time monitoring of high-risk indoor contaminant releases.* Atmospheric Environment, 2006. **40**(19): p. 3490-3502.

175. Sreedharan, P., et al., *Influence of indoor transport and mixing time scales on the performance of sensor systems for characterizing contaminant releases.* Atmospheric Environment, 2007. **41**(40): p. 9530-9542.

176. SteelFisher, Gillian, et al., *Public response to an anthrax attack: Reactions to mass prophylaxis in a scenario involving inhalation anthrax from an unidentified source.* Biosecurity and Bioterrorism: Biodefense Strategy, Practice, and Science, 2011.

177. Stephenson, Edward H., Edgar W. Larson, and Joseph W. Dominik, *Effect of environmental factors on aerosol-induced lassa virus infection.* Journal of Medical Virology, 1984. **14**(4): p. 295-303.

178. Stuart, Amy L. and Dean A. Wilkening, *Degradation of biological weapons agents in the environment: Implications for terrorism response.* Environmental Science & Technology, 2005. **39**(8): p. 2736-2743.

179. Szekely, A. V., *Beitrag zur lebensdauer der milzbrandsporen.* Z. Hyg. Infectionskrankh., 1903. **44**: p. 359-363.

180. Tarnvik, A. and L. Berglund, *Tularaemia.* Eur Respir J, 2003. **21**(2): p. 361-373.

181. Tarnvik, A., G. Sandstrom, and A. Sjostedt, *Epidemiological analysis of tularemia in sweden 1931-1993.* Fems Immunology and Medical Microbiology, 1996. **13**(3): p. 201-204.

182. Tellier, R., *Aerosol transmission of influenza a virus: A review of new studies.* Journal of the Royal Society Interface, 2009. **6**: p. S783-S790.

183. Thatcher, T. L., et al., *A concentration rebound method for measuring particle penetration and deposition in the indoor environment.* Aerosol Science and Technology, 2003. **37**(11): p. 847-864.

184. Thatcher, TL, Sextro R, and Ermak D, *Database of physical, chemical and toxicological properties of cb warfare agents for modeling airborne dispersion in and around buildings.* 2000.

185. Thatcher, Tracy L. and David W. Layton, *Deposition, resuspension, and penetration of particles within a residence.* Atmospheric Environment, 1995. **29**(13): p. 1487-1497.

186. Titball, R. W. and A. Sjostedt, *Francisella tularensis: An overview.* Asm News, 2003. **69**(11): p. 558-563.

187. U.S. Congress Office of Technology Assessment, *Proliferation of weapons of mass destruction: Assessing the risk.* 1993: Washington, DC.

188. USEPA, *Planning guidance for recovery following biological incidents*. 2009.

189. Waring, M. S. and J. A. Siegel, *Particle loading rates for hvac filters, heat exchangers, and ducts.* Indoor Air, 2008. **18**(3): p. 209-224.

190. Waterer, Grant W. and Hannah Robertson, *Bioterrorism for the respiratory physician.* Respirology, 2009. **14**(1): p. 5-11.

191. Watson, A. and D. Keir, *Information on which to base assessments of risk from environments contaminated with anthrax spores.* Epidemiology and Infection, 1994. **113**(3): p. 479-490.

192. Webb, G. F., *A silent bomb: The risk of anthrax as a weapon of mass destruction.* Proceedings of the National Academy of Sciences of the United States of America, 2003. **100**(8): p. 4355-4356.

193. Weber, T. P. and N. I. Stilianakis, *Inactivation of influenza a viruses in the environment and modes of transmission: A critical review.* Journal of Infection, 2008. **57**(5): p. 361-373.

194. Wehrle, P. F., et al., *An airborne outbreak of smallpox in a german hospital and its significance with respect to other recent outbreaks in europe.* Bulletin of the World Health Organization, 1970. **43**(5): p. 669-79.

195. Wein, L. M. and M. P. Atkinson, *Assessing infection control measures for pandemic influenza.* Risk Analysis, 2009. **29**(7): p. 949-962.

196. Wein, L. M., D. L. Craft, and E. H. Kaplan, *Emergency response to an anthrax attack.* Proceedings of the National Academy of Sciences of the United States of America, 2003. **100**(7): p. 4346-4351.

197. Wein, Lawrence M. and David L. Craft, *Evaluation of public health interventions for anthrax: A report to the secretary's council on public health preparedness.* Biosecurity and bioterrorism : biodefense strategy, practice, and science, 2005. **3**(4): p. 348-356.

198. Weis, C. P., *Personal communication*. 2010.

199. Weis, C. P., et al., *Secondary aerosolization of viable bacillus anthracis spores in a contaminated us senate office.* JAMA, 2002. **288**(22): p. 2853-8.

200. West, Jon S., et al., *Pcr to predict risk of airborne disease.* Trends in Microbiology, 2008. **16**(8): p. 380-387.

201. Whiting, R. C and R. L. Buchanan, *Predictive modeling and risk assessment*, in *Food microbiology: Fundamentals and frontiers* L.R.B. M. P.Doyle and T. J.Montville, Editors. 2001, ASM Press: Washington , DC.

202. WHO, *Health aspects of chemical and biological weapons*. 1970, Geneva.

203. WHO, *Human plague in 2002 and 2003.* Weekly Epidemiological Record, 2004. **79**(33): p. 6.

204. Wilkinso.Tr, *Survival of bacteria on metal surfaces.* Applied Microbiology, 1966. **14**(3): p. 303-307.

205. Won, William D. and Harold Ross, *Effect of diluent and relative humidity on apparent viability of airborne pasteurella pestis.* Applied and Environmental Microbiology, 1966. **14**(5): p. 742-745.

206. World Health, Organization. *Health aspects of chemical and biological weapons report of a who group of consultants*. 1970; Available from: http://catalog.hathitrust.org/api/volumes/oclc/98866.html.

207. Xu, M. D., et al., *Deposition of tobacco-smoke particles in a low ventilation room.* Aerosol Science and Technology, 1994. **20**(2): p. 194-206.

208. Zanini, Michele, *Middle eastern terrorism and netwar.* Studies in Conflict & Terrorism, 1999. **22**(3): p. 247-256.

209. Zink, Thomas K., *Anthrax attacks: Lessons learned on the 10th anniversary of the anthrax attacks.* Disaster medicine and public health preparedness, 2011. **5**(3): p. 173-4.

VITA

Tao Hong was born in Harbin, China. He received his bachelor's degree of Environmental Engineering from TongJi University, Shanghai, China in 2007. He joined the Department of Civil, Architectural, and Environmental Engineering at Drexel University in 2007, and received a Master degree in 2009. During his Ph.D. study, he focused on quantitative microbial risk assessment. He has published multiple research works on these topics. He is also a member of many professional affiliations such as the Society of Risk Assessment, American Society of Civil Engineers, etc.

Selected Publications

Tao Hong, P.L. Gurian, and N.F.D. Ward, "Setting Risk-Informed Environmental Standards for Bacillus Anthracis Spores", Risk Analysis, 2010. 30 (10).

Yin Huang, Tao Hong, Timothy Bartrand, et al., "How Sensitive is Safe? Risk-based Targets for Ambient Monitoring of Pathogens", IEEE Sensor Journal, 2010. 10 (3).

Tao Hong and P.L. Gurian, "Key Uncertainties in Risk Informed Standards for *B. Anthracis*", in 2nd International Conference on Risk Analysis and Crisis Response. 2009. Beijing, Atlantis Press.

Tao Hong, P.L. Gurian, Y. Huang, and C.N. Haas, "Prioritizing Risks and Uncertainties from Intentional Release of Selected Category A Pathogens" PLoS ONE (under revision).

Kyle C. Griffith, Tao Hong, Igor Burstyn, et al., "Comparison of Methods for Quantification of Surface Contamination with Microbial Spores in an Office Building" submitted to Applied and Environmental Microbiology